



# Study on Improvement of Evaluation Methodology of Cushioning Packaging

Chen, Zhong

---

(Degree)

博士 (工学)

(Date of Degree)

2013-09-25

(Date of Publication)

2014-09-01

(Resource Type)

doctoral thesis

(Report Number)

甲第5974号

(URL)

<https://hdl.handle.net/20.500.14094/D1005974>

※ 当コンテンツは神戸大学の学術成果です。無断複製・不正使用等を禁じます。著作権法で認められている範囲内で、適切にご利用ください。



博 士 論 文

**Study on Improvement of Evaluation  
Methodology of Cushioning Packaging**

(緩衝包装機能評価手法の高度化に関する研究)

平成 25 年 7 月

神戸大学大学院海事科学研究科

氏 名 : 仲 晨 (Chen ZHONG)



# ABSTRACT

## Study on Improvement of Evaluation Methodology of Cushioning Packaging

Chen ZHONG

Economic globalization is increasing the economic interdependence of national economies across the world through a rapid increase in cross-border movement of goods in recent years. Distribution of goods trends to globalization. This trend causes that package of goods is more important than ever.

For safe delivery of a product from manufacturer to consumers, adequate cushioning is indispensable. Using numerous cushioning materials and packaging methods, many package versions can be designed. Considering the relationship of product and package design, if the package cannot make up the difference between the product ruggedness and the environment inputs, 'under package' occurs and product damage will most likely result. Conversely, if the package is provided too much protection, the situation called 'over package' is economically wasteful because money is being wasted on protection which is not required. Therefore, packaging engineers seek 'optimal package' that provides sufficient protection to the products at an economical cost. To accomplish this, the performance of the cushioning materials that are used in transport packaging must be tested before the materials are applied in the packaging design. In addition, the whole cushioning package must be tested to confirm whether it provides sufficient protection to the products.

Cushioning package materials are usually evaluated by traditional drop testing methods, such as free fall and controlled shock tests. Both tests are considered to yield the same results when the test dummy is dropped from a given height. The basis for this assumption is the equivalent drop theory. Physical test methods can be supplemented by a number of widely used simulation methods.

In addition, a typical design procedure for the cushioning package comprises of the following four steps. Step 1—Define the distribution environment (i.e. the shock and vibration). The environment must be defined first to design package. Step 2—Define product fragility. The product fragility represents the product's sensitivity to shock and vibration. Step 3—Design the cushioning package. First, the cushioning material may need to be tested, and then the shock cushioning and vibration transmissibility curves are plotted. Second, from the test results, we can determine the type, size and thickness of the cushioning material. Finally, the entire cushioning package should be configured. Step 4—Perform verification tests for entire package. This step confirms whether the package design is optimized. If all testing requirements are met,

optimal package design is accomplished. Otherwise, the designers must return to Step 3 and repeat this procedure.

However, traditional drop test methods are limited by the following three shortcomings. First, in the traditional equivalent drop theory, the package is assumed to behave as a linear mass-spring model. Since no packaging materials satisfy this assumption, the applicability of the traditional equivalent drop theory is limited by experimental errors. Second, the safety of a test product is not guaranteed under traditional drop testing, while traditional simulation methods are not sufficiently accurate for the stringent requirements of packaging materials. Third, for traditional testing methods, design requirements are not usually met in a single verification testing in practice. Repetition of Steps 3 and 4 two or three times is normal. A worst-case scenario occurs when an inappropriate cushioning material was applied. In this case, large quantities of labor and material resources are undoubtedly required.

The objective of this study is to issue aforementioned questions. We resolve the first shortcoming by a new theory called the 'friction equivalent drop theory'. On the basis of this theory, we propose a new test method called 'the hybrid drop testing method' that integrates the traditional drop test and simulation methods. The hybrid drop test ensures the safety of the test product and improves test efficiency.

This dissertation comprises six chapters and an appendix.

Chapter 1 presents the research background, methods and purposes, focusing on two traditional evaluation testing methods for cushioning material and packaged product. Traditional and damping equivalent drop theories and digital simulation methods are also described.

Chapter 2 begins with the need for a new equivalent drop theory, and then introduces a new physical model called the 'friction viscous-damping model'. On the basis of this model, we theoretically deduced shock response equations of the free fall and controlled shock tests. Finally, a friction equivalent drop theory was theoretically elaborated. Due to a nonlinear characteristic of the friction viscous-damping model, some approximate solutions for nonlinear system such as average method and equivalent linearization method were applied during the deduction of the two shock response equations. Meanwhile, simulation software called MapleSim was used to carry out a digital simulation.

Chapter 3 describes a series of verification tests for proofing the feasibility of the friction equivalent drop theory. A preliminary verification test based on a simple corrugated sleeve was first performed. The equivalent free-fall height was decided as 60 cm. The results showed that the equivalent accuracy is improved after an application of the friction equivalent drop theory. To obtain robust proof, the further verification test was performed for a range of materials and stresses. A corrugated sleeve and pulp mould cushions were used as the test materials. Verification tests proofed the applicability of the friction equivalent drop theory to both

structural corrugated sleeve and pulp mould cushions. The corrective effects vary with stress but become more prominent toward the lowest point of the cushion curve. The predictive accuracy of the hybrid drop test is sufficiently high for practical application in cushion package design.

Chapter 4 introduces the hybrid drop test, a novel evaluation testing method based on the friction equivalent drop theory developed in Chapter 2. The chapter begins with a conceptual overview of the new testing method, followed by a flowchart. Finally, calculation of the parameters of the FVD model is explained in detail.

Chapter 5 describes the verification test which proves the feasibility of the hybrid drop test, similar to the friction equivalent drop theory in Chapter 3. A mockup was constructed to represent a real product—printer. Edge-coupling pulp mould was used as the cushioning material. The controlled shock tests were performed and the experimental data such as acceleration, velocity change were recorded. Data statistics was made on the basis of numerous experimental data. The results showed that hybrid drop test is sufficiently accurate for practical applications.

Chapter 6 presents the summary of this dissertation.

Appendix lists symbols and acronyms used in this dissertation.

Summarily, through developing a new equivalent drop theory and proposing a new evaluation testing method, we improved evaluation methodology of cushioning packaging. Using the hybrid drop testing method, we can predict the PRA for a specified package design at higher drop heights by performing a single, low-height drop test. The hybrid drop testing method provides packaging researchers with an alternative testing choice. It also ensures the safety of the test product and improves test efficiency. We expect that this new testing method will become of valuable assistance in future packaging design.

This page is intentionally left blank

# CONTENTS

<b>CHAPTER 1. INTRODUCTION.....</b>	<b>1</b>
1.1 OVERVIEW OF CUSHIONING PACKAGES .....	1
1.2 RESEARCH BACKGROUND .....	3
1.3 SHOCK HAZARD.....	4
1.4 EVALUATION TESTS FOR CUSHIONING MATERIALS .....	7
1.4.1 Dynamic compression test.....	7
1.4.2 Controlled shock test .....	9
1.5 EVALUATION TESTS FOR PACKAGED PRODUCTS.....	10
1.5.1 Free fall test .....	10
1.5.2 Controlled shock test .....	11
1.6 RELEVANT STANDARDS .....	13
1.7 EXISTING EQUIVALENT DROP THEORIES.....	14
1.7.1 Modeling of packaged product.....	14
1.7.2 Conception of test at free fall .....	15
1.7.3 Traditional equivalent drop theory .....	16
1.7.4 Damping equivalent drop theory.....	18
1.8 DIGITAL SIMULATION METHODS AND MAPLESIM .....	20
1.8.1 Simulation in MapleSim .....	21
1.8.2 Components used in this study .....	21
1.8.3 Digital simulation of Linear and VD models.....	23
1.9 RESEARCH PURPOSE AND METHOD .....	26
1.10 STRUCTURE OF DISSERTATION .....	27
1.11 REFERENCES .....	28
<b>CHAPTER 2. FRICTION EQUIVALENT DROP THEORY.....</b>	<b>33</b>
2.1 RATIONAL FOR DEVELOPING FRICTION EQUIVALENT DROP THEORY .....	33



2.2	PRELIMINARY TEST .....	33
2.2.1	Test equipment and materials .....	33
2.2.2	Test conditions .....	35
2.2.3	Test results .....	35
2.3	NEW PHYSICAL MODEL—FVD MODEL .....	36
2.3.1	Foundations of the FVD model .....	36
2.3.2	Rational for two springs .....	37
2.3.3	Types of friction .....	37
2.3.4	Building of friction component .....	38
2.4	DEDUCTION OF SR EQUATION OF TEST AT FREE FALL USING FVD MODEL .....	38
2.4.1	Calculating period of FVD model .....	38
2.4.2	Average method .....	40
2.4.3	Mathematical SR equation for test at free fall .....	41
2.4.4	Mathematical verification .....	44
2.5	DEDUCTION OF SR EQUATION OF CONTROLLED SHOCK TEST USING FVD MODEL .....	44
2.5.1	Equivalent linearization method .....	44
2.5.2	Calculation process .....	45
2.5.3	Mathematical SR equation for the controlled shock test .....	54
2.5.4	Mathematical verification .....	54
2.6	FRICTION EQUIVALENT DROP THEORY .....	54
2.7	REFERENCES .....	55

**CHAPTER 3. VERIFICATION OF FRICTION EQUIVALENT DROP THEORY...57**

3.1	PRELIMINARY VERIFICATION .....	57
3.1.1	Test equipment and materials .....	57
3.1.2	Test method .....	57
3.1.3	Test conditions .....	57
3.1.4	Correcting method .....	57
3.1.5	Results and discussion .....	62
3.2	FURTHER VERIFICATION .....	63

3.2.1	Test equipment and materials .....	63
3.2.2	Test design.....	65
3.2.3	Variance of friction.....	66
3.2.4	Probability distributions of dGs.....	67
3.2.5	Chi-square test.....	69
3.2.6	Evaluation of correction effect.....	73
3.2.7	Discussion .....	74
3.3	REFERENCES .....	78
<b>CHAPTER 4. THE HYBRID DROP TEST .....</b>		<b>81</b>
4.1	INTRODUCTION .....	81
4.2	CONCEPT OF NEW TESTING METHOD.....	82
4.3	HYBRID DROP TEST.....	82
4.4	EXPERIMENTAL STAGE .....	84
4.4.1	First controlled shock test.....	84
4.4.2	Second controlled shock test.....	84
4.5	CALCULATING PARAMETERS AND DATA TRANSFORM STAGE.....	84
4.5.1	Calculating $m$ .....	84
4.5.2	Calculating $k$ .....	86
4.5.3	Calculating $F_c$ .....	86
4.5.4	Calculating $c$ .....	87
4.5.5	Data transformation.....	88
4.6	DIGITAL SIMULATION STAGE .....	88
4.6.1	Simulation method.....	88
4.6.2	Simulation FVD model.....	88
4.6.3	Simulation result .....	89
4.7	PREDICTION STAGE .....	90
4.8	REFERENCES .....	90
<b>CHAPTER 5. VERIFICATION OF THE HYBRID DROP TEST .....</b>		<b>91</b>
5.1	TEST EQUIPMENT AND DUMMY .....	91

5.1.1	Test equipment.....	91
5.1.2	Test dummy.....	91
5.2	TEST METHOD .....	92
5.3	TEST RESULTS.....	93
5.4	DATA ANALYSIS FLOW .....	95
5.5	PARAMETER CALCULATION AND COMPARISON OF $PRA_{EXP}$ AND $PRA_{SIM}$ .....	95
5.6	DISCUSSION.....	99
5.7	REFERENCES .....	102
<b>CHAPTER 6. SUMMARY .....</b>		<b>103</b>
<b>ACKNOWLEDGEMENTS .....</b>		<b>105</b>
<b>APPENDIX .....</b>		<b>107</b>
	DATA OF $PRA_{EXP}$ VS. $PRA_{SIM}$ .....	107
	LIST OF SYMBOLS .....	116
	LIST OF ACRONYMS.....	118
	LIST OF FIGURE CAPTIONS.....	119
	LIST OF TABLES .....	121

# CHAPTER 1. INTRODUCTION

## 1.1 Overview of Cushioning Packages

The current trends toward economic globalization have placed increasingly competitive pressure on markets. Distribution of goods has become global in scope<sup>[1]</sup>, and goods are subjected to many hazards during transportation. Damage to the package systems of goods in transit is broadly classified into the following two categories: physical damage and chemical damage. Chemical damage includes rust and discoloration caused by the meteorological environment (temperature, humidity, rain and sunshine), while physical damage is caused by shocks and vibrations generated during transportation<sup>[2]</sup>.

If products are to be safely delivered from manufacturers to consumers, then they must be protected against these hazards during transportation. Therefore, packaging that protects the products against physical damage is indispensable. In particular, a cushioning package will provide an essential buffer between the product and distribution-related hazards<sup>[3]</sup>.

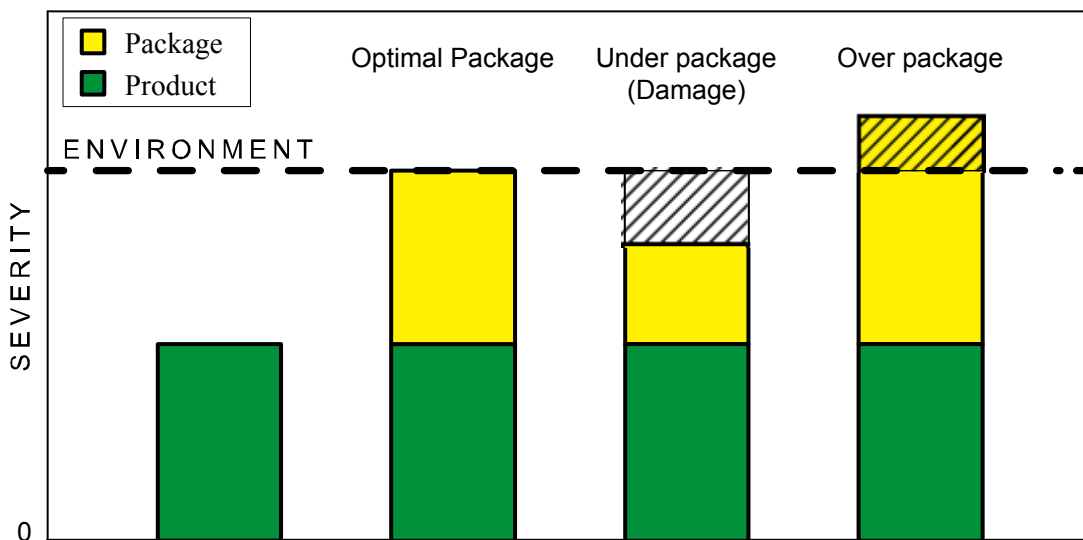


Figure 1-1 Cushioning Package Concept.

The bar chart of Figure 1-1 illustrates how packaging should be designed to suit the product and environment. The background can be regarded as the level of environmental severity for a given distribution channel. Although the product can inherently withstand a certain amount of abuse, it cannot usually withstand the rigors of shipment without support. The role of the package, therefore, is to compensate for the difference between environmental stress and ability of the product to withstand these stresses. In the ideal case, second bar in Figure 1-1, the package exactly makes up the difference between the product ruggedness and environmental inputs. The situation in which packaging is inadequate (third bar in Figure 1-1) is called 'under packaging' and likely leads to product damage. Conversely, the situation called 'over package' (depicted in the fourth bar in Figure 1-1) is economically wasteful because money is spent on protection that is not required. Thus, inappropriate choice of cushioning material will result in over

packaging or under packaging, neither of which is desirable. The optimal packaging can be ensured by testing the performance of the intended cushioning materials before applying them to the packaging design. In addition, the entire cushioning package must be tested to confirm whether it provides sufficient protection to the products.

Cushioning packages are widely used because they are relatively inexpensive and provide a large cushioning effect, while conforming to the sustainability mantra of ‘reduce, reuse, recycle’ [4]-[6]. As mentioned in Section 1.1, a vital consideration in packaging development is to determine whether a packaged product is likely to be damaged during its journey to the final customer. A fundamental role of packaging is to ensure the safety of a product during transportation and storage. If a product is damaged in transit, this primary objective fails and the customer will either return or refuse to purchase the product [7]. Therefore, an essential step in package design is evaluation testing for cushioning, which will verify the cushioning protection offered to component materials or packaged freight.

Package testing involves the measurement of characteristics or properties of the packaging, including packaging materials and components, primary packages, shipping containers and unit loads, as well as the associated processes. The various purpose of packaging testing are as follows [8].

- To determine whether, or verify that, the requirements of a specification, regulation or contract are met,
- To validate suitability for end-use,
- To provide a basis for technical communication,

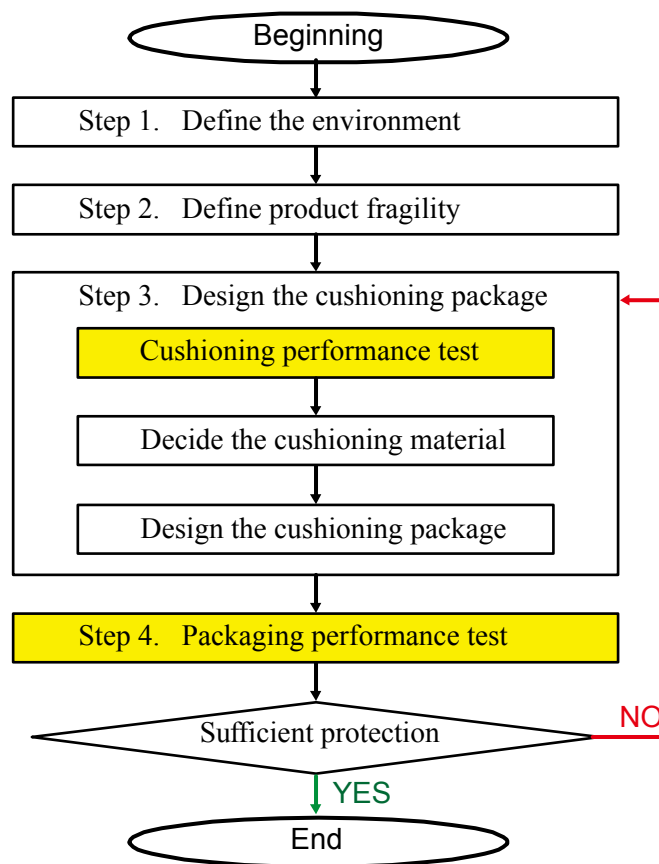


Figure 1-2 Cushioning Package Design Procedure.

- To assist with finding solutions to current packaging problems, and
- To help identify potential cost savings in packaging.

A typical design procedure for the cushioning package is shown in the flowchart of Figure 1-2. This procedure, developed in conjunction with the School of Packaging at Michigan State University<sup>[2]</sup>, has been accepted by a worldwide packaging designer. The procedure comprises of the following four main steps.

Step 1—Define the distribution environment (i.e. the shock and vibration environment<sup>[9]-[12]</sup>). The environment must be defined before the package is designed. By selecting the most severe drop height anticipated in the distribution environment, a representative acceleration vs. frequency profile is compiled.

Step 2—Define product fragility. The product fragility represents the product's sensitivity to shock and vibration. Shock and vibration fragility are characterized by the shock damage boundaries<sup>[13]-[15]</sup> and critical vibrational resonant frequency<sup>[16]-[19]</sup> of the product, respectively.

Step 3—Design the cushioning package. First, the cushioning material may need to be tested, and then the shock cushioning curves<sup>[20]-[25]</sup> and vibration transmissibility curves<sup>[26], [27]</sup> are plotted. Second, from the test results, we can determine the type, size and thickness of the cushioning material. Finally, the entire cushioning package should be configured<sup>[28]</sup>.

Step 4—Perform verification tests to confirm whether the package design has been optimized. These tests inform whether the provided protection is inadequate, sufficient or superfluous. If all testing requirements are met, optimal package design is accomplished. Otherwise, designers must return to Step 3 and repeat this procedure. In practice, design requirements are not usually met in a single verification testing, and repetition of Steps 3 and 4 two or three times is normal. A worst-case scenario occurs when the packaging fails because of inappropriate cushioning material applied. In this scenario, large quantities of labour and material resources are undoubtedly required.

## 1.2 Research Background

In Section 1.1, we highlighted the importance of verification testing in packaging design. The ability of the packaging to absorb shock and vibration hazards during distribution is verified by drop and vibration tests, respectively. TSUDA<sup>[29]-[33]</sup> and HOSOYAMA<sup>[34]-[37]</sup> conducted valuable research on vibration test. In this study, we focus on the drop test.

Traditional drop tests generally determine whether the peak response acceleration (PRA) is within the desired range and product is likely to be damaged (i.e. whether the package cushioning provides sufficient protection)<sup>[38]</sup>. However, the test dummy itself will likely be damaged under traditional drop test. This is often unacceptable, e.g. if the product is very valuable or in limited supply.

The following conditions are often encountered in packaging design and testing. Design requirements specify the drop height  $H$  as 80 cm. However, the product approaches its damage boundary if dropped from this height. As mentioned above, scarce or expensive products must remain undamaged through the verification test. Traditional testing methods are clearly inappropriate in this situation, because free fall and controlled shock tests confer a high risk of damage. On the basis of the above consideration, a simpler, more efficient verification testing technique is required in modern package design.

In addition to physical testing methods, such as free fall and controlled shock tests, a number of widely used simulation methods are available, including ANSYS<sup>®</sup><sup>[39], [40]</sup>, LS-DYNA<sup>®</sup><sup>[41], [42]</sup> and MSC Nastran<sup>™</sup><sup>[43]</sup>. In a typical digital simulation, the physical characteristics of the cushioning material are established in a series of preliminary tests. The test data are converted to native parameters that can be used by the simulation software, and the simulation is run. The cushioning performance of the transport

packaging can often be verified without repeated test. However, when repeated tests are needed, digital simulation is particularly advantageous.

Although simulation methods are sufficiently accurate in many engineering fields such as automobile manufacturing and aerospace<sup>[44]</sup>, they are insufficient for transport packaging because of the physical characteristics of the cushioning materials. The most widely used cushioning materials in package engineering are paper and plastic cushions, both of which display nonlinear characteristics. Consequently, simulating their physical characteristics with sufficient accuracy to satisfy the simulation requirements is difficult.

An important alternative approach is the equivalent drop theory, pioneered by Goff *et al.*<sup>[45],[46]</sup> in 1976. They first demonstrated the correlation of shock with the free fall height. The shock response, an important indicator of the performance of cushion materials<sup>[47]</sup>, is obtained from the results of a free fall or controlled shock test. Assuming that the cushion follows a linear mass–spring model<sup>[48]</sup>, the free fall and controlled shock tests yield the same results for equal free-fall heights. This result is known as the ‘traditional equivalent drop theory’. However, the linear mass–spring model is an idealized case that is not realized by any cushioning materials in the real world. Therefore, if the aforementioned precondition does not exist, is the equivalent free-fall height exactly equivalent?

Using expanded polyethylene as a test material, Saito *et al.*<sup>[49],[50]</sup> demonstrated the limitations of the linear model and that experimental errors may invalidate the traditional equivalent drop theory. They introduced viscous damping into the equivalent drop theory, and developed a new ‘damping equivalent drop theory’. An earlier study by Zhong *et al.*<sup>[48],[51]</sup> showed that the damping equivalent drop theory improves the precision of equivalent tests on quasi-linear cushioning materials; that is, the equivalent free-fall height under the damping equivalent drop theory for the quasi-linear packaging cushioning system can be considered to be equivalent. However, no researcher to date has dealt with the question of whether the equivalent free-fall height is still equivalent for nonlinear packaging cushioning system such as structural cushioning material (SCM). Therefore, to improve the precision of equivalent tests while providing a new theoretical basis for experimental analysis, researchers must develop an improved equivalent drop theory based on a new physical model.

### 1.3 Shock Hazard

Static cushioning packages always subjects the effect of gravitational acceleration  $g = 9.8 \text{ m/s}^2$ . A package in transit may be exposed to both gravitational force and hazard forces induced by shock or vibration. Since excessive forces are likely to damage the product, external forces applied during packaging design must not exceed the force tolerance of the product<sup>[20]</sup>.

According to Newton's second law of motion<sup>[52]</sup>, force  $F$  is expressed as

$$F = ma, \tag{1.1}$$

where  $m$  is mass and  $a$  is acceleration. Acceleration is typically used to assess the cushioning performance of the package.

A schematic of a generic packaged product is shown in Figure 1-3(a). The shock hazard to which the package is subjected is evaluated from an acceleration–time curve, shown in Figure 1-3(b). The force exerted on the package is represented by the input pulse, while the response pulse represents the force experienced by the product encased in the cushions. The horizontal and vertical axes denote time and acceleration, respectively.

Shock hazard is determined by the shock pulse, which comprises the following three parts: velocity change, peak acceleration and shock pulse shape<sup>[53]</sup>. The velocity change  $V_c$  is represented by the area

under the input pulse in Figure 1-3(b). According to Newton's fragility assessment theory<sup>[54]</sup>,  $V_c$  is a key parameter determining product fragility.

In Figure 1-3, two important data points are the peak input acceleration (PIA) and peak response acceleration (PRA). PIA and PRA are important indicators of the cushioning performance of the packaging systems. PIA defines the maximum force exerted on the package, while PRA is the maximum force experienced by the product.

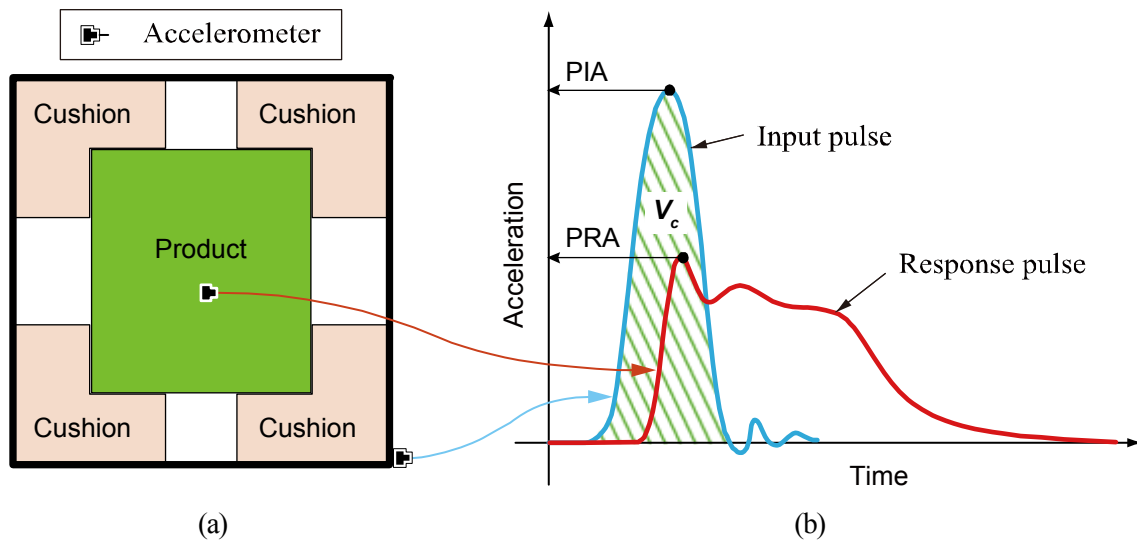


Figure 1-3 Generic Packaged Product and Acceleration–Time Curves.

(a) Schematic representation of packaged product, (b) Input and response curves.

Acceleration is measured using an acceleration pickup instrument, termed ‘shock manager’ is used. The shock manager (Figure 1-4(a)) is a suite of software and hardware manufactured by Yoshida Seiki Co., Ltd. In this study, the shock manager plays the following multiple roles<sup>[55]</sup>:

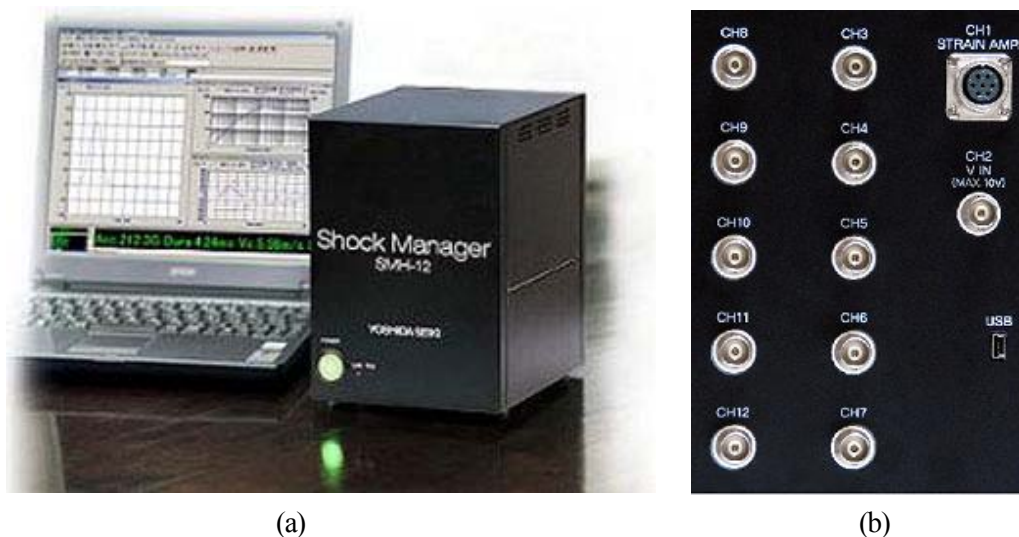


Figure 1-4 Shock Manager.

(a) Shock manager suit, (b) Rear panel of shock manager.



➤ Measurement of acceleration.

Input acceleration and the response acceleration from a maximum of 10 channels are measured (Figure 1-4(b)).

➤ Digital filter function

The digital filter function allows measurement of the waveforms filtered under filter conditions that are individually specified for each channel.

➤ Cushioning material characteristics analysis

The system plots a displacement waveform and an acceleration–displacement diagram, along with the acceleration waveform. These graphs allow the true effect of shock on the packaged freight, or the shock absorbing characteristics of the cushioning material, to be analysed.

➤ Shock response (SR)/shock response spectrum (SRS) analysis for damage prediction

When a natural frequency and damping coefficient are set for damage-prone parts of the product or the effect of an external force requires scrutiny, the system calculates and displays the response waveforms of the relevant parts.

To measure the input acceleration using the shock manager, the accelerometer, one end of which is embedded in a test machine in advance, is plugged into Channel 1 shown in Figure 1-4(b). The response acceleration is measured by attaching one end of another accelerometer to a product or weight dummy and plugging the other end into one of Channels 3–12.

The configuration of the test equipment is shown in Figure 1-10 in the next section, and the measured results are shown in Figure 1-5.

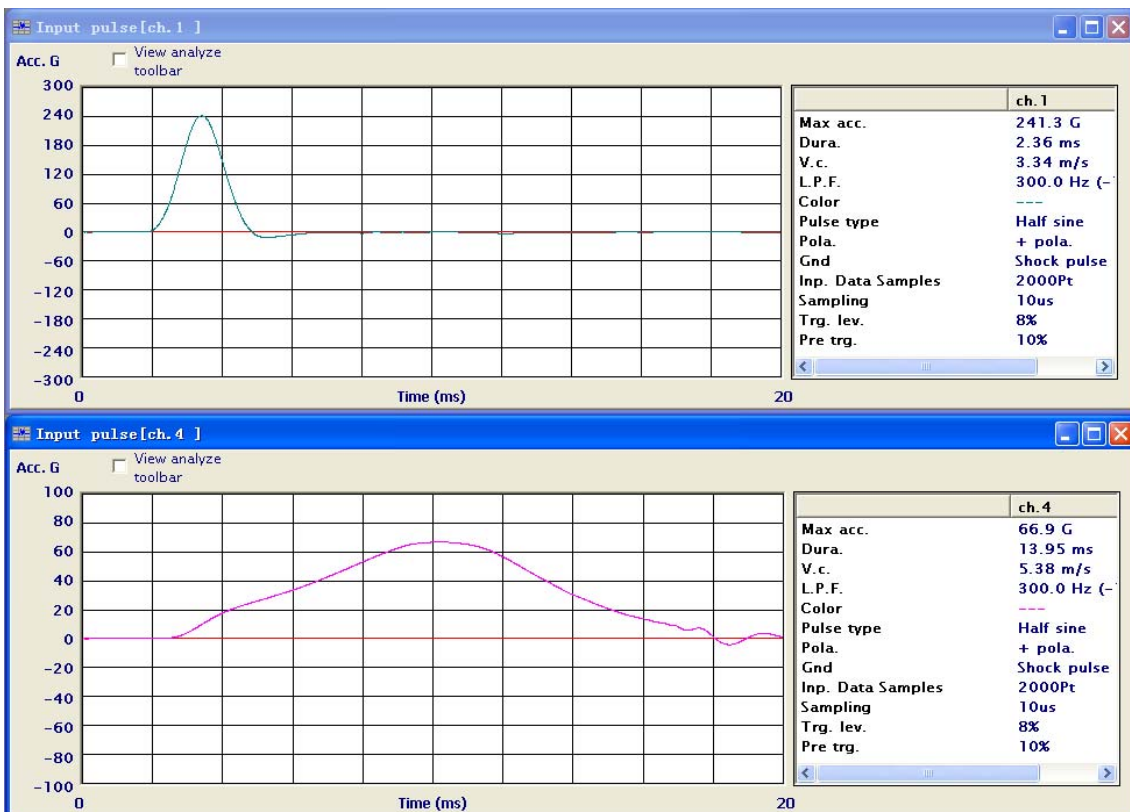


Figure 1-5 Screenshot for Acceleration–Time Curves of Input and Response Pulses.

According to Section 1.1, verification test is conducted on the following two broad packaging classes: cushioning materials and packaged product. Traditional tests applied to these two classes are introduced in the following section.

## 1.4 Evaluation Tests for Cushioning Materials

The cushioning materials determine the design and performance of the packaging. To aid the design process, packaging engineers require knowledge of the physical and (in some cases) chemical properties of the materials. Suppliers publish data sheets and other technical communications that include the typical or average relevant physical properties and test methods on which these are based. Sometimes these data are adequate; at other times, certain characteristics must be clarified by the packager or supplier, which requires additional cushioning material testing. These tests typically involve dynamic compression and controlled shock tests.

### 1.4.1 Dynamic compression test

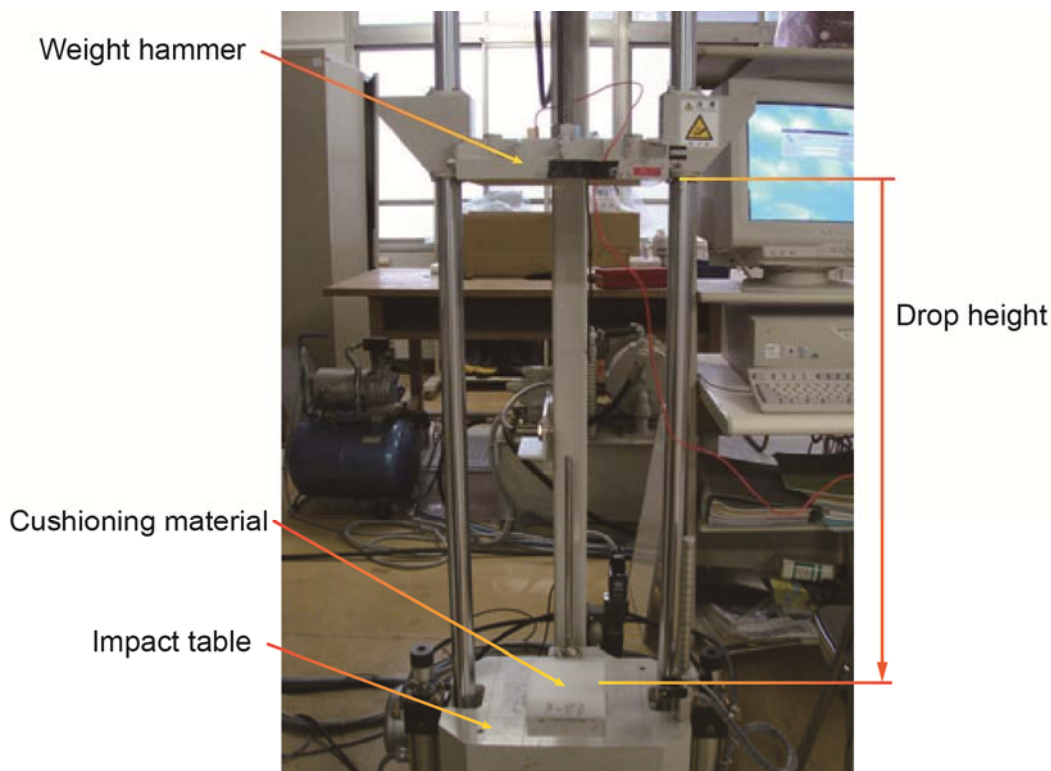


Figure 1-6 Dynamic Compression Tester.

The dynamic compression test requires a specially designed instrument known as a dynamic compression tester (Figure 1-6). In general, the dynamic compression test is applied to simple-shaped packaging materials, and it is not suitable for complex-shaped cushioning materials, such as pulp molding products. A schematic of the dynamic compression test for cushioning materials is illustrated in Figure 1-7. In the first step, the drop height is determined, and a hammer is raised to this level. Next, the test material is

placed at the centre of the platform, and the hammer is vertically withdrawn by the controller. The experimental data (e.g. response acceleration, impact velocity, rebound velocity and strain of the test material) are recorded when the hammer strikes the test material.

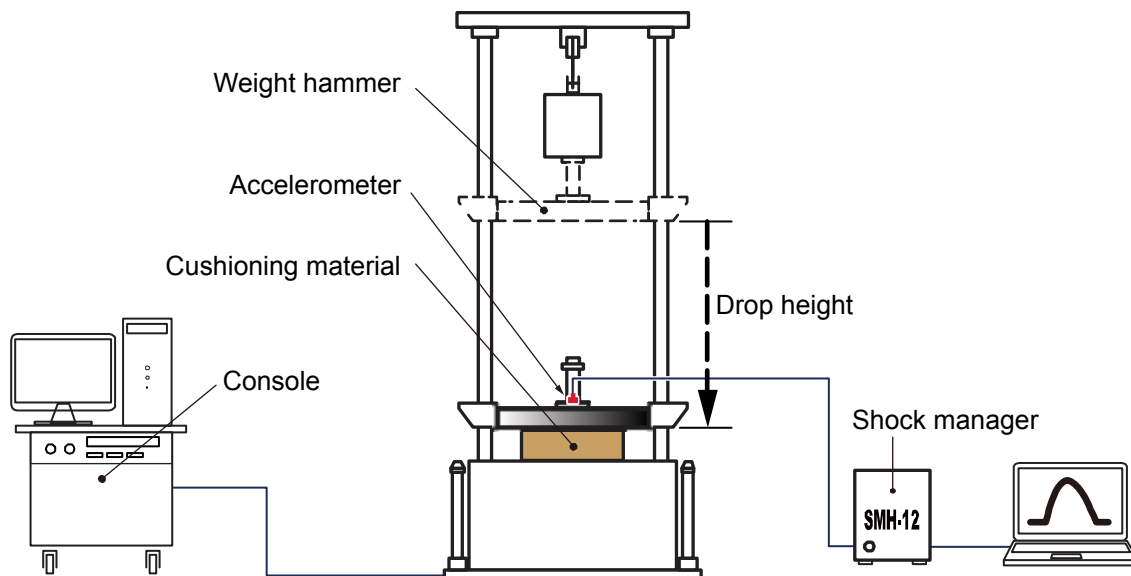


Figure 1-7 Schematic of the Dynamic Compression Test for Cushioning Materials.

Figure 1-8 shows a screenshot of the dynamic compression test results.

試験片	回数	重錘質量 (kgf)	面積 (cm <sup>2</sup> )	公称厚さ (mm)	実測厚さ (mm)	加速度 (G)	変位 (mm)	衝突速度 (m/s)	反撥速度 (m/s)
1	1	4.0	100.0	30.0	30.0	62.7	16.5	3.47	1.90
	2				30.0	63.8	16.4	3.38	1.88
	3				30.0	62.7	15.8	3.47	1.98
	4				30.0	58.6	16.2	3.42	1.90
	5				30.0	65.0	15.8	3.41	1.89
	6				30.0	59.7	16.6	3.43	1.84
	7				30.0	60.9	15.7	3.38	1.89
	8				30.0	63.2	15.6	3.38	1.78
	9				30.0	59.1	15.5	3.38	1.98

試験片 :	Test material	公称厚さ :	Nominal thickness
回数 :	Order	実測厚さ :	Actual thickness
重錘質量 :	Mass of hammer	加速度 :	Acceleration
面積 :	Area	変位 :	Displacement
衝突速度 :	Impact velocity	反撥速度 :	Rebound velocity

Figure 1-8 Screenshot of the Dynamic Compression Test Results.

## 1.4.2 Controlled shock test

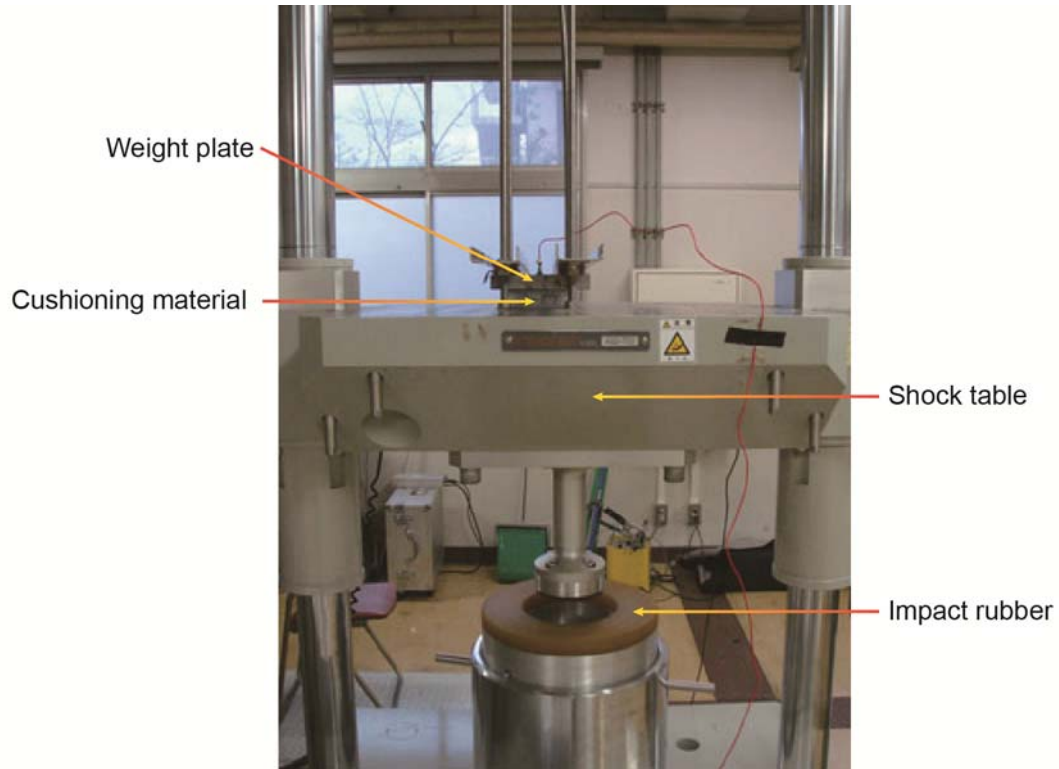


Figure 1-9 Shock Machine.

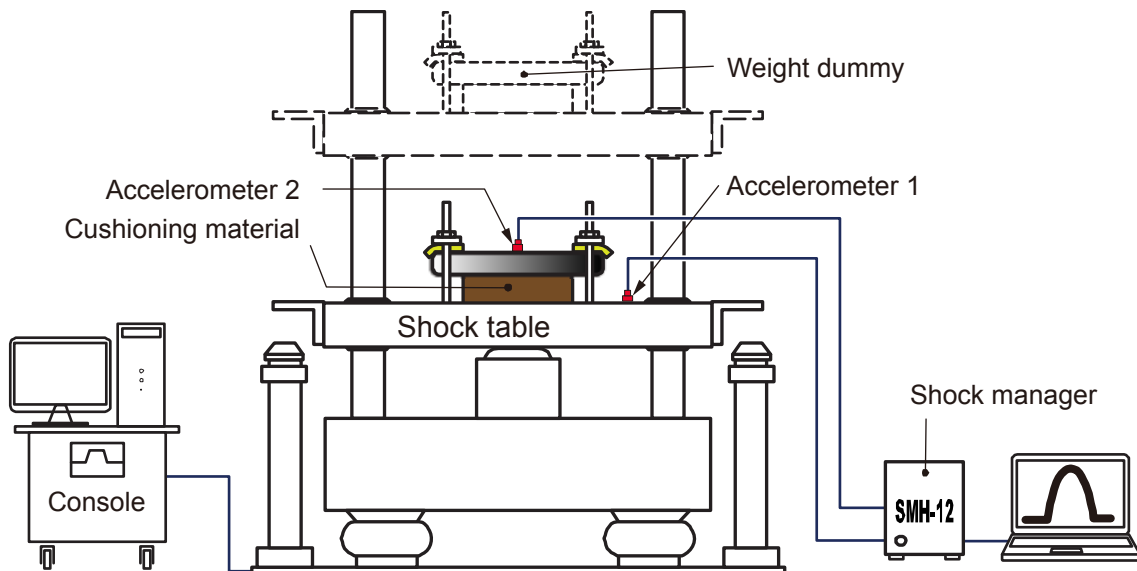


Figure 1-10 Schematic of the Controlled Shock Test for Cushioning Materials.

The controlled shock test is undertaken by a shock machine (see Figure 1-9), and it is configured as illustrated in Figure 1-10<sup>[57]</sup>. Similar to the dynamic compression test, the drop height is first determined, and the shock table is raised to this level. Next, the test material is fixed to the shock table. The test material and shock table are simultaneously dropped, and the experimental data (e.g. input acceleration, response acceleration, impact duration) are recorded when the shock table strikes an impact rubber. The input and output pulses are measured by two accelerometers (Accelerometers 1 and 2, in Figure 1-10).

## 1.5 Evaluation Tests for Packaged Products

Packaged products may be dropped or impacted by other items. Important properties of packaging are package integrity and the extent of product protection. Evaluation tests on packaged products assess the resistance of packages and products to controlled laboratory shock and vibration. Testing also determines the effectiveness of package cushioning in isolating fragile products from shock.

This section introduces free fall, dynamic compression and controlled shock tests.

### 1.5.1 Free fall test

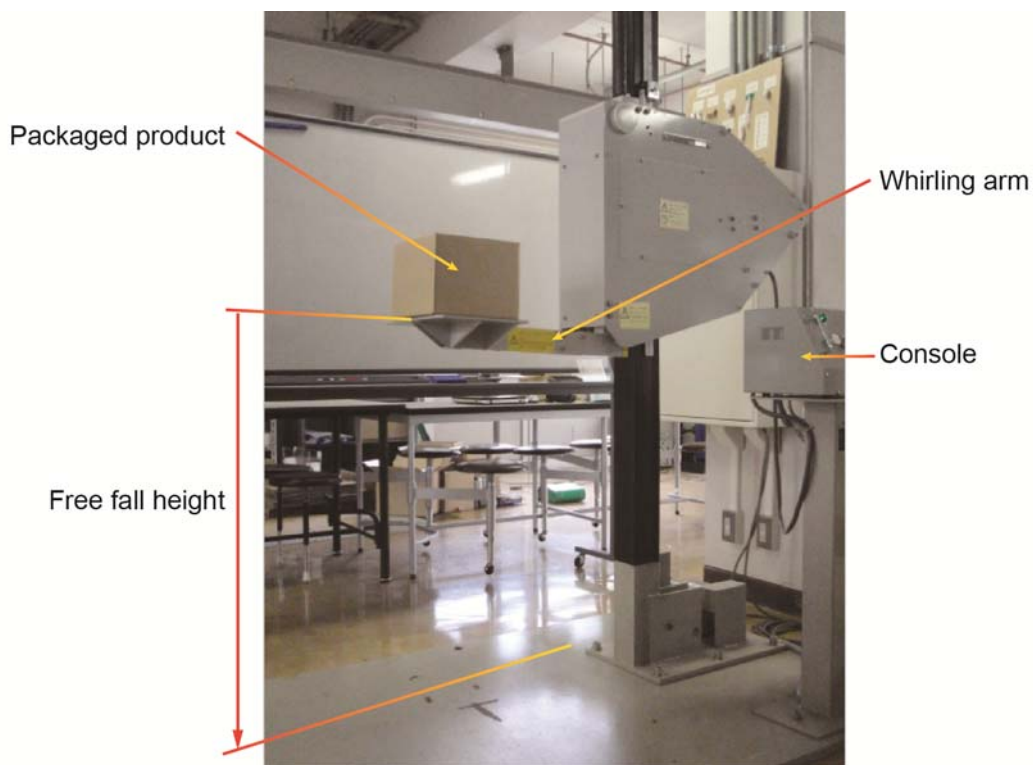


Figure 1-11 Free Fall Tester.

To date, the free fall test has been most frequently adopted because the necessary equipment is inexpensive, operation procedures are simple and a wide range of test dummies can be accommodated<sup>[38]</sup>. The components of the free fall test are illustrated in Figure 1-11, while Figure 1-12 is a schematic of the test method. In this test, the free fall height is first determined, and then the arm is raised to this level. Next,

a packaged product is placed on the arm, and the arm is rapidly withdrawn using the controller. The packaged product drops and experimental results are recorded<sup>[58]</sup>. However, because the packaged product drops in free fall, the bottom of the packaged product does not remain parallel to the ground during the drop process. Accurate results cannot be achieved if the packaged product drops non-horizontally.

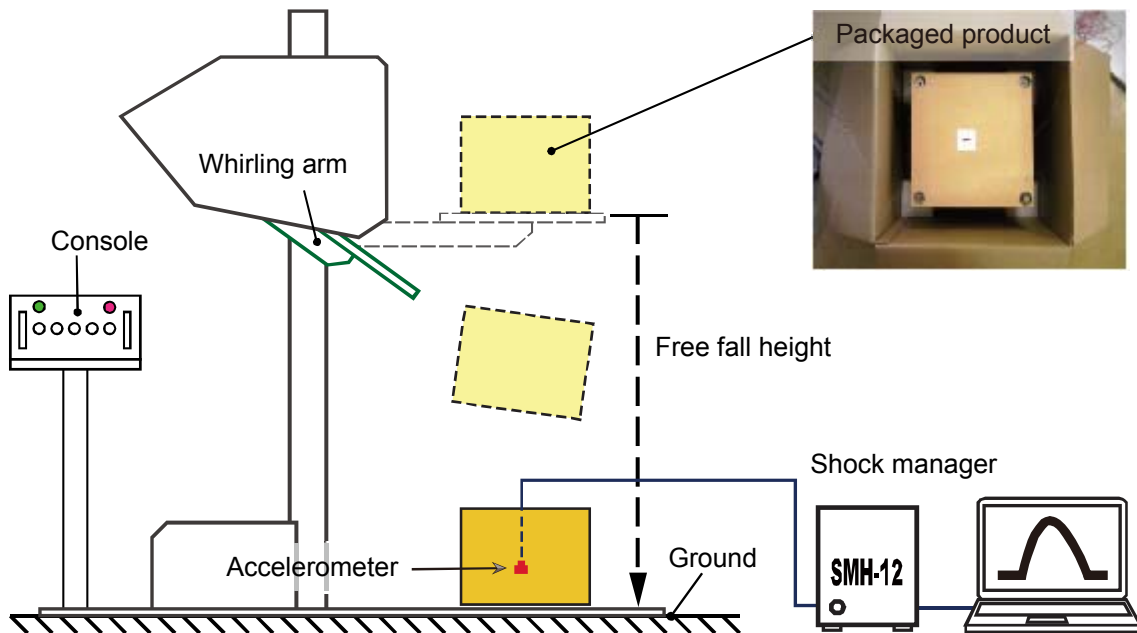


Figure 1-12 Schematic of the Free Fall Test for Packaged Product.

### 1.5.2 Controlled shock test

The departure from horizontal falling of the packaged product is illustrated in Figure 1-12. As shown in this figure, the test dummy almost inevitably tilts during the surface drop test<sup>[59]</sup>. To circumvent this problem, the free fall test was substituted with a controlled shock test (Figure 1-14).

The controlled shock test confers the following advantages:

1. The package can be precisely orientated throughout the entire drop process.
2. It is potentially considerably more accurate than the dynamic compression test because the input pulse is an actual waveform.
3. Since one machine can fulfill the functions of two machines, testing costs may be reduced. That is, if a laboratory already stocks a shock machine for analyzing product fragility, staff need not buy a separate drop test machine used solely for that purpose.

The test method differs from that of the cushioning material only in the cushioning material or packaged product used.

Figures 1-13 and 1-14 display a photograph and schematic of the controlled shock test for the packaged products, respectively.



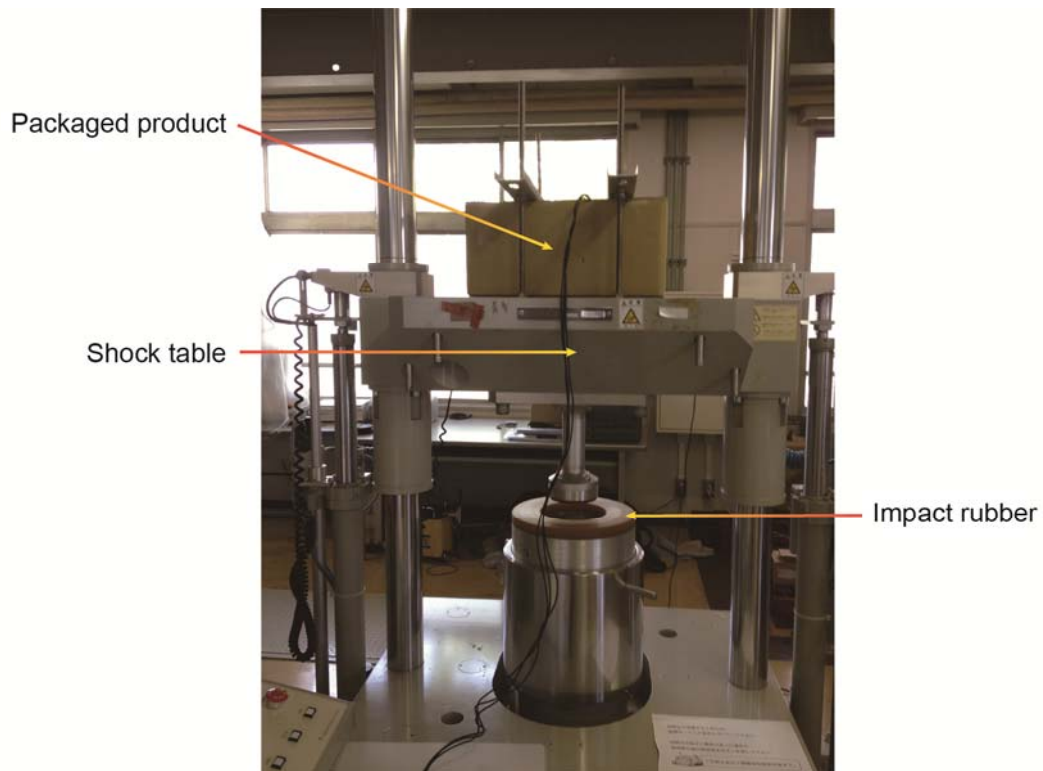


Figure 1-13 Scene of the Controlled Shock Test for Packaged Product.

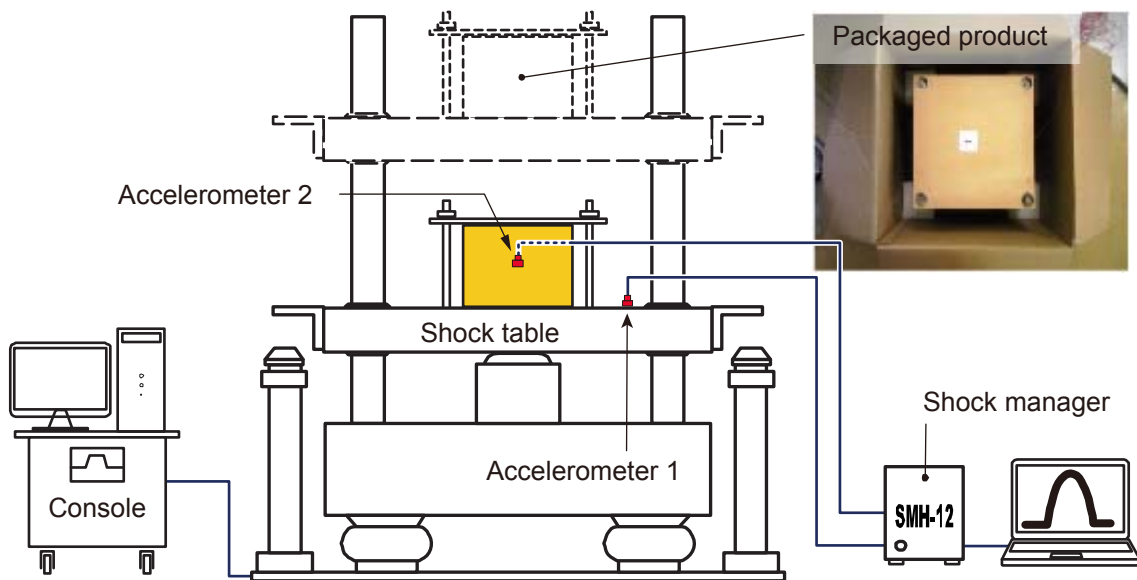
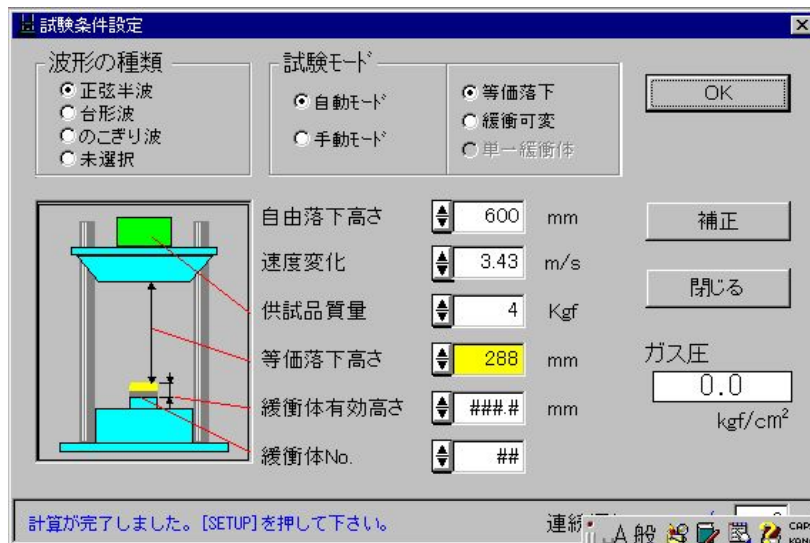


Figure 1-14 Schematic of the Controlled Shock Test for Packaged Product.



正弦半波 :	Half sine	自由落下高さ :	Free fall height
台形波 :	Trapezoidal wave	速度変化 :	Velocity change
のこぎり波 :	Sawtooth	供試品質量 :	Mass of sample
未選択 :	No selection	等価落下高さ :	Equivalent free-fall height
自動モード :	Auto mode	緩衝体有効高さ :	Effective height of cushion
手動モード :	Manual mode	緩衝体No. :	Cushion No.
等価落下 :	Equivalent drop	補正 :	Correct
緩衝可変 :	Buffered	閉じる :	Close

Figure 1-15 Settings Screenshot of the Controlled Shock Test for Packaged Product.

## 1.6 Relevant Standards

Methods for package testing are published in several standards organizations, such as International Organization for Standard (ISO) <sup>[60]</sup>, American Society for Testing and Material (ASTM) <sup>[61]</sup>, European Committee for Standardization (CEN) <sup>[62]</sup>, Technical Association of the Pulp and Paper Industry (TAPPI) <sup>[63]</sup>, and International Safe Transit Association (ISTA) <sup>[64]</sup>. Testing standards for cushioning materials and packaged product are summarized in Tables 1-1 and 1-2, respectively.

Table 1-1 Testing Standards for Cushioning Materials.

Standard Number	Standard Title
JIS Z 0235: 2002	Cushioning materials for packaging-Determination of cushioning performance
JIS Z 0240: 2002	Structural cushioning materials for packaging-Determination of cushioning performance

The JIS Z 0235 standard <sup>[65]</sup> specifies the cushioning performance and compression creep tests of packaging components such as regular shape cushions, cellular rubbers and plastics.

The JIS Z 0240 standard <sup>[66]</sup> specifies the drop test method for SCM. In general, SCMs are random-shaped cushions.



Table 1-2 Testing Standards for Packaged Products.

Standard Number	Standard Title
JIS Z 0119: 2002	Mechanical-shock fragility testing methods for packaging and products design
JIS Z 0200: 1999	Packaged freights-General rules of testing
JIS Z 0202: 1994	Method of drop test for packaged freights
JIS Z 0212: 1998	Packaged freights and containers-Method of compression test

As mentioned above, a product in transit is exposed to numerous distribution hazards such as vibration, shock and compression. The JIS Z 0200 standard<sup>[68]</sup> specifies general test methods for confirming whether the package optimally protects the product from these hazards.

Two parameters frequently used in package design are the critical acceleration and critical velocity change, from which package engineers can construct a damage boundary curve. The JIS Z 0119 standard<sup>[67]</sup> defines the test methods to obtain these technical targets.

The JIS Z 0202 standard<sup>[69]</sup> specifies drop test methods for packaged products.

The JIS Z 0212 standard<sup>[70]</sup> specifies compression test methods for packaged products.

## 1.7 Existing Equivalent Drop Theories

Two equivalent drop theories are commonly used today. We refer to these as the traditional equivalent drop theory and damping equivalent drop theory.

### 1.7.1 Modeling of packaged product

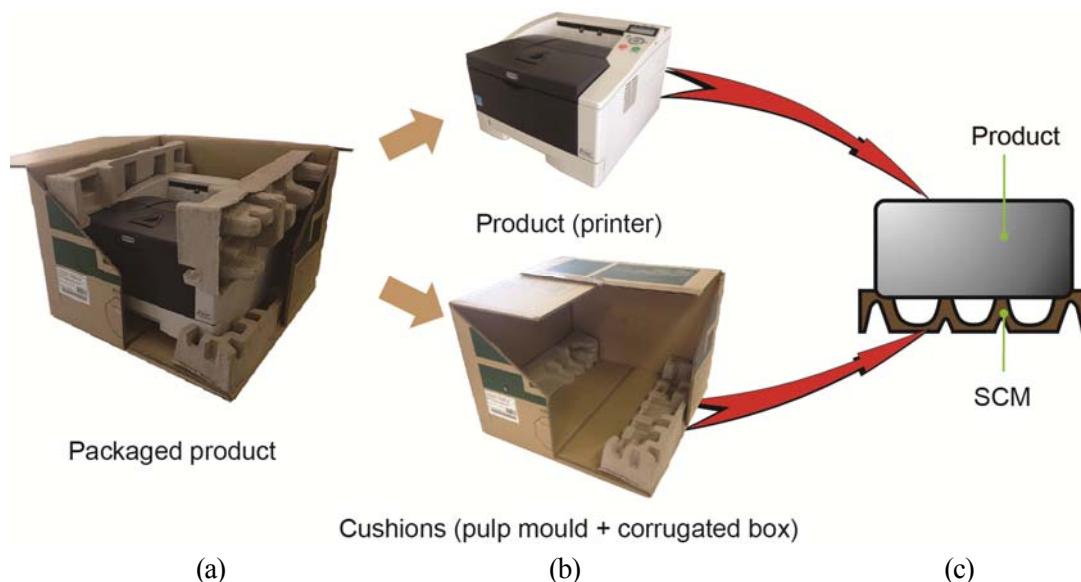


Figure 1-16 Modeling of Packaged Product.  
 (a) Packaged product, (b) Product and cushions, (c) Modeling.

To assist packaging research, the package should be conceptually modeled. Figure 1-16(a) shows an example of a common cushioning package. The package can be divided into product and cushions (see Figure 1-16(b)). Here the printer is referred to as the ‘product’. In addition, according to JIS Z 0240 standard (enclosed by the solid rectangle in Figure 1-17 and equivalent to ASTM D4168 [72] or ISO 8568 [73] standards), the corrugated box and pulp mould belong to SCM and are collectively referred to as the ‘SCM’ in the model (Figure 1-16(c)).

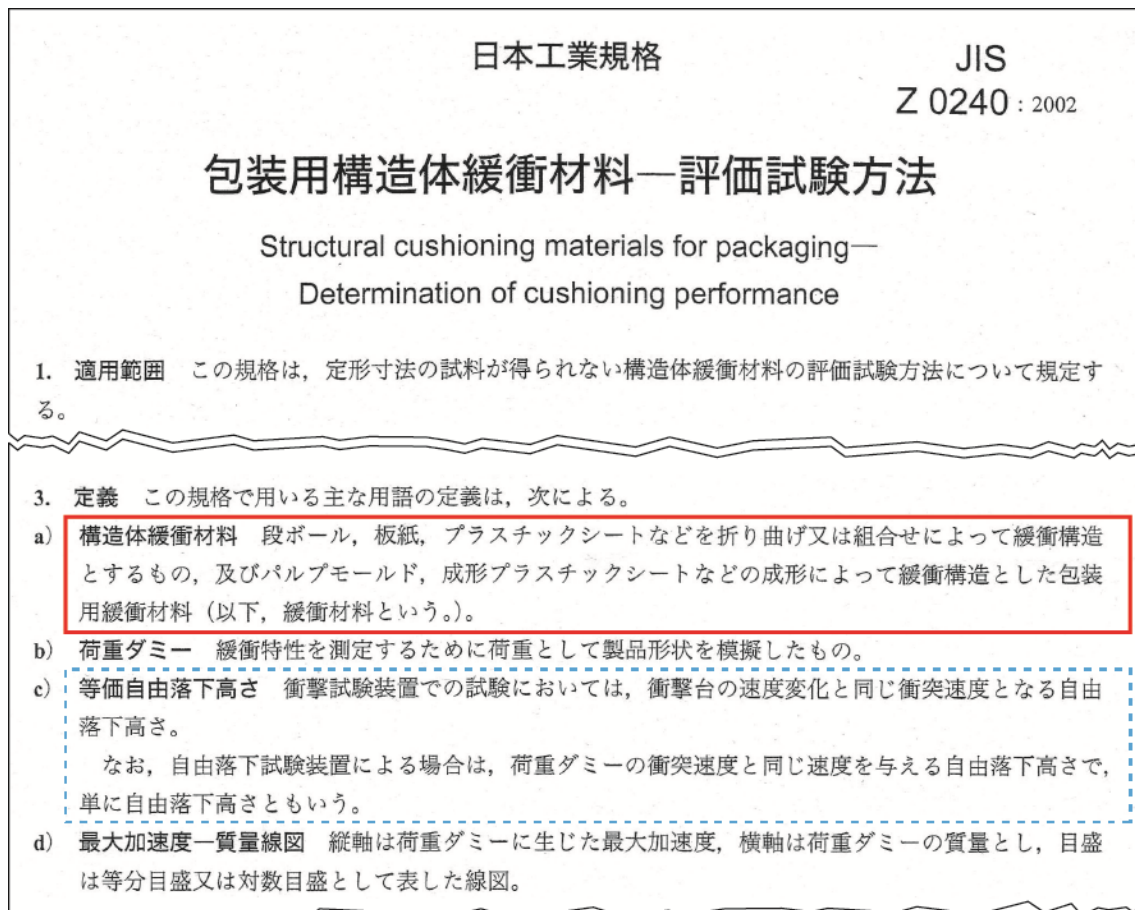


Figure 1-17 Section of JIS Z 0240: 2002 Standard.

## 1.7.2 Conception of test at free fall

According to Figure 1-16, the cushion mechanism is the same in the free fall and dynamic compression tests. Therefore, the free fall and dynamic compression tests are jointly called the ‘*Test at free fall*’ in this study.

### 1.7.3 Traditional equivalent drop theory

#### A) Linear model

The simplest mathematical model<sup>[74]</sup> that describes the behavior of the cushioning materials is the linear spring–mass model (Figure 1-18), hereafter abbreviated as the ‘Linear model’.

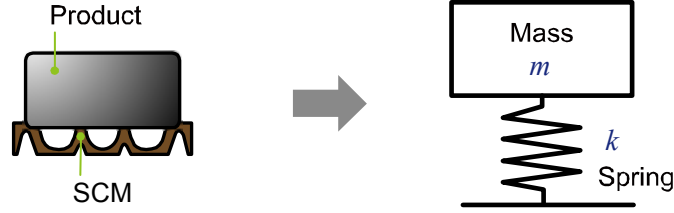


Figure 1-18 Linear Model.

#### B) Test at free fall

Applying law of conservation of energy to the Linear model, the following equation is obtained:

$$mgH = \frac{mV^2}{2} = \frac{kx_{\max}^2}{2},$$

where  $k$  is the spring constant,  $H$  is the drop height,  $V$  is the impact velocity of the weight dummy and  $x_{\max}$  is the maximum strain of the spring.

Rearranging,  $x_{\max}$  is obtained as follows:

$$x_{\max} = \sqrt{\frac{2gH \cdot m}{k}}. \quad (1.2)$$

According to the equation of motion, following is obtained

$$F = m\ddot{x} = kx_{\max}, \quad (1.3)$$

where  $F$  is the force.

Eq. (1.3) is rewritten as

$$\ddot{x} = \frac{kx}{m}. \quad (1.4)$$

The PRA on a weight dummy of the test at free fall  $PRA_{ff}$  occurs when the spring is most compressed. Therefore, substituting Eq. (1.2) in Eq. (1.4),  $PRA_{ff}$  is obtained as

$$PRA_{ff} = \frac{kx}{m} = \sqrt{\frac{2gH \cdot k}{m}} = \omega_n \cdot V, \quad (1.5)$$

where

$$V = \sqrt{2gh},$$

$$\omega_n = \sqrt{\frac{k}{m}} \quad (\omega_n \text{ is the undamped natural angular frequency}).$$

### C) Controlled shock test

In the controlled shock test, the SRS of the system is recorded when an extremely short half-sine shock pulse is applied to the system, as shown in Figure 1-19. Here the model is regarded as a ‘soft spring’ and SRS curve is linear with slope  $2\pi$  when  $f_n \cdot D_e$  is smaller than  $1/2\pi$  (where  $f_n$  is the undamped natural frequency and  $D_e$  is the effective impact duration). Hence, shock transmissibility  $T_r$  is equal to  $2\pi f_n D_e$ , and  $T_r$  is represented as follows<sup>[71]</sup>:

$$T_r = \frac{\text{PRA}_{cs}}{\text{PIA}} = 2\pi \cdot f_n \cdot D_e, \quad (1.6)$$

$$\text{PRA}_{cs} = \omega_n \cdot V_c, \quad (1.7)$$

$$\therefore \omega_n = 2\pi \cdot f_n, \quad V_c = D_e \cdot \text{PIA}, \quad D_e = 2D/\pi,$$

where  $\text{PRA}_{cs}$  is PRA of the controlled shock test,  $V_c$  is the velocity change recorded on the shock table and  $D$  is the impact duration.

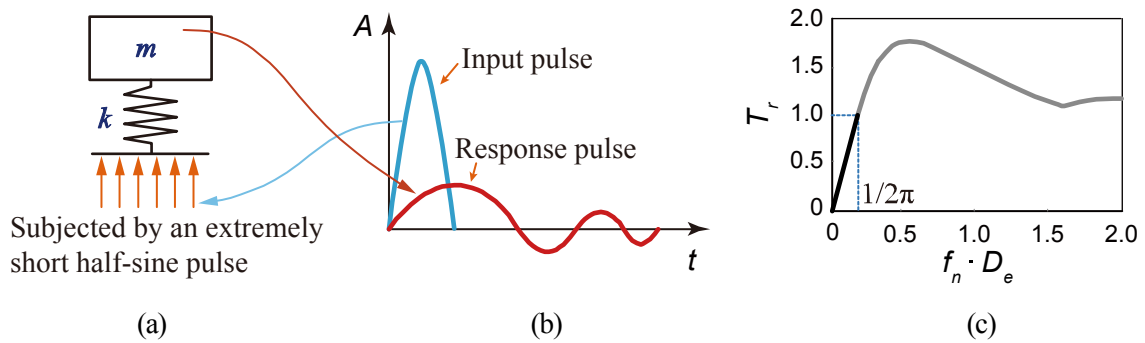


Figure 1-19 SRS for Linear model.

(a) Dynamic model, (b) Input and response pulses, (c) SRS curve.

### D) Equivalent free-fall height

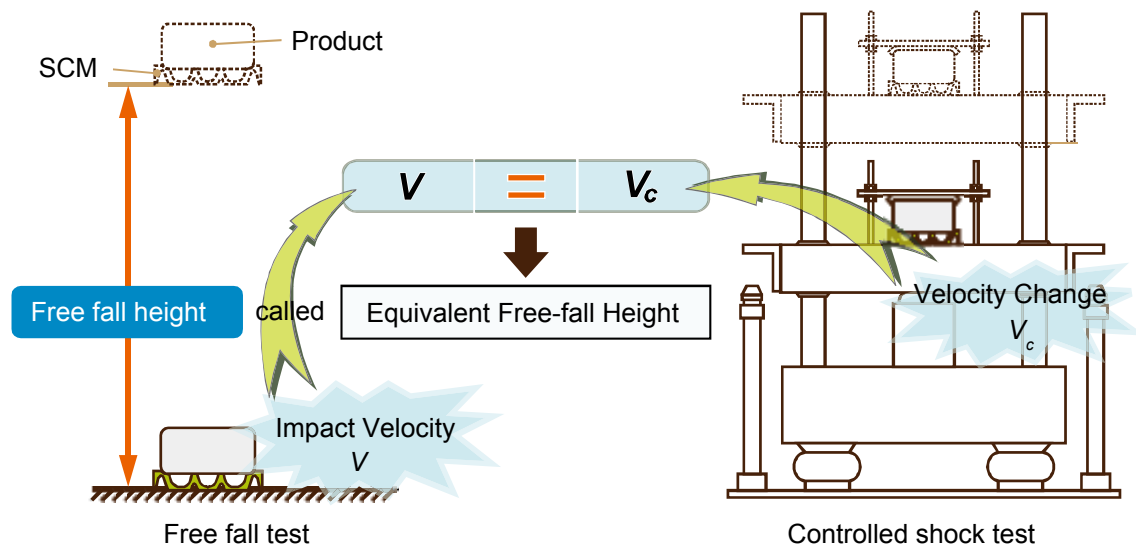


Figure 1-20 Schematic of Equivalent Free-fall Height.

JIS Z 0240 (the contents enclosed by the dashed rectangle in Figure 1-17) recommends that drop tests be conducted as the so-called ‘equivalent free-fall height’. The equivalent free-fall height is defined as the height for which the impact velocity of the free fall test equals the velocity change of the controlled shock test (Figure 1-20). This recommendation assumes that the cushioning materials can be modeled as the Linear model of Figure 1-18. If this assumption holds, then the test at free fall and controlled shock test are equivalent.

### E) Traditional equivalent drop theory

Comparing Eqs. (1.5) and (1.7), if  $V = V_c$  when the test at free fall and the controlled shock test are performed, the PRAs of these two tests should be theoretically same. In other words, the two tests can be concluded to be equivalent. This idea forms the basis of the traditional equivalent drop theory and is hereafter abbreviated as the ‘traditional theory’ (Figure 1-21).

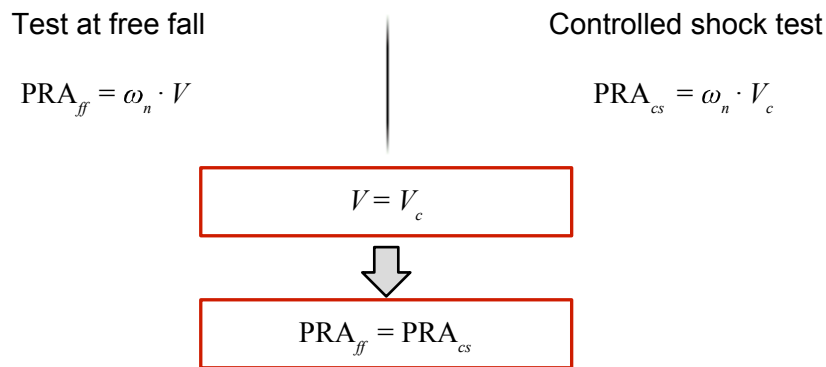


Figure 1-21 Schematic of the Traditional Equivalent Drop Theory.

## 1.7.4 Damping equivalent drop theory

### A) VD model

Although Linear model is mathematically convenient, no completely linear cushioning materials exist in practice. Therefore, researchers have developed the viscous damping (VD) model, which incorporates the effects of attenuation (Figure 1-22). Here the cushioning material is assumed to obey a one-dimensional attenuation model.

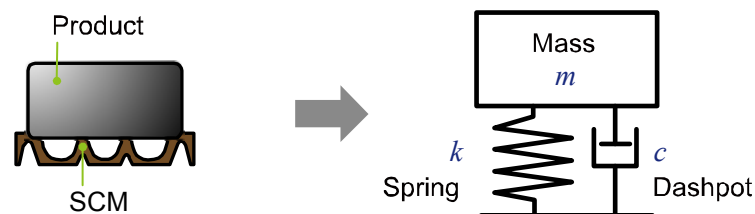


Figure 1-22 VD Model.

## B) Test at free fall

The damping model is based on the following differential equation of motion:

$$m\ddot{x} + \xi\dot{x} + kx = 0, \quad (1.8)$$

where  $\xi$  is the damping ratio.

After solving Eq. (1.8),  $PRA_{ff}$  is obtained as follows:

$$PRA_{ff} = n_{ff} \cdot \omega_n \cdot V, \quad (1.9)$$

$$n_{ff} = \left| \frac{2\xi^2 - 1}{\sqrt{1 - \xi^2}} \right| \cdot \exp\left(\frac{-\pi\xi}{2\sqrt{1 - \xi^2}}\right), \quad (1.10)$$

where  $n_{ff}$  is the correction coefficient of the test at free fall.

## C) Controlled shock test

In the shock test, the PRA of the VD model initially accelerated by a half-sine wave can be obtained theoretically (Figure 1-23). Subsequently,  $T_r$  can be calculated from the input and response accelerations.

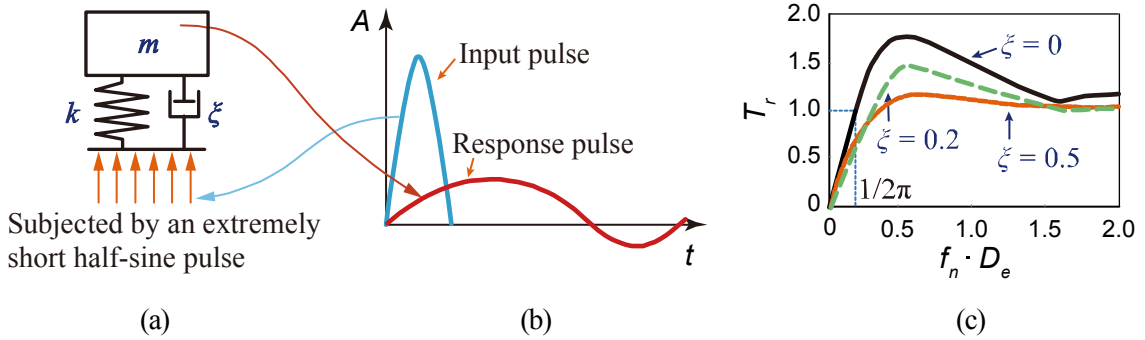


Figure 1-23 SRS for VD Model.

(a) Dynamic model, (b) Input and response pulses, (c) SRS curve.

In Section 1.7.3, the SRS curve is assumed to be line with slope  $2\pi$  through the origin. However, by introducing  $\xi$ ,  $T_r$  is expressed as follows.<sup>[75]</sup>

$$T_r = \begin{cases} a \cdot \ddot{g}(t) & \text{when } \ddot{x}(t)_{\max} \text{ is in range } 0 < t < D \\ a \cdot (\ddot{g}(t) + \ddot{g}(t - D)) & \text{when } \ddot{x}(t)_{\max} \text{ is in range } t > D \end{cases},$$

$$\ddot{g}(t) = \frac{(2a^2\omega^2 - 4a^2\omega^2\xi^2 - 2\omega^4) \sin(\omega\sqrt{1 - \xi^2}t) + 4a^2\omega^2\xi\sqrt{1 - \xi^2} \cos(\omega\sqrt{1 - \xi^2}t)}{2\omega\sqrt{1 - \xi^2} [\omega^4 + (4\xi^2 - 2)a^2\xi^2 + a^4]} e^{(-\omega\xi t)}$$

$$+ \frac{(4a^2\omega^2\xi^2 + \omega^4 - a^2\omega^2) \sin(at) - 2a^3\omega\xi \cos(at)}{a [\omega^4 + (4\xi^2 - 2)a^2\omega^2 + a^4]}, \quad (1.11)$$

where

$$a = \pi/T_0,$$

$\ddot{x}(t)_{\max}$  is the PRA function and  $T_0$  is the initial impact duration.

This equation determines a new SRS (Figure 1-23(c)). The form of the SRS curve depends on the value of  $\xi$ . Thus, defining  $n_{cs}$  as the ratio of  $T_r$  to the approximation of the shock transmissibility  $2\pi f_n D_e$ , estimated from the traditional equivalent drop theory, we obtain

$$n_{cs} = \frac{T_r}{2\pi \cdot f_n \cdot D_e}. \quad (1.12)$$

From which  $PRA_{cs}$  is obtained as follows:

$$PRA_{cs} = n_{cs} \cdot \omega_n \cdot V_c, \quad (1.13)$$

where  $n_{cs}$  is the correction coefficient of the controlled shock test.

#### D) Damping equivalent drop theory

From the preceding discussion, it is clear that a correction is required if the results of the test at free fall and controlled shock test are equivalent under the attenuation model. This so-called ‘correction coefficient’ is expressed as follows:

$$V_c = \frac{n_{ff}}{n_{cs}} V \quad \text{or} \quad (1.14)$$

$$V = \frac{n_{cs}}{n_{ff}} V_c. \quad (1.15)$$

This theory is called the damping equivalent drop theory and is hereafter abbreviated as the ‘damping theory’ (Figure 1-24).

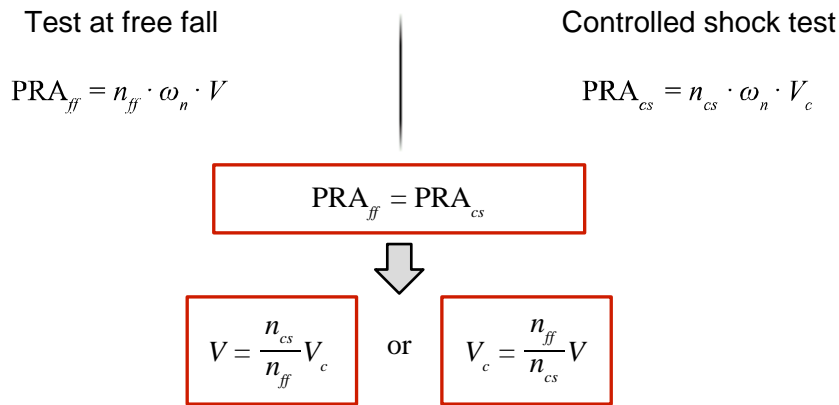


Figure 1-24 Schematic of the Damping Equivalent Drop Theory.

## 1.8 Digital Simulation Methods and MapleSim

MapleSim (Maplesoft Inc., Canada) is a physical modeling tool founded on symbolic computation technology. It is widely used in engineering field such as automobile manufacturing and aerospace<sup>[76]</sup> and is a suitable choice for packaging engineering. Because MapleSim is based on Maple, it can vastly reduce

the model development time and provides an extensive range of analytical tools for greater insight into engineering systems.

### 1.8.1 Simulation in MapleSim

Simulations are performed in MapleSim as follows (the MapleSim window is shown in Figure 1-25)<sup>[77]</sup>.

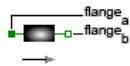
1. A physical model is constructed from built-in or custom components.
2. Appropriate parameters are set for each component.
3. The model is simulated by pressing the button labeled ‘simulate the model’. The obtained simulation results are shown in Figure 1-25(b).

### 1.8.2 Components used in this study

One features of MapleSim is drag-and-drop physical modeling environment. With MapleSim, users avoid having to translate their design into equations and manipulate them into signal-flow block diagrams. Users can simply recreate the system diagram on their screen using components that represent the physical model. The MapleSim component library contains over 500 components that are divided into 1-D mechanical, electrical, hydraulic, magnetic, multibody mechanical, signal blocks and thermal.

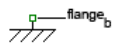
The components, those belong to 1-D mechanical and signal blocks, used in this study are as follows<sup>[78]</sup>:

- Sliding mass component



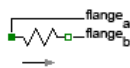
This component models sliding mass with inertia and two rigidly connected flanges, without friction. The sliding mass has the length,  $L$ , and the position coordinate,  $s$ , is in the middle.

- Translational fixed component



This component models the flange of a one-dimensional translational mechanical system fixed at position,  $s_0$ , in the housing. This component can be used to connect a compliant element (e.g., a spring or damper) between a sliding mass and the housing, or to fix a rigid element (e.g., a sliding mass) at a specific position.

- Spring component

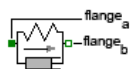


This component models a linear one-dimensional translational spring. Its governing equations are

$$f = c \cdot (s_{rel} - s_{rel0}), \quad s_{rel} = s_b - s_a,$$

$$f = f_b, \quad f_a + f_b = 0.$$

- Damp-spring component



This component comprises the spring and damper components connected in parallel. Its governing equations are

$$f = c \cdot (s_{rel} - s_{rel0}) + d \cdot v_{rel},$$



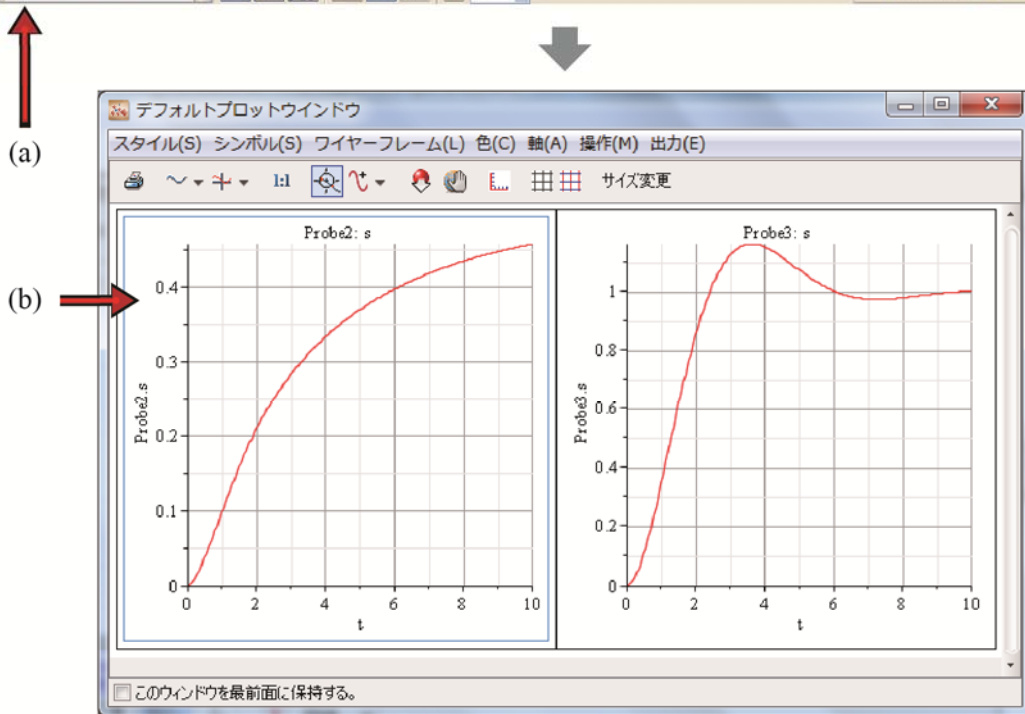
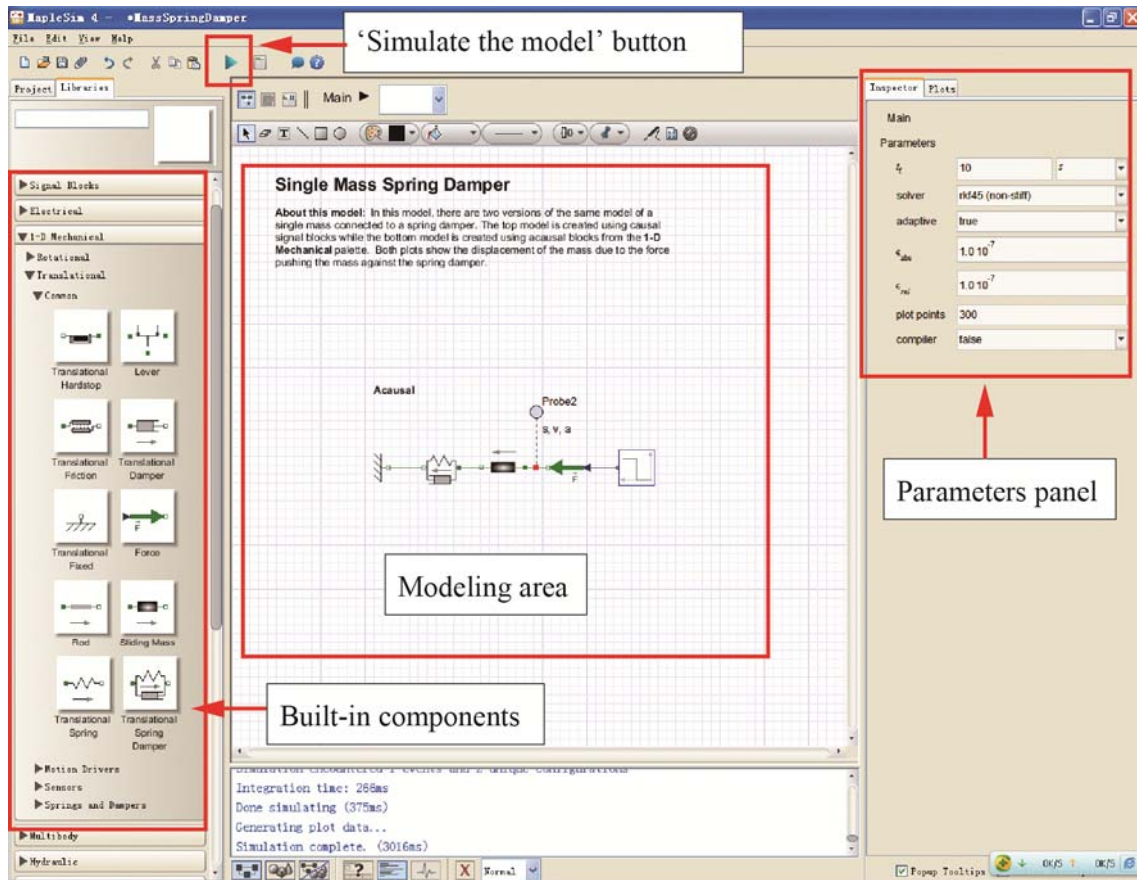


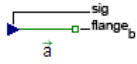
Figure 1-25 MapleSim Window and Simulation Results.

(a) MapleSim window and software panels; (b) Simulation results.

$$s_{rel} = s_b - s_a, \quad v_{rel} = \dot{s}_{rel},$$

$$f = f_b, \quad f_a + f_b = 0.$$

- Translational acceleration component



This component generates a forced one-dimensional acceleration at  $flange_b$  proportional to the input signal. The velocity and the position of the flange are determined by the integration of the acceleration.

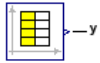
Its component equations are

$$a = \text{sig} \left[ \frac{m}{s^2} \right],$$

$$\dot{v} = a, \quad \dot{s} = v,$$

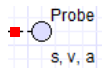
$$v(0) = v_0, \quad s(0) = s_0.$$

- Time lookup table component



This component generates an output signal,  $y$ , by interpolation using time as the input value.

- Probe



A model must contain at least one probe with a set quantity, otherwise the simulation will fail. Adding probes to a model, we can measure graph and obtain specific information about various quantities, such as acceleration, velocity, distance and volume, for different components and connections. Probes do not affect the quantities being measured.

### 1.8.3 Digital simulation of Linear and VD models

As mentioned above, MapleSim is a widely used simulation tool<sup>[79]</sup>. However, author found no reported applications of MapleSim to packaging engineering. Therefore, whether MapleSim can be applied in packaging research must be verified by a feasibility study. To this end, we used MapleSim to plot mathematical curves of the Linear and VD models.

#### A) Linear model

As the simplest basic model, the Linear model is an obvious choice for an initial assessment. For comparisons with actual test data, the mass was specified as 4 kg and the free fall height  $h_{ff}$  was assumed as 60 cm; therefore, the initial velocity of the mass was  $v_0 = -3.43$  m/s from  $v_0 = \sqrt{2gh_{ff}}$  (note that the positive direction is vertically upward). The spring constant  $k$  (denoted  $c$  in MapleSim) was set at  $10^5$  N/m. The construction of the Linear model in MapleSim is shown in Figure 1-26.

In terms of parameters  $k$ ,  $m$  and  $v_0$ , the theoretical response acceleration is

$$\ddot{x}_{\max} = v_0 \sqrt{\frac{k}{m}} = 3.43 \times \sqrt{\frac{10^5}{4}} \doteq 542.33 \text{ (m/s}^2\text{)}.$$

The result of this simulation is shown in Figure 1-27. The curve peaks at  $542.329 \text{ m/s}^2$ , the exact value of the theoretical response acceleration.

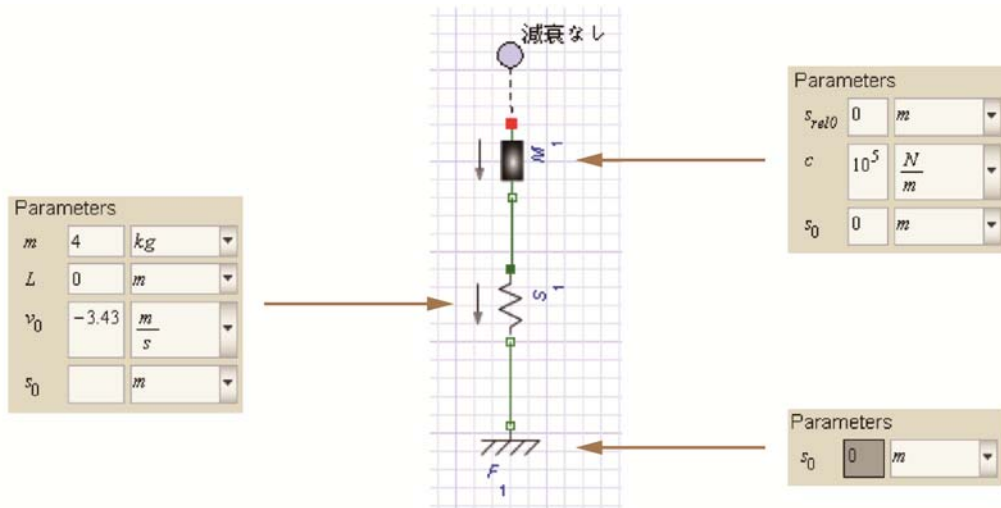


Figure 1-26 Linear Model in MapleSim.

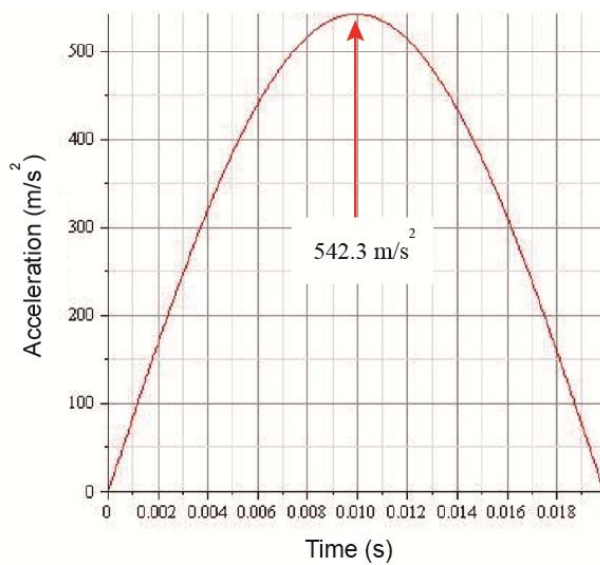


Figure 1-27 Simulation Result of Linear Model.

### B) VD model

Next, the VD model was constructed in MapleSim, as shown in Figure 1-28. Here  $m$  was specified as 4 kg. The spring constant  $k$  and damping coefficient  $c$  ( $c$  and  $d$  in MapleSim, respectively) were obtained from experimental data.

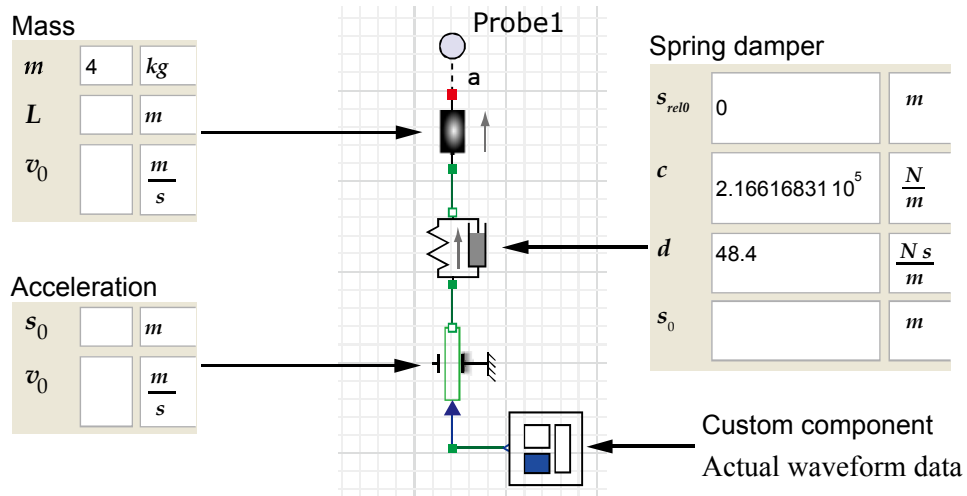


Figure 1-28 VD Model in MapleSim.

Prior to inputting the waveform data to MapleSim, the data were converted to a compatible format. First, the data obtained from the shock manager were converted to a '\*.txt' file. Next, having determined an appropriate measuring time, the '\*.txt' file was converted to a '\*.csv' file. Finally, the '\*.csv' file was imported into MapleSim using the 'Time lookup table' model component (Figure 1-29).

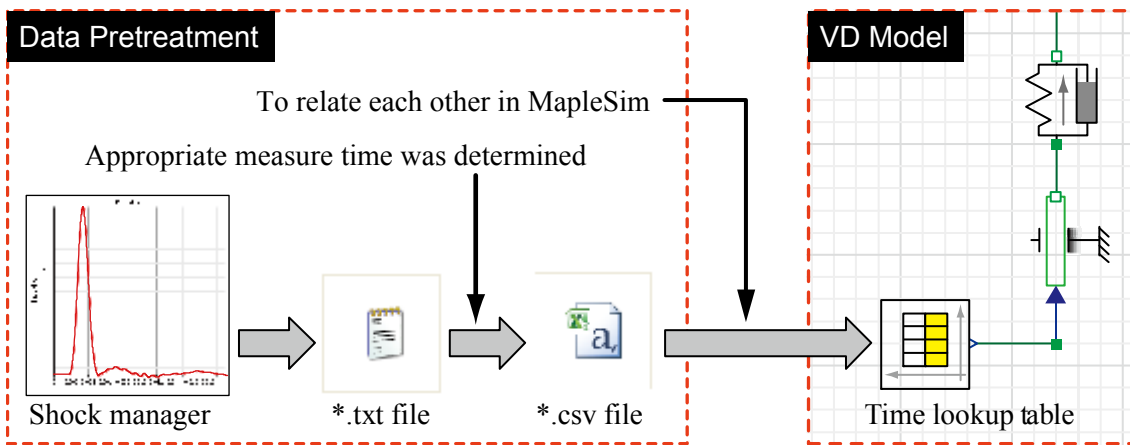


Figure 1-29 Flowchart for Importing Actual Waveform into MapleSim.

For the controlled shock test,  $f_n$ ,  $\xi$  and  $m$  had been experimentally determined, while  $k$  and  $c$  were calculated by Eqs. (1.16) and (1.17), respectively.

$$k = m \cdot \omega_n^2 = 4m\pi^2 f_n^2, \quad (1.16)$$

$$\xi = \frac{c}{c_c} = \frac{c}{2\sqrt{k \cdot m}} \Rightarrow c = 2\xi\sqrt{k \cdot m}. \quad (1.17)$$

The waveform data were supplied as the input acceleration, and the calculated values of  $m$ ,  $k$  and  $c$  were input to the model of Figure 1-28. Figure 1-30 compares the resulting SR curve of the VD model

with those of previous studies <sup>[21]</sup>. This figure reveals an exact match between the simulated and theoretical response curves. Therefore, it can be concluded that packaging engineers can construct mathematical models and verify them by running simulations in MapleSim, thereby saving considerable time, improving research efficiency and laying the foundation for further research.

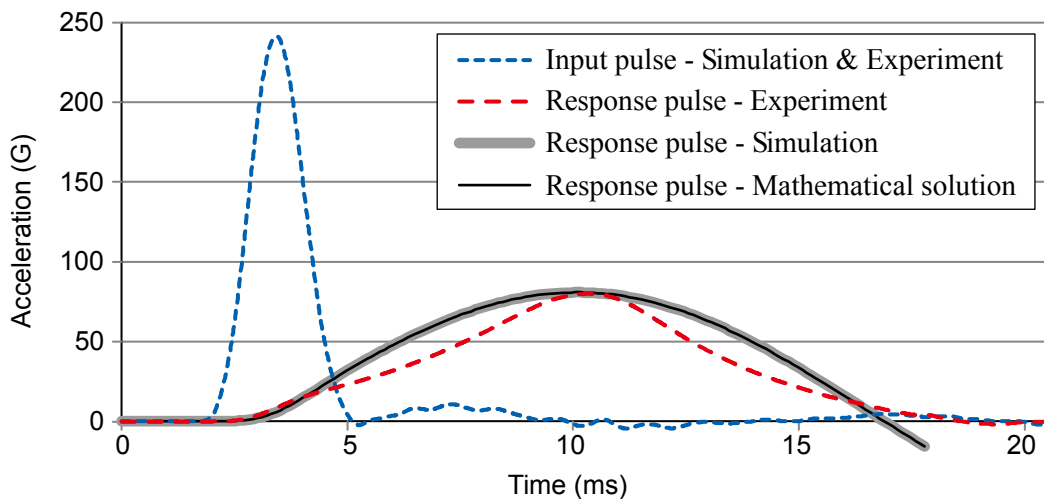


Figure 1-30 Comparison between Simulated and Experimental SR Results in the VD Model.

## 1.9 Research Purpose and Method

Aforementioned discussion leads us to the purpose of this study; to improve the efficiency and extend the applicability of traditional drop testing methods.

This study is based on the equivalent drop theory, which is an important extension of traditional drop testing. However, the equivalent drop theory in its current form has been shown to deviate from experimental findings. To correct this inconsistency, we first develop a novel equivalent drop theory based on a new physical model, from which we deduce the mathematical equations for the test at free fall and controlled shock test. From these two equations, we then deduce an appropriate correction condition. The applicability of the new theory to common package materials is assessed in a series of verification tests.

On the basis of the new equivalent drop theory, we propose a new drop testing method, designated as the hybrid drop test method. This section develops both the experimental and digital simulation methods. Similar to the verification of the equivalent drop theory, the feasibility of the hybrid drop test is demonstrated in verification tests.

If successful, this study will accomplish the following objectives.

- Improve accuracy of package testing.
- Establish a theoretical foundation for developing a more precise JIS standard.
- Improve the efficiency of verification testing.
- Reduce packaging cost.

## 1.10 Structure of Dissertation

This dissertation comprises six chapters and an appendix.

Chapter 1 presents the research background, methods and purposes, focusing on two traditional evaluation testing methods for cushioning material and packaged product. Traditional and damping equivalent drop theories and digital simulation methods are also described.

Chapter 2 discusses the need for a new equivalent drop theory and then introduces the theoretical foundations of the friction equivalent drop theory.

In Chapter 3, the feasibility of the friction equivalent drop theory is evaluated in preliminary and more extensive verification tests. The test materials are two compositionally different paper cushions. By considering cushioning materials and stress, we prove that the friction equivalent drop theory is applicable to SCM.

Chapter 4 introduces the hybrid drop test, a novel evaluation testing method based on the friction equivalent drop theory developed in Chapter 2. The chapter begins with a conceptual overview of the new testing method, followed by a flowchart. Finally, calculation of the parameters of the FVD model is explained in detail.

The hybrid drop testing method is verified in Chapter 5, similar to the friction equivalent drop theory in Chapter 3.

Chapter 6 presents a summary of this dissertation.

Symbols and acronyms used in this dissertation are provided in the Appendix.

### **The papers realized on the basis of this dissertation are listed below.**

1. Chen ZHONG and Katsuhiko SAITO. Equivalent Drop Test Modification for Determination of Cushioning Performance. *Journal of Packaging Science & Technology, Japan*. 2010; 19(2): 123–135.
2. Chen ZHONG and Katsuhiko SAITO. Modified Simulated Drop Test for Transmitted Shock Characteristics of Structural Corrugated Fiberboard. *Journal of Applied Packaging Research*. 2010; 4(4): 189–201.
3. Chen ZHONG, Katsuhiko SAITO and Kazuaki KAWAGUCHI. Shock Response of Frictional-viscous Damping Model for Cushioning Package. *Journal of Applied Packaging Research*. 2011; 5(4): 197–214.
4. Chen ZHONG and Katsuhiko SAITO. Modified Equivalent Drop Test for Structural Corrugated Fiberboard Cushioning. *Journal of Packaging Science & Technology, Japan*. 2012; 21(4): 281–293.
5. Chen ZHONG and Katsuhiko SAITO. Equivalent Drop Test for Structural Pulp Mould Cushion. *Journal of Applied Packaging Research*. 2012; 6(3): 185–201.
6. Chen ZHONG, Katsuhiko SAITO and Kazuaki KAWAGUCHI. Improvement of Equivalent Drop Theory for Transport Packaging. *International Journal of Packaging Technology and Science*. 2013; 26(2): 67–81.
7. Chen ZHONG, Katsuhiko SAITO, Kazuaki KAWAGUCHI and Hiroshi SETOUE. The Hybrid Drop Test. *International Journal of Packaging Technology and Science*. (Under review)

### **International conferences**

1. Katsuhiko SAITO and Chen ZHONG. Modified Simulated Drop Test for Transmitted Shock Characteristics of Structural Plastic Foam Cushioning Materials. *17th IAPRI World Conference on Packaging*. Tianjin, China, Oct. 12–15, 2010.
2. Chen ZHONG, Katsuhiko SAITO and Kazuaki KAWAGUCHI. Improvement of Equivalent Drop

Theory for Transport Packaging. *18th IAPRI World Conference on Packaging*. California Polytechnic State University, San Luis Obispo, California, USA, June 17–21, 2012.

3. Chen ZHONG and Katsuhiko SAITO. Equivalent Drop Test for Structural Corrugated Fiberboard and Pulp Mould Cushions. *26th IAPRI Symposium on Packaging 2013*. VTT Technical Research Centre of Finland, Espoo, Finland, June 10–13, 2013.

## 1.11 References

- [1] Jahre, M. and Hatteland, C-J. Packages and Physical Distribution—Implications for Integration and Standardization. *International Journal of Physical Distribution and Logistics Management*. 2004; 34(2): 123–139.
- [2] Katsuhiko SAITO. *The Basic Technology of Transport Packaging*, 2001.
- [3] McKinlay, A. H. Pinpointing Loss and Damage. *Distribution Worldwide*, 1972.
- [4] Zabaniotou and A. Kassidi. Life Cycle Assessment Applied to Egg Packaging Made from Polystyrene and Recycled Paper. *Journal of Cleaner Production*. 2003; 11 (5): 549–559.
- [5] Lijiang HUO, Katsukiko SAITO and Yukiomi NAKAGAWA. Establishment of Sustainability Indicator for Cushioning Packaging. *Journal of Packaging Science & Technology, Japan*. 2009; 18(4): 259–269.
- [6] Lijiang HUO and Katsukiko SAITO. Sustainability Assessment for Optimizing Logistics-oriented Protective Packaging Design. *Journal of Packaging Science & Technology, Japan*. 2010; 19(3): 203–213.
- [7] Kiyohide Hasegawa. Recent Trend of Transport Packaging Test. *JPI Journal*. 2010; 42(9): 716–722.
- [8] Soroka W, CPP. *Fundamentals of Packaging Technology*. DEStech Publications, Inc.: Lancaster, 2009.
- [9] Vanee Chonhenchob, Sher Paul Singh, Jay Jagjit Singh, Sukasem Sittipod, Dathpan Swasdee and Supoj Pratheepthinthong. Measurement and Analysis of Truck and Rail Vibration Levels in Thailand. *International Journal of Packaging Technology and Science*. 2010; 23: 91–100.
- [10] Daisuke Nei, Nobutaka Nakamura, Poritosh Roy, Takahiro Orikasa, Yutaka Ishikawa, Hiroaki Kitazawa and Takeo Shiina. Wavelet Analysis of Shock and Vibration on the Truck Bed. *International Journal of Packaging Technology and Science*. 2008; 21(8): 491–499.
- [11] Fei Lu, Yutaka Ishikawa, Hiroaki Kitazawa and Takaaki Satake. Effect of Vehicle Speed on Shock and Vibration Levels in Truck Transport. *International Journal of Packaging Technology and Science*. 2008; 23(2): 101–109.
- [12] Fei Lu, Yutaka Ishikawa, Takeo Shiina and Takaaki Satake. Analysis of Shock and Vibration in Truck Transport in Japan. *International Journal of Packaging Technology and Science*. 2008; 21(8): 479–489.
- [13] Wang Z-W. On Evaluation of Product Dropping Damage. *International Journal of Packaging Technology and Science*. 2002; 15(3): 115–120.
- [14] Wang Z-W. Dropping Damage Boundary Curves for Cubic and Tangent Package Cushioning Systems. *International Journal of Packaging Technology and Science*. 2002; 15(5): 263–266.
- [15] Wang Z-W, Jiang J-H. Evaluation of Product Dropping Damage Based on Key Component. *International Journal of Packaging Technology and Science*. 2010; 23(4): 227–238.
- [16] Gary J. Burgess. Product Fragility and Damage Boundary Theory. *International Journal of Packaging Technology and Science*. 1988; 1(1): 5–10.

- [17] Changfeng Ge. Model of Accelerated Vibration Test. *International Journal of Packaging Technology and Science*. 2000; 13(1): 7–11.
- [18] Vincent Rouillard and Robert Richmond. A Novel Approach to Analysing and Simulating Railcar Shock and Vibrations. *International Journal of Packaging Technology and Science*. 2007; 20(1): 17–26.
- [19] Bresk, F. C. Application of Product Fragility Information in Package Design, *Packaging Technology*. 1986;16(5): 10–20.
- [20] Yam KL. Encyclopedia of Packaging Technology. John Wiley & Sons, Inc.: New York, 2009.
- [21] Chen ZHONG and Katsuhiko SAITO. Equivalent Drop Test Modification for Determination of Cushioning Performance. *Journal of Packaging Science & Technology, Japan*. 2010; 19(3): 123–136.
- [22] Saito K, Hasegawa K. Foundation and Applications of Transport Package (in Japanese). Saiwaishobo Inc., Tokyo, 11–24. 2008.
- [23] Gary Burgess. Consolidation of Cushion Curves. *International Journal of Packaging Technology and Science*. 1990; 3(4): 189–194.
- [24] Patricia Navarro-Javierre, Manuel-Alfredo Garcia-Romeu-Martinez, Vicente-Agustin Cloquell-Ballester and Enrique de-la-Cruz-Navarro. Evaluation of Two Simplified Methods for Determining Cushion Curves of Closed Cell Foams. *International Journal of Packaging Technology and Science*. 2012; 25(4): 217–231.
- [25] Sek M, Kirkpatrick J. Characteristics of Corrugated Fibreboard as a Cushioning Material in Protective Packaging. *10th IAPRI World Conference on Packaging*, Melbourne, 257–266, 1997.
- [26] Sek M, Bruscella B, Rouillard V. Limitations of Standard Procedures for Performance Testing of Protective Packaging for Transportation. *10th IAPRI World Conference on Packaging*, Melbourne, 567–574, 1997.
- [27] Sek MA, Rouillard V and Parker A. Characterisation of Nonlinear Behaviour of Expanded Polystyrene Cushions. *Journal of Applied Mechanics and Materials*. 2007; 7(8): 283–288.
- [28] Hiroshi Setoue. Transport Package Design (3)—Cushioning Package Method (in Japanese). *Journal of Packaging Science & Technology, Japan*. 2011; 20(3): 209–219.
- [29] Kazuki TSUDA and Takamasa NAKAJIMA. Numerical Investigation on Vibration of Package with Gap (in Japanese). *Journal of Packaging Science & Technology, Japan*. 2005; 14(1): 35–47.
- [30] Kazuki TSUDA and Takamasa NAKAJIMA. Theoretical Investigation on Vibration of Package with Gap (in Japanese). *Journal of Packaging Science & Technology, Japan*. 2005; 14(3): 181–190.
- [31] Kazuki TSUDA, Takamasa NAKAJIMA and Katsuhiko SAITO. Experimental Investigation on Vibration of Package with Gap (in Japanese). *Japan Institute of Navigation*. 2006; 114: 201–207.
- [32] Kazuki TSUDA, Takamasa NAKAJIMA and Katsuhiko SAITO. Experimental Verification on Non-linear Gap Vibration of Packaged Product (in Japanese). *Journal of Packaging Science & Technology, Japan*. 2007; 16(1): 53–61.
- [33] Kazuki TSUDA, Takamasa NAKAJIMA and Katsuhiko SAITO. Investigation on Vibration Durability of Package with Gap (in Japanese). *Japan Institute of Navigation*. 2007; 117: 111–117.
- [34] Akira HOSOYAMA, Katsuhiko SAITO and Takamasa NAKAJIMA. Experimental Verification on the Effectiveness of Non-Gaussian Vibration Test. *Journal of Packaging Science & Technology, Japan*. 2012; 21(2): 107–114.
- [35] Akira HOSOYAMA and Takamasa NAKAJIMA. The Method of Generating Non-Gaussian Random Vibration Using Kurtosis. *Journal of Packaging Science & Technology, Japan*. 2011; 20(1): 27–34.



- [36] Akira HOSOYAMA and Takamasa NAKAJIMA. Comparative Study of Accumulated Fatigues Caused by Vibrations of a Cart and a Testing Machine. *Journal of Packaging Science & Technology, Japan*. 2010; 19(2): 113–121.
- [37] Akira HOSOYAMA, Katsuhiko SAITO and Takamasa NAKAJIMA. Effect of Non-Gaussian Random Vibration on Packaging Response Using Numerical Simulation. *Journal of Packaging Science & Technology, Japan*. 2012; 21(6): 471–478.
- [38] Daniel Goodwin and Dennis Young. Protective Packaging for Distribution. DEStech Publications Inc., 2011.
- [39] Andreas Menrad, Thomas Goedecke, Klaus-Peter Gruender and Manfred H. Wagner. Method for Deriving the Correlation between Free Fall and Shock Machine Drop Height. *International Journal of Packaging Technology and Science*. (paper presented at IAPRI world conference 2012).
- [40] Abdelmajid Lajmi, Henri Champlaud and Van Ngan Lê. Computation of the Maximum Torque of a Cap Liner Using a Power-Law Friction and Finite Element Analysis. *International Journal of Packaging Technology and Science*. 2011; 24: 103–121.
- [41] N. J. Mills and Y. Masso-Moreu. Finite Element Analysis (FEA) Applied to Polyethylene Foam Cushions in Package Drop Tests. *International Journal of Packaging Technology and Science*. 2005; 18: 29–38.
- [42] A. Yoxall, J. Luxmoore, J. Rowson, J. Langley and R. Janson. Size Does Matter: Further Studies in Hand—Pack Interaction Using Computer Simulation. *International Journal of Packaging Technology and Science*. 2008; 21: 61–72.
- [43] M. E. Biancolini and C. Brutti. Numerical and Experimental Investigation of the Strength of Corrugated Board Packages. *International Journal of Packaging Technology and Science*. 2003; 16: 47–60.
- [44] Benedettini, O. and Tjahjono, B.. Towards an Improved Tool to Facilitate Simulation Modeling of Complex Manufacturing Systems. *International Journal of Advanced Manufacturing Technology*. 2008; 43 (1–2): 191–199.
- [45] Goff JW, Chateman R. The Correlation of Shock with Free-fall Drop Height. Technical Report N. 24. Multi-Sponsor Research Program, School of Packaging, Michigan State University /East Lansing, MI, 1976.
- [46] Goff JW, Chateman R, Iwahimizu H and Collins K. Shock Machine and Free-fall Drop Correlation, Unpublished data. School of Packaging, Michigan State University/East Lansing, MI, 1976.
- [47] Brandenburg RK, Lee JJ-L. Fundamentals of Packaging Dynamics. L.A.B. Equipment, Inc.: Itasca. 1993; 50–73.
- [48] Zhong C, Saito K. Equivalent Drop Test Modification for Determination of Cushioning Performance. *Journal of Packaging Science & Technology, Japan*. 2010; 19(2): 123–135.
- [49] Saito K, Kawaguchi K. Equivalent Drop Theory with Damping. *23rd International Association of Packaging Research Institutes Symposium*, 2007.
- [50] Kawaguchi K, Saito K. Experimental Verification of Equivalent Drop Testing with Damping for Packaged Freight. *Journal of Packaging Science & Technology, Japan*. 2008; 17(1): 39–45.
- [51] Saito K, Zhong C. Modified Simulated Drop Test for Transmitted Shock Characteristics of Structural Plastic Foam Cushioning Materials. *17th IAPRI World Conference on Packaging*. 2009; 491–495.
- [52] Benjamin Crowell. Newtonia Physics. Fullerton, Colifornia, USA, 2006.
- [53] Li F, Twede D, Goff JW. Method for Deriving the Correlation between Free Fall and Shock Machine Drop Height. *International Journal of Packaging Technology and Science*. 1993; 6(4): 139–146.

- [54] Newton RE. Fragility Assessment Theory and Test Procedure. Monterey Research Laboratory, Monterey, CA, 1968.
- [55] Yoshida Seiki Co., Ltd. Specification of Shock Manager (in Japanese). SM-500 serial.
- [56] Yoshida Seiki Co., Ltd. Dynamic Compression Tester User's Guide (in Japanese). ACST-200 serial.
- [57] Yoshida Seiki Co., Ltd. Shock Machine User's Guide (in Japanese). ASQ-700 serial.
- [58] Yoshida Seiki Co., Ltd. Free Fall Tester User's Guide (in Japanese). DT-100B serial.
- [59] ISO 2248. Packaging—Complete, Filled Transport Packages—Vertical Impact Test by Dropping.
- [60] <http://www.iso.org/iso/home.html> (accessed in May 2013)
- [61] <http://www.astm.org/Standard/index.shtml> (accessed in May 2013)
- [62] <http://www.cen.eu/cen/pages/default.aspx> (accessed in May 2013)
- [63] <http://www.tappi.org/Bookstore/Standards--TIPs/Standards.aspx> (accessed in May 2013)
- [64] <http://www.ista.org/> (accessed in May 2013)
- [65] JIS Z 0235, “Cushioning Materials for Packaging—Determination of Cushioning Performance”, Japanese Industrial Standard, 2002.
- [66] JIS Z 0240, Structural Cushioning Materials for Packaging—Determination of Cushioning Performance, Japanese Industrial Standard, 2002.
- [67] JIS Z 0119, Mechanical-shock Fragility Testing Methods for Packaging and Products Design, Japanese Industrial Standard, 2002.
- [68] JIS Z 0200, Packaged Freights—General Rules of Testing, Japanese Industrial Standard, 1999.
- [69] JIS Z 0202, Method of Drop Test for Packaged Freights, Japanese Industrial Standard, 1994.
- [70] JIS Z 0212, Packaged Freights and Containers—Method of Compression Test, Japanese Industrial Standard, 1998.
- [71] Katsuhiko SAITO and Kazuaki KAWAGUCHI. Equivalence of Drop Test for Packaging Freight, *23rd International Association of Packaging Research Institutes Symposium*. 2007; 3(5): 255–260.
- [72] ASTM D 4168. Standard Test Methods for Transmitted Shock Characteristics of Foam-in-Place Cushioning Materials, American Society of Testing Materials, 1995.
- [73] ISO 8568. Mechanical Shock—Testing Machines—Characteristics and Performance, International Organization for Standardization, 1989.
- [74] Katsuhiko SAITO and Kiyohide HASEGAWA. Foundation and Applications of Transport Package (in Japanese). Saiwaishobo, Inc., 2008.
- [75] Kazuaki KAWAGUCHI. Study on Equivalent Drop Test of Cushioning Packaging, *Master's Thesis*, Kobe University, 2005.
- [76] <http://www.maplesoft.com/> (accessed in May 2013)
- [77] Maplesoft Co. Ltd. *MapleSim User's Guide*, MapleSim Ver. 4.5.
- [78] Maplesoft Co. Ltd. *MapleSim help*, MapleSim Ver. 4.5.
- [79] <http://www.maplesoft.com/products/maplesim/>

This page is intentionally left blank

# CHAPTER 2. FRICTION EQUIVALENT DROP THEORY

## 2.1 Rational for Developing Friction Equivalent Drop Theory

The equivalent drop theory is an important concept in packaging engineering. Goff *et al.* <sup>[1],[2]</sup>, who pioneered the theory, demonstrated that shock is correlated with the free fall height. As mentioned in Section 1.7, the traditional theory predicts that the free fall and controlled shock tests yield identical test results at a specified drop height. Section 1.5 highlights the importance of controlled shock testing of the packaged products. Nevertheless, in some instances, the controlled shock tests are precluded by high price of the machine required to conduct such tests. On the other hand, by adopting the equivalent drop theory, researchers can substitute the expensive shock machine with much cheaper free fall or compression testers.

As mentioned earlier, the traditional theory is strictly applicable only to products that follow the Linear model (see Figure 1-18), which excludes all real-time cushioning materials. In this case, the equivalence of the free fall height is questionable. Saito *et al.* <sup>[3],[4]</sup>, demonstrated the limits of the Linear model and errors inherent in the traditional theory. From these insights, they developed the damping theory, as discussed in Section 1.7.4.

Zhong *et al.* <sup>[5],[6]</sup> showed that the damping theory can improve the precision of equivalent tests that use a quasi-linear cushion; i.e. equivalence of free fall height in quasi-linear packaging cushioning systems is achieved if the system is damped. Wang *et al.* <sup>[7]-[9]</sup> researched the effect of shock hazard on linear and nonlinear packaging cushioning systems, but their analysis was limited to the damage boundary curve. Whether equivalent free-fall height is equivalent in nonlinear packaging cushioning systems such as SCM remains unexplored.

To solve this contention, a new equivalent drop theory is required. In this chapter, we first propose a new physical model that considers friction and viscous damping. Next, mathematical equations describing the free fall and shock responses of the new model are deduced from simulation codes written in Maple and MapleSim. Finally, we propose a friction equivalent drop theory.

## 2.2 Preliminary Test

### 2.2.1 Test equipment and materials

#### A) Test equipment

The controlled shock and dynamic compression tests were conducted using a shock machine and dynamic compression tester, respectively (see Section 1.4).

#### B) Test materials

New cushioning materials are being continuously discovered and applied in packaging engineering. Nevertheless, paper cushions (such as corrugated boxes) and expanded polyethylene (EPE) remain popular cushioning materials because they are low cost, exhibit strong cushioning properties and environmentally friendly. A glance at Table 2-1 will justify this sentiment. This table shows the

proportion of different materials used in packaging and containers in Japan (2011)<sup>[10]</sup>. Paper and corrugated fiberboard cushions are by far the most widely used packaging materials, comparing 2/3 of all manufactured packaging materials. Therefore, testing the cushioning characteristics of paper cushions is a priority.

Table 2-1 Proportion of Materials Manufactured for Packaging and Containers in Japan (2011).

Package Materials	Outgoing Freight Amount	
	Weight ( $\times 10^3$ Ton)	Proportion
Paper · Corrugated board	11,743	62.4 %
Plastic material	3,531	18.7 %
Metal material	1,627	8.6 %
Glass material	1,335	7.1 %
Wood material	597	3.2 %
Other	-	-
Total	18,833	100 %

Figure 2-1 shows a corrugated box commonly used as a cushioning package. In this example, a corrugated fiberboard is folded into concave and convex shapes that buffer the product from transport-associated hazards. The compressive strength of the corrugated fiberboard is maximized when the applied force is parallel to the direction of the flute. We reproduced these cushioning characteristics by creating a corrugated fiberboard (A-flute with dimension  $110 \times 110 \times 50$  (mm)) as the test material after being folded to form a sleeve cushion, as shown in Figure 2-2.



Figure 2-1 Example of a Common Cushioning Package.

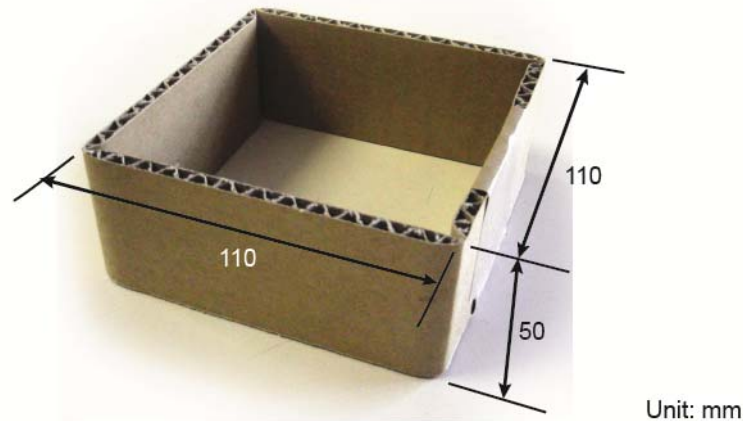


Figure 2-2 Structural Corrugated Sleeve in Preliminary Test.

### 2.2.2 Test conditions

The test at free fall and controlled shock test were performed under the following conditions.

1. As recommended in JIS Z 0240, 300 Hz low-pass filtering was applied.
2. Test materials were placed in a controlled atmospheric environment at 23°C and a relative humidity of 50 % for 24 hours.
3. In both tests, a 4 kg weight dummy was used, and the accelerometer used for measuring the PRA was fixed in the centre above the weight dummy.
4. A new sleeve was used for each test.
5. The equivalent free-fall height  $h$  was set at 0.6 m, as recommended in JIS Z 0240.
6. Data collection: When  $h = 0.6$  m, the impact velocity  $V$  was 3.43 m/s using  $V = \sqrt{2gh}$ . In the test at free fall, the drop height was adjusted to ensure that impact velocity  $V$  of the weight dummy was 3.43 m/s. In the controlled shock test, an adjusting function in the controlling software<sup>[11]</sup> was iterated until  $V_c$  on the shock table was 3.43 m/s. For both tests, the data were considered to be effective only when  $V = 3.43$  m/s or  $V_c = 3.43$  m/s; 10 data sets were collected for each test.

### 2.2.3 Test results

The preliminary experimental results are shown in Figure 2-3. The central regions of the shock response curves output by both tests are trapezoidal rather than parabolic. However, the traditional theory predicts an output response similar to a half-sine pulse (dashed-dotted line in Figure 2-3) that peaks nearly half way through the recording. Furthermore, PRA does not match the response curves of either the Linear or VD model. Therefore, we infer that the current theories are imperfect for measuring the cushioning performance of SCM, possibly because the physical models themselves are imperfect, leading to offset of the equivalent free-fall height. A potential defect in the VD model is that viscous damping and linear spring factors alone are considered. Therefore, developing a new model to explain this newly observed phenomenon is necessary.

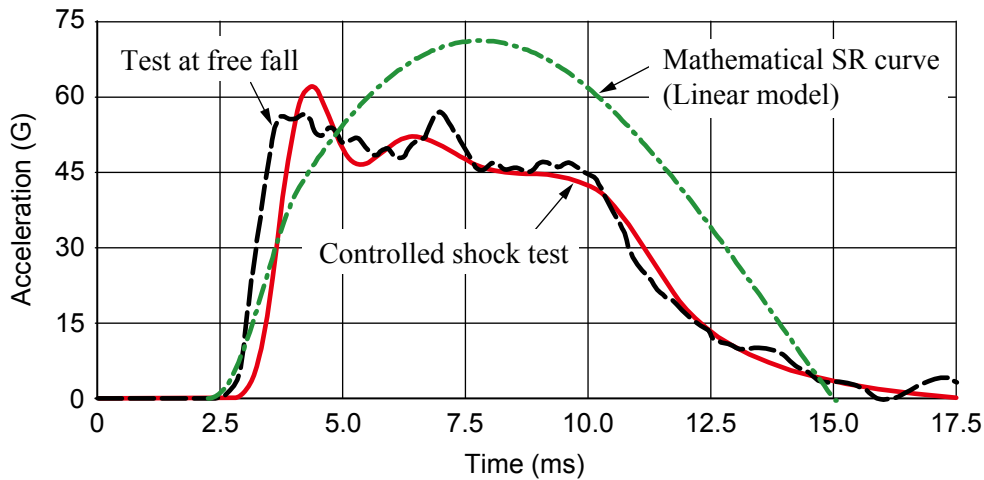


Figure 2-3 Results of Preliminary Experiments.

## 2.3 New Physical Model—FVD Model

### 2.3.1 Foundations of the FVD model

This chapter proposes a new mathematical damping model that incorporates friction and viscous damping. Figure 2-3 indicates the following:

1. No real cushioning materials behaves perfectly elastically; therefore, an attenuation factor is required.
2. The results of a previous study<sup>[5],[6]</sup> indicated that softer springs should be used in the new model.
3. The central region of the SCM waveform presents as a jagged curve with no obvious peak; this result can arise from friction.

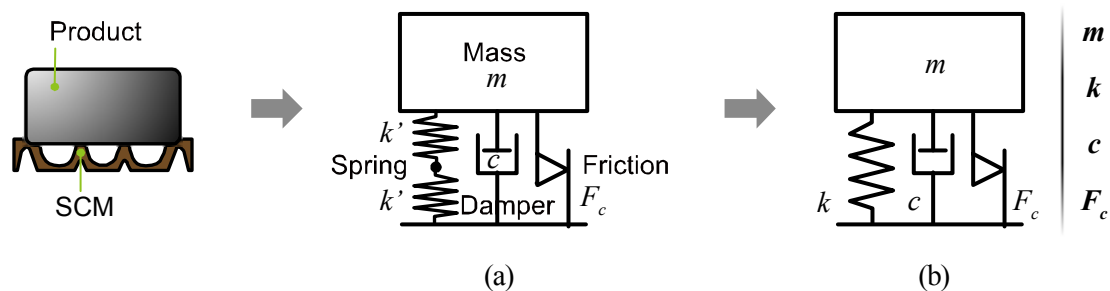


Figure 2-4 Frictional-viscous Damping (FVD) Models.  
(a) Original model, (b) Simplified model.

The new model built from the aforementioned analysis is shown as a schematic in Figure 2-4(a). The system comprises a mass and two linear springs subject to damping and friction. According to the laws of mechanics<sup>[12]</sup>, two springs in series behave as a single spring; therefore, the new model can be simplified to that shown in Figure 2-4(b). This model is called a frictional-viscous damping (FVD) model.

Note that the spring constant in the simplified model is  $k = k' / 2$ .

### 2.3.2 Rational for two springs

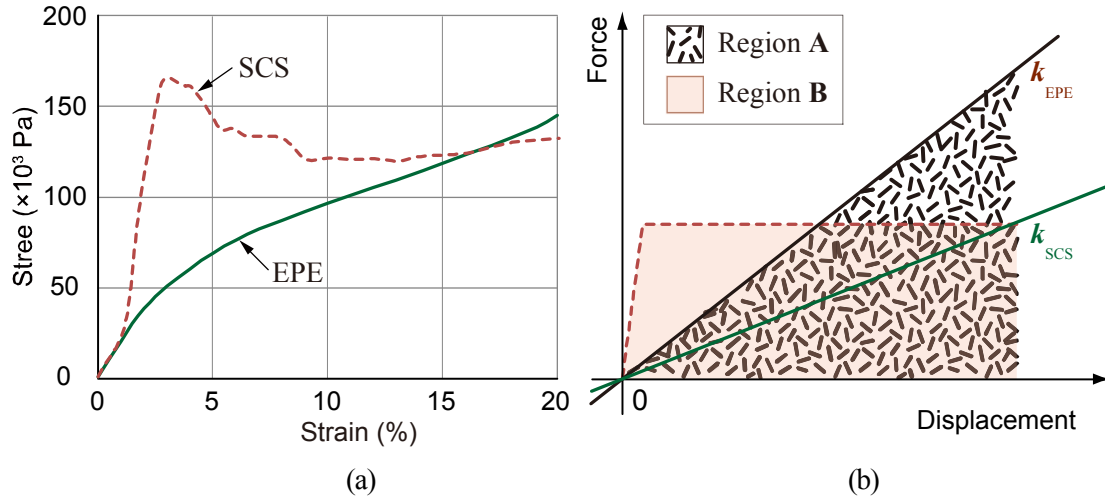






Figure 2-5 Interpretation of  $k/2$ .

(a) Stress–strain curve, (b) Schematic of displacement–force curve

The reason for applying two series-connected springs in the new model is described below. Figure 2-5(a) shows the stress–strain curves of structural corrugated sleeve (SCS) and EPE obtained from the static compression test. The curve for EPE is smooth and passes through the origin, while that of the structural corrugated sleeve increases sharply at 3% strain, then declines slowly and remains approximately constant. Figure 2-5(a) can be generalized to Figure 2-5(b), where the horizontal and vertical axes represent displacement and force, respectively, and  $k$  is the slope of the line. The shock energies that can be absorbed by EPE and SCS are delineated by regions  and , respectively. To determine  $k$  for SCS that yields the same  $k_{EPE}$ , the area of regions  and  should be equal. Therefore,  $k_{SCS} = k_{EPE}/2 \rightarrow k_e = k_{(calculated)}/2$ .

### 2.3.3 Types of friction

Friction is the force that resists the relative motion of solid surfaces, fluid layers and material elements sliding against each other. Friction can be classified as follows<sup>[13]</sup>:

$$\text{Friction} \begin{cases} \text{Rotational Friction} \\ \text{Sliding Friction} \begin{cases} \text{Coulomb Friction} \\ \text{Viscous Friction} \\ \text{Stribeck Friction} \end{cases} \end{cases}$$

This study considers only Coulomb friction, defined by

$$F_c = \begin{cases} \mu N \cdot \text{sign}(\dot{x}) & \dot{x} > 0 \\ F_a & \dot{x} = 0 \ \& \ F_a < \mu N \end{cases}, \quad (2.1)$$

where  $F_c$  is the Coulomb friction,  $\mu$  is the coefficient of friction,  $N$  is the normal force exerted between surfaces,  $F_a$  is the force exerted by friction (in the case of equality, the maximum possible magnitude of this force) and  $\dot{x}$  is the velocity.



### 2.3.4 Building of friction component

The friction component is defined in MapleSim on the basis of Eq. (2.1). Here  $srel(t)$  and  $vrel(t)$  denote the relative displacement and velocity, respectively.  $f(t)$ ,  $f(a)$  and  $f(b)$  are the forces of the flanges,  $vth$  is the linear-region velocity threshold and  $sa(t)$  and  $sb(t)$  are the absolute positions of the flanges.  $fa(t)$ ,  $fb(t)$  are defined as the input variables and  $sa(t)$ ,  $sb(t)$  are defined as the output variables (Figure 2-6)<sup>[13]</sup>.

```

eq := [ f(t) = [ Fc * [ 1 vrel(t) > 0 |vrel(t)| > vth, srel(t) = sb(t) - sa(t), vrel(t) = d/dt srel(t), f(t) = fb(t), fa(t) + fb(t) = 0
                -1 vrel(t) <= 0 |vrel(t)| > vth
                0 |vrel(t)| <= vth ] ]
      [ f(t) = [ Fc * [ 1 0 < vrel(t) |vth < |vrel(t)|, srel(t) = sb(t) - sa(t), vrel(t) = d/dt srel(t), f(t) = fb(t), fa(t) + fb(t) = 0
                -1 vrel(t) <= 0 |vrel(t)| > vth
                0 |vrel(t)| <= vth ] ] ]
params := [Fc = 100, vth = 0.0001]
[Fc = 100, vth = 0.0001]
sys := DynamicSystems[DiffEquation](eq, inputvariable = [fa(t), fb(t)], outputvariable = [sa(t), sb(t)]);
Warning, diff-eg is not a polynomial

```

**Diff. Equation**  
 continuous  
 2 output(s); 2 input(s)  
 inputvariable = [fa(t), fb(t)]  
 outputvariable = [sa(t), sb(t)]

Figure 2-6 Definition of Friction Component in Maple.

## 2.4 Deduction of SR Equation of Test at Free Fall Using FVD Model

As a first step in developing a new equivalent drop theory, we establish the mathematical SR equations of the free fall and controlled shock tests. On the basis of the FVD model, this section deduces the mathematical SR equation of the free fall test. The input acceleration pulse is a half-sine wave.

### 2.4.1 Calculating period of FVD model

The equation of motion in the FVD model is

$$m\ddot{x} + c\dot{x} + kx + F_c \text{sign}(\dot{x}) = 0. \quad (2.2)$$

Defining

$$\frac{c}{m} = 2\epsilon, \quad \frac{k}{m} = \omega_n^2, \quad b = \frac{F_c}{k},$$

Eq. (2.2) is rewritten as

$$\ddot{x} + 2\epsilon\dot{x} + \omega_n(x + b \text{sign}(\dot{x})) = 0. \quad (2.3)$$

Letting  $y = x + b \text{sign}(\dot{x})$ , Eq. (2.3) becomes

$$\ddot{x} + 2\epsilon\dot{x} + \omega_n y = 0. \quad (2.4)$$

For  $y = x + b \text{sign}(\dot{x})$ , we obtain

$$\dot{y} = \dot{x}, \quad \ddot{y} = \ddot{x}.$$

Replacing  $\ddot{x}$  with  $\ddot{y}$  and  $\dot{x}$  with  $\dot{y}$ , Eq. (2.4) becomes

$$\ddot{y} + 2\epsilon\dot{y} + \omega_n^2 y = 0. \quad (2.5)$$

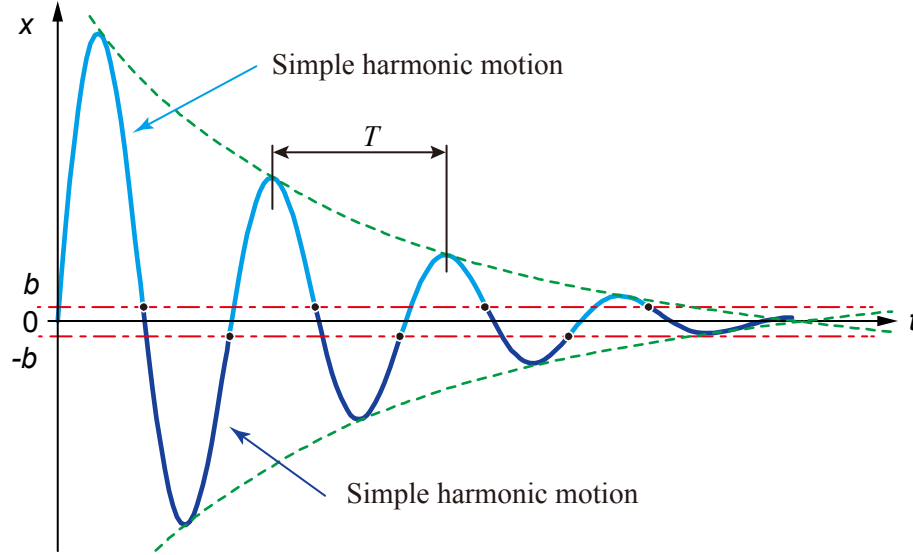


Figure 2-7 Period of FVD Model.

Eq. (2.5) reduces to the VD model when  $\xi < 1$  (i.e.  $\epsilon < \omega_n$ ; see Figure 2-7). In this case, the solution to Eq. (2.5) is

$$y = e^{-\epsilon t} (A \cos(\omega_d t) + B \sin(\omega_d t)), \quad (2.6)$$

where  $\omega_d = \omega_n \sqrt{1 - \xi^2}$ .

In terms of the given conditions  $t = 0, x = 0$  and  $\dot{x} = v_0$ ,  $y$  is expressed as follows:

$$y = x - b = \frac{v_0}{\omega_d} \cdot e^{-\epsilon t} \sin(\omega_d t). \quad (2.7)$$

From which  $x$  is obtained as follows:

$$x = \frac{v_0}{\omega_d} \cdot e^{-\epsilon t} \sin(\omega_d t) + b. \quad (2.8)$$

Therefore, the period of the FVD model is expressed as

$$T = \frac{2\pi}{\omega_d} = \frac{2\pi}{\omega_n \sqrt{1 - \xi^2}}. \quad (2.9)$$

## 2.4.2 Average method

The FVD model is nonlinear because of the Coulomb friction term, and nonlinear systems are extremely difficult to solve precisely. However, approximate solutions can be obtained in the following ways<sup>[13],[15]</sup>:

- ◆ Series expanding method,
- ◆ Lindstedt–Poincaré method,
- ◆ Average method,
- ◆ Multidimensional scaling method, and
- ◆ Harmonic balance method.

Here we adopt the average method because the other four methods are not applicable to this study. For example, the harmonic balance is a method used to calculate the steady-state response of nonlinear differential equations, and is mostly applied to electrical circuits<sup>[16],[17]</sup>; the Lindstedt–Poincaré method is often used to weakly nonlinear problems with finite oscillatory solutions<sup>[18]</sup>.

The general form of nonlinear vibration is

$$\ddot{x} + \omega_n^2 x = \epsilon f(x, \dot{x}).$$

When  $\epsilon = 0$ , this equation reduces to linear vibration,

$$\ddot{x} + \omega_n^2 x = 0.$$

Solving this equation yields Eq. (2.10).

$$x = a \sin(\omega_n t + \phi), \tag{2.10}$$

where  $a$  and  $\phi$  are constants.

If  $\epsilon \neq 0$ , the solution of nonlinear vibration is

$$x(t) = a(t) \sin(\omega_n t + \phi(t)), \tag{2.11}$$

where  $a$  and  $\phi$  are functions of time  $t$ .

Solving Eq. (2.11), we obtain

$$\dot{a}(t) = -\frac{1}{2\pi\omega_n m} \int_0^{2\pi} f(a(t) \sin \phi, \omega_n a(t) \cos \phi) \cos \phi \, d\phi, \tag{2.12}$$

$$\dot{\phi}(t) = -\frac{1}{2\pi\omega_n m a(t)} \int_0^{2\pi} f(a(t) \sin \phi, \omega_n a(t) \cos \phi) \sin \phi \, d\phi. \tag{2.13}$$

In Eqs. (2.12) and (2.13), when the nonlinear term is related only to speed  $\dot{x}(t)$ , we have

$$\dot{\phi}(t) \equiv 0.$$

Thus,  $\phi(t) = \phi_0$ ,

and Eq. (2.11) can be rewritten as

$$x(t) = a(t) \sin(\omega_n t + \phi_0). \tag{2.14}$$

For convenience and without loss of generality, we assume that  $\phi_0 = 0$ , Eq. (2.14) then becomes

$$x(t) = a(t) \sin(\omega_n t),$$

and Eq. (2.13) can be rewritten as

$$\dot{a}(t) = -\frac{1}{2\pi\omega_n m} \int_0^{2\pi} f(\omega_n a(t) \cos \phi) \cos \phi \, d\phi. \quad (2.15)$$

### 2.4.3 Mathematical SR equation for test at free fall

#### A) Outline of deduction

Equation of motion:  $m\ddot{x} + c\dot{x} + kx + F_c \text{sign}(\dot{x}) = 0$



Equation of displacement:  $x = \delta_1(t)$



Equation of velocity:  $\dot{x} = \delta_2(t)$



Equation of acceleration:  $\ddot{x} = \delta_3(t)$



Substitute the time when the peak acceleration is reached

Equation of PRA:  $\text{PRA}_{ff} = \ddot{x} = \delta_3(t) \Big|_{t=\tau}$

#### B) Calculation process

The equation of motion of the dynamic compression test is given by

$$m\ddot{x} + kx + c\dot{x} + F_c \text{sign}(\dot{x}) = 0. \quad (2.16)$$

By the average method, the equation of motion of the test at free fall is

$$m\ddot{x} + kx + f(x, \dot{x}) = 0. \quad (2.17)$$

Therefore,

$$f(x, \dot{x}) = c\dot{x} + F_c \text{sign}(\dot{x}) = c\dot{x} + F_c \frac{\dot{x}}{|\dot{x}|}. \quad (2.18)$$

Let  $a(t)$  be the amplitude of the response, based on the average method. Then,

$$\dot{a}(t) = -\frac{1}{2\pi\omega_n m} \int_0^{2\pi} f(\omega_n a(t) \cos \phi) \cos \phi \, d\phi. \quad (2.19)$$

Substituting Eq. (2.18) into Eq. (2.19),

$$\begin{aligned} \dot{a}(t) &= -\frac{1}{2\pi\omega_n m} \left( \int_0^{2\pi} F_c \frac{\omega_n a(t) \cos \phi}{|\omega_n a(t) \cos \phi|} \cos \phi \, d\phi + \int_0^{2\pi} c \omega_n a(t) \cos \phi \cos \phi \, d\phi \right) \\ &= -\frac{1}{2\pi\omega_n m} \left( \int_0^{\frac{\pi}{2}} F_c \cos \phi \, d\phi - \int_{\frac{\pi}{2}}^{\frac{3\pi}{2}} F_c \cos \phi \, d\phi + \int_{\frac{3\pi}{2}}^{2\pi} F_c \cos \phi \, d\phi \right) \end{aligned} \quad (2.20)$$

$$\begin{aligned}
& + \int_0^{2\pi} c \omega_n a(t) \cos \phi \cos \phi \, d\phi \\
& = -\frac{c a(t)}{2m} - \frac{2F_c}{\pi \omega_n m}.
\end{aligned} \tag{2.21}$$

Eq. (2.21) has a global solution

$$a(t) = -\frac{4F_c}{c\pi\omega_n} + e^{-\frac{c}{2m}t} + C. \tag{2.22}$$

Substituting initial condition  $\dot{x} = V_0$  ( $V_0 = \sqrt{2gh}$ ) into Eq. (2.22), the exact solution is obtained as

$$a(t) = -\frac{2mV_0 \cdot \exp(-\frac{c}{2m}t)}{c} - \frac{4F_c}{c\pi\omega_n}. \tag{2.23}$$

Furthermore, the equation of displacement is given by

$$x = a(t) \sin(\omega_d t), \tag{2.24}$$

Substituting Eq. (2.23) into Eq. (2.24), we obtain

$$x(t) = -\left(\frac{2mV_0 \cdot \exp(-\frac{c}{2m}t)}{c} + \frac{4F_c}{c\pi\omega_n}\right) \sin(\omega_d t). \tag{2.25}$$

Let

$$\frac{c}{m} = 2\epsilon, \quad \frac{k}{m} = \omega_n^2, \quad b = \frac{F_c}{k},$$

Eq. (2.25) is rewritten as

$$x(t) = -\left(\frac{V_0}{\epsilon} e^{-\epsilon t} + \frac{2b\omega_n}{\pi\epsilon}\right) \sin(\omega_d t). \tag{2.26}$$

Differentiating Eq. (2.26), we get

$$\dot{x}(t) = V_0 e^{-\epsilon t} \sin(\omega_d t) - \left(\frac{V_0 e^{-\epsilon t}}{\epsilon} + \frac{2b\omega_n}{\pi\epsilon}\right) \omega_d \cos(\omega_d t), \tag{2.27}$$

and the second-order differential is

$$\ddot{x}(t) = \left[-V_0 \epsilon e^{-\epsilon t} + \left(\frac{V_0 e^{-\epsilon t}}{\epsilon} + \frac{2b\omega_n}{\pi\epsilon}\right) \omega_d^2\right] \sin(\omega_d t) + 2V_0 \omega_d e^{-\epsilon t} \cos(\omega_d t) \tag{2.28}$$

$$= \left[\frac{(\omega_d^2 - \epsilon^2)V_0 e^{-\epsilon t}}{\epsilon} + \frac{2b\omega_n \omega_d^2}{\pi\epsilon}\right] \sin(\omega_d t) + 2V_0 \omega_d e^{-\epsilon t} \cos(\omega_d t).$$

The period is defined as

$$T = \frac{2\pi}{\omega_d}. \tag{2.29}$$

Time  $t$  to reach the peak response is expressed as

$$t = \tau = \frac{T}{4} = \frac{\pi}{2\omega_d}, \quad (2.30)$$

Substituting Eq. (2.30) into Eq. (2.28), we get

$$\ddot{x}(t)_{\max} = \frac{(\omega_d^2 - \epsilon^2)V_0 \cdot \exp\left(\frac{-\pi\epsilon}{2\omega_d}\right)}{\epsilon} + \frac{2b\omega_n\omega_d^2}{\pi\epsilon}. \quad (2.31)$$

Letting  $\epsilon = \xi\omega_n$ ,  $\omega_d = \omega_n\sqrt{1 - \xi^2}$ , Eq. (2.31) becomes

$$\ddot{x}(t)_{\max} = \left| \frac{2\xi^2 - 1}{\xi} \right| \exp\left(-\frac{\pi\xi}{2\sqrt{1 - \xi^2}}\right) \cdot V_0 \cdot \omega_n + \frac{2(1 - \xi^2)}{\pi\xi} \cdot b \cdot \omega_n^2. \quad (2.32)$$

The spring constant (derived earlier) is given by  $k = k_0/2$ ; thus, we obtain

$$\omega_n = \frac{1}{\sqrt{2}}\omega_0, \quad \xi = \sqrt{2}\xi_0, \quad b = 2b_0. \quad (2.33)$$

Therefore, Eq. (2.32) is rewritten as

$$\ddot{x}(t)_{\max} = \left| \frac{4\xi^2 - 1}{2\xi} \right| \exp\left(-\frac{\pi\xi}{\sqrt{2 - 4\xi^2}}\right) \cdot V_0 \cdot \omega_n + \frac{\sqrt{2}(1 - 2\xi^2)}{\pi\xi} \cdot b \cdot \omega_n^2. \quad (2.34)$$

Defining

$$b \cdot \omega_n^2 = \frac{F_c}{m} = A_F, \quad (2.35)$$

We obtain the final mathematical equation for the test at free fall  $\text{PRA}_{ff}$  as

$$\begin{aligned} \text{PRA}_{ff} &= \ddot{x}(t)_{\max} = u_{ff} \cdot \omega_n \cdot V_0 + \mu_{ff} \cdot A_F \\ &= u_{ff} \cdot \omega_n \cdot V_0 + \mu_{ff} \cdot \omega_n \cdot V_F, \end{aligned} \quad (2.36)$$

where

$$u_{ff} = \left| \frac{4\xi^2 - 1}{2\xi} \right| \exp\left(-\frac{\pi\xi}{\sqrt{2 - 4\xi^2}}\right), \quad (2.37)$$

$$\mu_{ff} = \frac{\sqrt{2}(1 - 2\xi^2)}{\pi\xi}, \quad (2.38)$$

$$A_F = \frac{F_c}{m}, \quad (2.39)$$

$$V_F = \frac{A_F}{\omega_n} = \frac{F_c}{m\omega_n}. \quad (2.40)$$

## 2.4.4 Mathematical verification

Equation (2.36) can be verified on test data. If Eq. (2.36) is correct, then the calculated results should approximately match the experimental and simulated results. In this case, given test data  $\omega_n = 301$  Hz,  $\xi = 0.286$ ,  $F_c = 74$  N and  $m = 4$  kg, Eq. (2.36) yield a  $PRA_{ff}$  of 64.48 G, while the simulated and experimental results were 65.50 G and 62.40 G, respectively. Thus, Eq. (2.36) is applicable to the test at free fall.

## 2.5 Deduction of SR Equation of Controlled Shock Test Using FVD

### Model

As mentioned above, the FVD model is a nonlinear system and difficult to solve precisely<sup>[13]</sup>. Therefore, approximate solutions to the SR equation of the controlled shock test were obtained by the following approach. First, the equivalent spring constant  $k_e$  and equivalent damping coefficient  $c_e$  were calculated using the equivalent linearization method<sup>[15]</sup>. Second, on the basis of the equation of motion of the FVD model that is expressed by  $k_e$  and  $c_e$ , a mathematical solution to the FVD model was derived from the Laplace and the inverse Laplace transforms. The calculation procedure is shown as a flowchart in Figure 2-8.

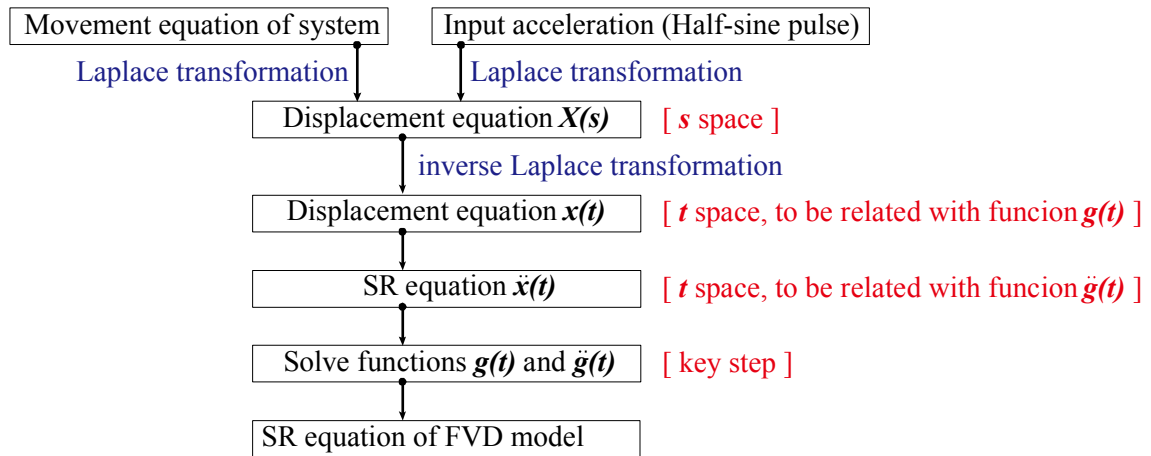


Figure 2-8 Deduction Flowchart for SR Equation of Controlled Shock Test.

### 2.5.1 Equivalent linearization method

To minimize the error in the square integral of the equivalent linearization method in each iteration, an evaluation function  $J$  is introduced, defined by

$$\begin{aligned}
 J &= \int_0^{2\pi} [f(x, \dot{x}) - (c_e \dot{x} + k_e x)]^2 d\theta \\
 &= \int_0^{2\pi} (f(x, \dot{x}))^2 d\theta - 2aAc_e \int_0^{2\pi} f(x, \dot{x}) \cos \theta d\theta
 \end{aligned}$$

$$-2Ak_e \int_0^{2\pi} f(x, \dot{x}) \sin \theta \, d\theta + \pi a^2 A^2 c_e^2 + \pi A^2 k_e^2. \quad (2.41)$$

Because  $J$  is the function that relates to  $k_e$  and  $c_e$ ,

$$\text{according to } \frac{\partial J}{\partial K_e} = 0, \quad K_e = \frac{1}{\pi A} \int_0^{2\pi} f(A \sin \theta, Aa \cos \theta) \sin \theta \, d\theta, \quad (2.42)$$

$$\text{according to } \frac{\partial J}{\partial C_e} = 0, \quad C_e = \frac{1}{\pi Aa} \int_0^{2\pi} f(A \sin \theta, Aa \cos \theta) \cos \theta \, d\theta. \quad (2.43)$$

The equation of motion of the FVD model is

$$m\ddot{x} + c\dot{x} + kx + F_c \text{sign}(\dot{x}) = A \sin at, \quad (2.44)$$

where  $x$  is the displacement,  $\dot{x}$  is the velocity and  $\ddot{x}$  is the acceleration.

Therefore,  $f(x, \dot{x})$  is expressed as

$$f(x, \dot{x}) = c\dot{x} + kx + F_c \text{sign}(\dot{x}) = c\dot{x} + kx + F_c \frac{\dot{x}}{|\dot{x}|}. \quad (2.45)$$

Substituting Eq. (2.45) into Eqs. (2.42) and (2.43), we obtain

$$k_e = k, \quad c_e = c + \frac{4F_c}{\pi Aa}, \quad (2.46)$$

where  $a = \pi/T_0$  ( $T_0$  is the initial impact duration).

## 2.5.2 Calculation process

The equivalent linearization method gives  $k_e$  and  $c_e$  as

$$k_e = k, \quad c_e = c + \frac{4F_c}{\pi Aa}, \quad (2.47)$$

and the equation of motion of the controlled shock test is expressed as

$$m\ddot{x} + c_e(\dot{x} - \dot{x}_0) + k_e(x - x_0) = 0. \quad (2.48)$$

Substituting Eq. (2.47) into Eq. (2.48), we get

$$m\ddot{x} + \left(c + \frac{4F_c}{\pi Aa}\right)(\dot{x} - \dot{x}_0) + k(x - x_0) = 0, \quad (2.49)$$

which is rewritten as

$$\ddot{x} + \left(\frac{c}{m} + \frac{4F_c}{\pi mAa}\right)(\dot{x} - \dot{x}_0) + \frac{k}{m}(x - x_0) = 0. \quad (2.50)$$

Defining

$$c = 2m\omega\xi, \quad \omega^2 = \frac{k}{m}, \quad B = \frac{4F_c}{\pi mAa},$$



Eq. (2.50) becomes

$$\ddot{x} + (2\omega\xi + B)(\dot{x} + \dot{x}_0) + \omega^2(x - x_0) = 0. \quad (2.51)$$

We now apply the following Laplace transformations:

$$L[x] = X(s),$$

$$L[x_0] = X_0(s),$$

$$L[\dot{x}] = sX(s) - x(0),$$

$$L[\ddot{x}] = s^2X(s) - sx(0) - \dot{x}(0).$$

After Laplace transformation, Eq. (2.51) becomes

$$s^2X(s) + 2\omega\xi sX(s) - 2\omega\xi sX_0(s) + BsX(s) - BsX_0(s) + \omega^2X(s) - \omega^2X_0(s) = 0, \quad (2.52)$$

with solutions

$$X(s) = \frac{(2\omega\xi + B)s + \omega^2}{s^2 + (2\omega\xi + B)s + \omega^2} \cdot X_0(s). \quad (2.53)$$

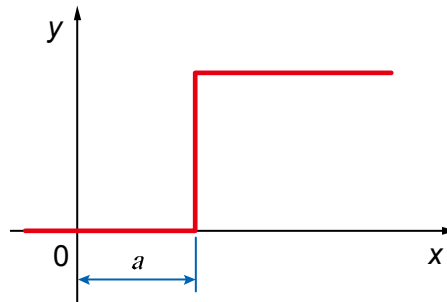


Figure 2-9 Step Function.

Step function (Figure 2-9) is given by

$$\begin{aligned} L[U(t - a)] &= \int_0^{\infty} e^{-st} \cdot U(t - a) dt \\ &= \int_0^a e^{-st} \cdot 0 dt + \int_a^{\infty} e^{-st} \cdot 1 dt \\ &= \frac{1}{s} \cdot e^{-as}. \end{aligned} \quad (2.54)$$

when  $a = 0$ ,

$$L[U(t)] = \frac{1}{s}. \quad (2.55)$$

A half-sine input pulse is expressed in terms of the step function as follows:

$$\ddot{x}_0 = A_0 \left[ \sin \frac{\pi}{T_0} \cdot U(t) - \sin \frac{\pi(t - T_0)}{T_0} \cdot U(t - T_0) \right] \quad (2.56)$$

and  $L[\sin at] = a/(s^2 + a^2)$ ;

therefore, the Laplace transformation of Eq. (2.56) is

$$\ddot{X}_0(s) = L[\ddot{x}_0] = A_0 \left\{ L\left[\sin \frac{\pi t}{T_0}\right] + e^{-T_0 s} L\left[\sin \frac{\pi t}{T_0}\right] \right\}. \quad (2.57)$$

Let  $a = \pi/T_0$ , Eq. (2.57) becomes

$$\begin{aligned} \ddot{X}_0(s) &= A_0(1 + e^{-T_0 s}) \frac{\pi/T_0}{s^2 + (\frac{\pi}{T_0})^2} \\ &= \frac{A_0 a}{s^2 + a^2} (1 + e^{-T_0 s}). \end{aligned} \quad (2.58)$$

If  $x(0) = 0$  and  $\dot{x}(0) = 0$ ,

$$\begin{aligned} L[\ddot{x}_0] &= s^2 X_0(s) - sx(0) - \dot{x}(0) \\ &= s^2 X_0(s). \end{aligned} \quad (2.59)$$

Eq. (2.59) is rewritten as

$$X_0(s) = \frac{1}{s^2} \ddot{X}_0(s). \quad (2.60)$$

Substituting Eq. (2.58) into Eq. (2.53),

$$X_0(s) = \frac{A_0 a}{s^2(s^2 + a^2)} (1 + e^{-T_0 s}). \quad (2.61)$$

Next, substituting Eq. (2.61) into Eq. (2.53),

$$X(s) = \frac{(2\omega\xi + B)s + \omega^2}{s^2 + (2\omega\xi + B)s + \omega^2} \cdot \frac{A_0 a(1 + e^{-T_0 s})}{s^2(s^2 + a^2)}. \quad (2.62)$$

Second transition theorem and Laplace transformation with higher-order poles are used in the following contents. In the second transition theorem,

Let  $f(t) = L^{-1}[\varphi(s)]$ ,

from which Eq. (2.63) is obtained as

$$L^{-1}[e^{-as} \cdot \varphi(s)] = f(t - a) \cdot U(t - a). \quad (2.63)$$

Under Laplace transformation, Eq. (2.63) becomes

$$L[f(t - a) \cdot U(t - a)] = e^{-as} \cdot \varphi(s). \quad (2.64)$$

A Laplace transformation with higher-order poles is expressed as follows.

Defining

$$\varphi(s) = L[f(t)] = \frac{C(s)}{D(s)},$$

where

$$D(s) = (s - a_1)^k (s - a_2)(s - a_3) \cdots (s - a_n).$$

Thus, Eq. (2.65) may be tenable.

$$\varphi(s) = \frac{c_{11}}{(s - a_1)^k} + \frac{c_{12}}{(s - a_1)^{k-1}} + \cdots + \frac{c_{1k}}{(s - a_1)} + \frac{c_2}{s - a_2} + \frac{c_3}{s - a_3} + \cdots + \frac{c_n}{s + a_n}, \quad (2.65)$$

where

$$c_{11} = \left[ (s - a_1)^k \cdot \varphi(s) \right]_{s=a_1},$$

$$c_{12} = \left[ \frac{d}{ds} (s - a_1)^k \cdot \varphi(s) \right]_{s=a_1},$$

$$c_{13} = \frac{1}{2!} \left[ \frac{d^2}{ds^2} (s - a_1)^k \cdot \varphi(s) \right]_{s=a_1},$$

...

$$c_{1k} = \frac{1}{k-1} \left[ \frac{d^{k-1}}{ds^{k-1}} (s - a_1)^k \cdot \varphi(s) \right]_{s=a_1}.$$

Therefore, the following equation is obtained.

$$\begin{aligned} f(t) &= \left[ c_{11} \frac{t^{k-1}}{(k-1)!} + c_{12} \frac{t^{k-2}}{(k-2)!} + \cdots + c_{1k} \right] \cdot e^{a_1 t} + c_2 \cdot e^{a_2 t} + c_3 \cdot e^{a_3 t} + \cdots + c_n \cdot e^{a_n t} \\ &= \sum_{r=0}^{k-1} \frac{t^{k-1-r}}{r!(k-1-r)} \left[ \frac{d^r}{ds^r} \left( (s - a_1)^k \cdot \varphi(s) \right) \cdot e^{st} \right]_{s=a_1} + \sum_{i=2}^n \left[ (s - a_i) \varphi(s) \cdot e^{st} \right]_{s=a_i}. \end{aligned} \quad (2.66)$$

Next, applying the second transition theorem and inverse Laplace transformation with higher-order poles, we obtain the displacement equation of the controlled shock test as follows.

$$\begin{aligned} x(t) &= A_0 a [g(t) \cdot U(t) + g(t - T_0) \cdot U(t - T_0)] \\ &= \begin{cases} A_0 a \cdot [g(t) \cdot 0 + g(t - T_0) \cdot 0] & t < 0 \\ A_0 a \cdot [g(t) + g(t - T_0) \cdot 0] & 0 < t < T_0 \\ A_0 a \cdot [g(t) + g(t - T_0)] & T_0 < t \end{cases} \\ &= \begin{cases} 0 & t < 0 \\ A_0 a \cdot g(t) & 0 < t < T_0 \\ A_0 a \cdot [g(t) + g(t - T_0)] & T_0 < t \end{cases}. \end{aligned} \quad (2.67)$$

The second-order differential is performed for Eq. (2.67), and the acceleration equation of the controlled shock test is obtained as

$$\ddot{x}(t) = \begin{cases} 0 & t < 0 \\ A_0 a \cdot \ddot{g}(t) & 0 < t < T_0 \\ A_0 a \cdot [\dot{g}(t) + \dot{g}(t - T_0)] & T_0 < t \end{cases} \quad (2.68)$$

Eq. (2.68) implies that solving function  $g(t)$  subsequently yields  $\ddot{g}(t)$ . Therefore,  $g(t)$  is solved by the following steps.

We apply the Laplace transformation with higher-order poles and define

$$\begin{cases} \alpha + \beta = -(2\omega\xi + B) & t < 0 \\ \alpha \cdot \beta = \omega^2 & 0 < t < T_0 \end{cases} \quad (2.69)$$

Solving Eq. (2.69), we obtain

$$\begin{cases} \alpha = -(\omega\xi + B/2) + i\sqrt{4(\omega^2 - \omega^2\xi^2 - \omega\xi B) - B^2}/2 \\ \beta = -(\omega\xi + B/2) - i\sqrt{4(\omega^2 - \omega^2\xi^2 - \omega\xi B) - B^2}/2 \end{cases} \quad (2.70)$$

Substituting Eq. (2.70) into Eq. (2.62), gives

$$\begin{aligned} X(s) &= \frac{[(2\omega\xi + B)s + \omega^2]A_0 a}{s^2(s - \alpha)(s - \beta)(s + ia)(s - ia)} \\ &= \frac{c_{11}}{s^2} + \frac{c_{12}}{s} + \frac{c_2}{s - \alpha} + \frac{c_3}{s - \beta} + \frac{c_4}{s + ia} + \frac{c_5}{s - ia}, \end{aligned} \quad (2.71)$$

where

$$\begin{aligned} c_{11} &= \left[ \frac{(2\omega\xi + B)s + \omega^2}{s^2 + (2\omega\xi + B)s + \omega^2} \cdot \frac{1}{s^2 + a^2} \right]_{s=0} = \frac{1}{a^2}, \\ c_{12} &= \left[ \frac{d}{ds} \left( \frac{(2\omega\xi + B)s + \omega^2}{s^2 + (2\omega\xi + B)s + \omega^2} \cdot \frac{1}{s^2 + a^2} \right) \right]_{s=0} = 0, \\ c_2 &= \left[ \frac{(2\omega\xi + B)s + \omega^2}{s^2(s - \beta)(s + ia)(s - ia)} \right]_{s=\alpha} = \frac{(2\omega\xi + B)s + \omega^2}{\alpha^2(\alpha - \beta)(\alpha^2 + a^2)}, \\ c_3 &= \left[ \frac{(2\omega\xi + B)s + \omega^2}{s^2(s - \alpha)(s^2 + a^2)} \right]_{s=\beta} = \frac{(2\omega\xi + B)s + \omega^2}{\beta^2(\beta - \alpha)(\beta^2 + a^2)}, \\ c_4 &= \left[ \frac{(2\omega\xi + B)s + \omega^2}{s^2(s - \alpha)(s - \beta)(s - ia)} \right]_{s=-ia} = \frac{\omega^2 - ia(2\omega\xi + B)}{i2a^3(\alpha + ia)(\beta + ia)}, \\ c_5 &= \left[ \frac{(2\omega\xi + B)s + \omega^2}{s^2(s - \alpha)(s - \beta)(s + ia)} \right]_{s=ia} = \frac{\omega^2 + ia(2\omega\xi + B)}{-i2a^3(-\alpha + ia)(-\beta + ia)}. \end{aligned}$$

Substituting  $c_1 - c_5$  into Eq. (2.66),  $g(t)$  is expressed as

$$\begin{aligned}
g(t) = & \frac{1}{a^2} t + 0 + \frac{(2\omega\xi + B)s + \omega^2}{\alpha^2(\alpha - \beta)(\alpha^2 + a^2)} e^{\alpha t} + \frac{(2\omega\xi + B)s + \omega^2}{\beta^2(\beta - \alpha)(\beta^2 + a^2)} e^{\beta t} \\
& + \frac{\omega^2 - ia(2\omega\xi + B)}{i2a^3(\alpha + ia)(\beta + ia)} e^{-iat} + \frac{\omega^2 + ia(2\omega\xi + B)}{-i2a^3(-\alpha + ia)(-\beta + ia)} e^{iat}. \tag{2.72}
\end{aligned}$$

The second-order derivative of Eq. (2.72)  $\ddot{g}(t)$  is

$$\begin{aligned}
\ddot{g}(t) = & \frac{(2\omega\xi + B)\alpha + \omega^2}{(\alpha - \beta)(\alpha^2 + a^2)} e^{\alpha t} + \frac{(2\omega\xi + B)\beta + \omega^2}{(\beta - \alpha)(\beta^2 + a^2)} e^{\beta t} \\
& + \frac{-\omega^2 + ia(2\omega\xi + B)}{i2a(\alpha + ia)(\beta + ia)} e^{-iat} + \frac{\omega^2 + ia(2\omega\xi + B)}{i2a(-\alpha + ia)(-\beta + ia)} e^{iat}. \tag{2.73}
\end{aligned}$$

Because this equation is extremely complex, it is divided into two parts for convenience.

$$\ddot{g}(t) = \text{Part I} + \text{Part II},$$

where

$$\begin{aligned}
\text{Part I} = & \frac{(2\omega\xi + B)\alpha + \omega^2}{(\alpha - \beta)(\alpha^2 + a^2)} e^{\alpha t} + \frac{(2\omega\xi + B)\beta + \omega^2}{(\beta - \alpha)(\beta^2 + a^2)} e^{\beta t}, \\
\text{Part II} = & + \frac{-\omega^2 + ia(2\omega\xi + B)}{i2a(\alpha + ia)(\beta + ia)} e^{-iat} + \frac{\omega^2 + ia(2\omega\xi + B)}{i2a(-\alpha + ia)(-\beta + ia)} e^{iat}.
\end{aligned}$$

**For Part I:**

Defining  $D = 2\omega\xi + B$ , Part I is rewritten as

$$\begin{aligned}
\text{Part I} = & \frac{D\alpha + \omega^2}{(\alpha - \beta)(\alpha^2 + a^2)} e^{\alpha t} - \frac{D\beta + \omega^2}{(\alpha - \beta)(\beta^2 + a^2)} e^{\beta t} \\
= & \frac{(D\alpha + \omega^2)(\beta^2 + a^2)e^{\alpha t} - (D\beta + \omega^2)(\alpha^2 + a^2)e^{\beta t}}{(\alpha - \beta)(\alpha^2 + a^2)(\beta^2 + a^2)} \\
= & \frac{(D\alpha + \omega^2)(\beta^2 + a^2)e^{\alpha t} - (D\beta + \omega^2)(\alpha^2 + a^2)e^{\beta t}}{(\alpha - \beta)(\alpha^2 + a^2)(\beta^2 + a^2)} \\
= & \frac{-\alpha^2(\beta^2 + a^2)e^{\alpha t} + \beta^2(\alpha^2 + a^2)e^{\beta t}}{(\alpha - \beta)(\alpha^2 + a^2)(\beta^2 + a^2)}. \tag{2.74}
\end{aligned}$$

From Eq. (2.70), we obtain

$$\begin{cases} -\alpha^2 = \omega^2 + D\alpha \\ -\beta^2 = \omega^2 + D\beta \end{cases} \tag{2.75}$$

Substituting Eq. (2.75) into Eq. (2.74), Part I becomes

$$\begin{aligned}
\text{Part I} &= \frac{\alpha^2 \beta^2 (e^{\beta t} - e^{\alpha t}) + a^2 (\beta^2 e^{\beta t} - \alpha^2 e^{\alpha t})}{(\alpha - \beta)(\alpha^2 + a^2)(\beta^2 + a^2)} \\
&= \frac{\alpha^2 \beta^2 (e^{\beta t} - e^{\alpha t}) + a^2 (\beta^2 e^{\beta t} - \alpha^2 e^{\alpha t})}{iQ[\omega^4 + (4\omega^2 \xi^2 + \frac{5}{2}B^2 + 4\omega \xi B - 2\omega^2)a^2 + a^4]}, \tag{2.76}
\end{aligned}$$

where

$$Q = \sqrt{4(\omega^2 - \omega^2 \xi^2 - \omega \xi B) - B^2}.$$

Because Eq. (2.76) is still complex, its numerator and denominator are solved separately.

For the numerator, we introduce Euler's formula, expressed as

$$e^{ix} = \cos x + i \sin x. \tag{2.77}$$

Applying this formula,  $\alpha$  and  $\beta$  are rewritten as

$$\begin{aligned}
\alpha^2 &= [2(\omega^2 \xi^2 + B^2/4 + \omega \xi B) - \omega^2] - i(\omega \xi + B/2)Q \\
&= E - i(\omega \xi + B/2)Q, \tag{2.78}
\end{aligned}$$

$$\begin{aligned}
\beta^2 &= [2(\omega^2 \xi^2 + B^2/4 + \omega \xi B) + \omega^2] - i(\omega \xi + B/2)Q \\
&= E + i(\omega \xi + B/2)Q, \tag{2.79}
\end{aligned}$$

where

$$E = 2(\omega^2 \xi^2 + B^2/4 + \omega \xi B) - \omega^2.$$

Therefore, the following equations are obtained:

$$\begin{aligned}
e^{\alpha t} &= e^{-(\omega \xi + \frac{B}{2})t} \cdot e^{i\frac{Q}{2}t} \\
&= e^{-(\omega \xi + \frac{B}{2})t} \cdot (\cos \frac{Q}{2}t + i \sin \frac{Q}{2}t), \tag{2.80}
\end{aligned}$$

$$\begin{aligned}
e^{\beta t} &= e^{-(\omega \xi + \frac{B}{2})t} \cdot e^{-i\frac{Q}{2}t} \\
&= e^{-(\omega \xi + \frac{B}{2})t} \cdot (\cos \frac{Q}{2}t - i \sin \frac{Q}{2}t), \tag{2.81}
\end{aligned}$$

$$\begin{aligned}
\alpha^2 e^{\alpha t} &= e^{-(\omega \xi + B/2)t} \{ [E \cos \frac{Q}{2}t + (\omega \xi + B/2)Q \sin \frac{Q}{2}t] \\
&\quad + i[E \sin \frac{Q}{2}t - (\omega \xi + B/2)Q \cos \frac{Q}{2}t] \}, \tag{2.82}
\end{aligned}$$

$$\begin{aligned}
\beta^2 e^{\beta t} &= e^{-(\omega \xi + B/2)t} \{ [E \cos \frac{Q}{2}t + (\omega \xi + B/2)Q \sin \frac{Q}{2}t] \\
&\quad - i[E \sin \frac{Q}{2}t - (\omega \xi + B/2)Q \cos \frac{Q}{2}t] \}, \tag{2.83}
\end{aligned}$$

$$\begin{aligned}
e^{\beta t} - e^{\alpha t} &= \left[ \left( \cos \frac{Q}{2}t - i \sin \frac{Q}{2}t \right) - \left( \cos \frac{Q}{2}t + i \sin \frac{Q}{2}t \right) \right] \cdot e^{-(\omega\xi + \frac{1}{2}b)t} \\
&= -i2 \sin \frac{Q}{2}t \cdot e^{-(\omega\xi + \frac{1}{2}b)t},
\end{aligned} \tag{2.84}$$

$$\alpha^2 \beta^2 = \omega^4, \tag{2.85}$$

$$\beta^2 e^{\beta t} - \alpha^2 e^{\alpha t} = -i \left[ 2E \sin \frac{Q}{2}t - 2(\omega\xi + B/2)Q \cos \frac{Q}{2}t \right] \cdot e^{-(\omega\xi + B/2)t}. \tag{2.86}$$

Substituting Eqs. (2.80)–(2.86) into the numerator of Eq. (2.76), we obtain

$$\begin{aligned}
\text{Numerator of Part I} &= \alpha^2 \beta^2 (e^{\beta t} - e^{\alpha t}) + a^2 (\beta^2 e^{\beta t} - \alpha^2 e^{\alpha t}) \\
&= i2 \left\{ -\omega^4 \sin \frac{Q}{2}t - a^2 \left[ E \sin \frac{Q}{2}t - (\omega\xi + B/2)Q \cos \frac{Q}{2}t \right] \right\} e^{-(\omega\xi + B/2)t}.
\end{aligned} \tag{2.87}$$

Therefore, Part I is expressed as

$$\begin{aligned}
\text{Part I} &= \frac{\alpha^2 \beta^2 (e^{\beta t} - e^{\alpha t}) + a^2 (\beta^2 e^{\beta t} - \alpha^2 e^{\alpha t})}{iQ[\omega^4 + (4\omega^2\xi^2 + \frac{5}{2}B^2 + 4\omega\xi B - 2\omega^2)a^2 + a^4]} \\
&= \frac{2 \left\{ -\omega^4 \sin \frac{Q}{2}t - a^2 \left[ E \sin \frac{Q}{2}t - (\omega\xi + \frac{B}{2})Q \cos \frac{Q}{2}t \right] \right\}}{Q[\omega^4 + (4\omega^2\xi^2 + \frac{5}{2}B^2 + 4\omega\xi B - 2\omega^2)a^2 + a^4]} \cdot e^{-(\omega\xi + \frac{B}{2})t} \\
&= \frac{-2(\omega^4 + a^2 E) \sin \frac{Q}{2}t + 2a^2(\omega\xi + \frac{B}{2})Q \cos \frac{Q}{2}t}{Q[\omega^4 + (4\omega^2\xi^2 + \frac{5}{2}B^2 + 4\omega\xi B - 2\omega^2)a^2 + a^4]} \cdot e^{-(\omega\xi + \frac{B}{2})t},
\end{aligned} \tag{2.88}$$

where

$$Q = \sqrt{4(\omega^2 - \omega^2\xi^2 - \omega\xi B) - B^2}.$$

**For Part II:**

$$\begin{aligned}
\text{Part II} &= \frac{-\omega^2 + iaD}{i2a(\alpha + ia)(\beta + ia)} e^{-iat} + \frac{\omega^2 + iaD}{i2a(-\alpha + ia)(-\beta + ia)} e^{iat} \\
&= \frac{-\omega^2 + iaD}{i2a[-a^2 + ia(\alpha + \beta) + \alpha\beta]} e^{-iat} + \frac{\omega^2 + iaD}{i2a[-a^2 - ia(\alpha + \beta) + \alpha\beta]} e^{iat} \\
&= \frac{-\omega^2 + iaD}{i2a[-a^2 - iaD + \omega^2]} e^{-iat} + \frac{\omega^2 + iaD}{i2a[-a^2 + iaD + \omega^2]} e^{iat} \\
&= \frac{-Y}{i2a[Y - a^2]} e^{-iat} + \frac{X}{i2a[X - a^2]} e^{iat} \\
&= \frac{1}{i2a} \left[ \frac{X e^{iat}}{X - a^2} - \frac{Y e^{-iat}}{Y - a^2} \right]
\end{aligned}$$

$$\begin{aligned}
&= \frac{1}{i2a} \frac{XY(e^{iat} - e^{-iat}) + a^2(Ye^{-iat} - Xe^{iat})}{XY - a^2(X + Y) + a^4} \\
&= \frac{1}{i2a} \frac{2(\omega^4 + a^2D^2)i \sin at - 2a^2(aDi \cos at + \omega^2i \sin at)}{\omega^4 + a^2D^2 - 2a^2\omega^2 + a^4} \\
&= \frac{[\omega^4 + a^2(2\omega\xi + B)^2 - a^2\omega^2] \sin at - a^3(2\omega\xi + B) \cos at}{a[\omega^4 + a^2(2\omega\xi + B)^2 - 2a^2\omega^2 + a^4]}, \tag{2.89}
\end{aligned}$$

where

$$\begin{cases} X = iaD + \omega^2 \\ Y = -iaD + \omega^2 \end{cases} \tag{2.90}$$

Combining Eqs. (2.89) and (2.88),  $\ddot{g}(t)$  is obtained as

$$\begin{aligned}
\ddot{g}(t) &= \frac{-2(\omega^4 + a^2E) \sin \frac{Q}{2}t + 2a^2(\omega\xi + \frac{B}{2})Q \cos \frac{Q}{2}t}{Q[\omega^4 + (4\omega^2\xi^2 + \frac{5}{2}B^2 + 4\omega\xi B - 2\omega^2)a^2 + a^4]} \cdot e^{-(\omega\xi + \frac{B}{2})t} \\
&\quad + \frac{[\omega^4 + a^2(2\omega\xi + B)^2 - a^2\omega^2] \sin at - [a^3(2\omega\xi + B)] \cos at}{a[\omega^4 + a^2(2\omega\xi + B)^2 - 2a^2\omega^2 + a^4]}. \tag{2.91}
\end{aligned}$$

Substituting Eq. (2.91) into Eq. (2.68) yields the SR equation of the controlled shock test, expressed as

$$A_{cs}(t) = \ddot{x}(t) = \begin{cases} 0 & t < 0 \\ A_0a \cdot \ddot{g}(t) & 0 < t < T_0, \\ A_0a \cdot [\ddot{g}(t) + \ddot{g}(t - T_0)] & T_0 < t \end{cases} \tag{2.92}$$

where

$$a = \frac{\pi}{T_0},$$

$$B = \frac{4F_c}{\pi mAa},$$

$$E = 2(\omega^2\xi^2 + B^2/4 + \omega\xi B) - \omega^2,$$

$$Q = \sqrt{4(\omega^2 - \omega^2\xi^2 - \omega\xi B) - B^2},$$

$$\begin{aligned}
\ddot{g}(t) &= \frac{-2(\omega^4 + a^2E) \sin \frac{Q}{2}t + 2a^2(\omega\xi + \frac{B}{2})Q \cos \frac{Q}{2}t}{Q[\omega^4 + (4\omega^2\xi^2 + \frac{5}{2}B^2 + 4\omega\xi B - 2\omega^2)a^2 + a^4]} \cdot e^{-(\omega\xi + \frac{B}{2})t} \\
&\quad + \frac{[\omega^4 + a^2(2\omega\xi + B)^2 - a^2\omega^2] \sin at - [a^3(2\omega\xi + B)] \cos at}{a[\omega^4 + a^2(2\omega\xi + B)^2 - 2a^2\omega^2 + a^4]}.
\end{aligned}$$



### 2.5.3 Mathematical SR equation for the controlled shock test

On the basis of Eq. (2.92), we can calculate the peak value of the SR equation, i.e.  $PRA_{cs}$  in the friction theory. Similar to the damping theory,  $PRA_{cs}$  is expressed as

$$PRA_{cs} = u_{cs} \cdot \omega_n \cdot V_c, \quad (2.93)$$

where

$$u_{cs} = \frac{T_r}{2\pi f_n D_e}. \quad (2.94)$$

### 2.5.4 Mathematical verification

The mathematical solution of the FVD model reduces to that of the VD model when  $F_c = 0$ . The SR equations are of the same form (Eq. (2.92)), although their  $\ddot{g}(t)$  functions differ. Therefore, the mathematical solution can be verified by comparing the two  $\ddot{g}(t)$  functions. In other words, if  $\ddot{g}(t)$  of the new model yields the same solution as that of the established model under the same condition, then the mathematical solution of the FVD model is correct and it can be proved.

When  $F_c = 0$ , we obtain the following equations:  $B = 0$ ,  $E = \omega^2(2\xi^2 - 1)$  and  $Q = 2\omega\sqrt{1 - \xi^2}$ . Substituting these three parameters into Eq. (2.91),  $\ddot{g}(t)$  becomes equal to Eq. (1.11).

## 2.6 Friction Equivalent Drop Theory

The new correcting conditions can be deduced from the new mathematical equations for the test at free fall and the controlled shock test.

Comparing Eqs. (2.36) and (2.93) and setting

$$PRA_{ff} = PRA_{cs},$$

we obtain

$$u_{ff} \cdot \omega_n \cdot V + \mu_{ff} \cdot \omega_n \cdot V_F = u_{cs} \cdot \omega_n \cdot V_c. \quad (2.95)$$

Rearranging terms gives

$$u_{ff} \cdot V + \mu_{ff} \cdot V_F = u_{cs} \cdot V_c. \quad (2.96)$$

Rearranging Eq. (2.96), the following two correcting conditions are obtained:

$$V_c = \frac{u_{ff}}{u_{cs}} V + \frac{\mu_{ff}}{u_{cs}} V_F \quad \text{or} \quad (2.97)$$

$$V = \frac{u_{cs}}{u_{ff}} V_c - \frac{\mu_{ff}}{u_{ff}} V_F. \quad (2.98)$$

From Eqs. (2.97) and (2.98), we observe that the test at free fall and controlled shock test are mathematically equivalent in the FVD model. This new theory is called the friction equivalent drop theory and hereafter abbreviated as the ‘friction theory’ (Figure 2-10).

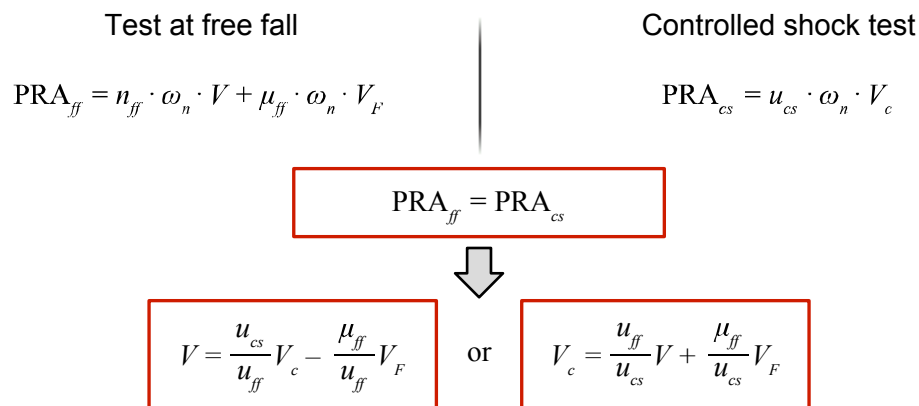


Figure 2-10 Schematic of the Friction Equivalent Drop Theory.

## 2.7 References

- [1] Goff J W and Chateman R. The Correlation of Shock with Free-fall Drop Height. Technical Report N. 24. Multi-Sponsor Research Program, School of Packaging, Michigan State University/East Lansing, MI, 1976.
- [2] Goff J W, Chateman R, Iwahimizu H, and Collins K. Shock Machine and Free-fall Drop Correlation, Unpublished Data. School of Packaging, Michigan State University/East Lansing, MI, 1976.
- [3] Katsuhiko SAITO and Kazuaki KAWAGUCHI. Equivalent Drop Theory with Damping. *23rd International Association of Packaging Research Institutes Symposium*. 3–5 Sep. 2007.
- [4] Kazuaki KAWAGUCHI and Katsuhiko SAITO. Experimental Verification of Equivalent Drop Testing with Damping for Packaged Freight. *Journal of Packaging Science & Technology, Japan*. 2008; 17(1): 39–45.
- [5] Chen ZHONG and Katsuhiko SAITO. Equivalent Drop Test Modification for Determination of Cushioning Performance. *Journal of Packaging Science & Technology, Japan*. 2010; 19(2): 123–135.
- [6] Katsuhiko SAITO and Chen ZHONG. Modified Simulated Drop Test for Transmitted Shock Characteristics of Structural Plastic Foam Cushioning Materials. *17th IAPRI World conference on Packaging*, 2009.
- [7] Wang Z. W. On evaluation of product dropping damage. *International Journal of Packaging Technology and Science*. 2002; 15(3): 115–120.
- [8] Wang Z. W. Dropping damage boundary curves for cubic and tangent package cushioning systems. *International Journal of Packaging Technology and Science*. 2002; 15(5): 263–266.
- [9] Wang Z. W. and Jiang J. H. Evaluation of product dropping damage based on key component. *International Journal of Packaging Technology and Science*. 2010; 23(4): 227–238.
- [10] <http://www.jpi.or.jp/toukei/H23.html> (Accessed in May 2013)
- [11] Yoshida Seiki Co., Ltd. Shock Machine User's Guide (in Japanese). ASQ-700 serial.
- [12] Singiresu S. Rao. *Mechanical Vibrations* (5th Edition), Pearson Education, 2010.
- [13] S. Bran, D. Ewins, S. S Rao. *Encyclopedia of Vibration*, Academic Press, 2002.
- [14] Maplesoft Co. Ltd. *Maple User's Guide*, Maple Ver. 14.
- [15] Cyril M. Harris, Allan G. Piersol. *Harris' Shock and Vibration Handbook* (Fifth Edition), McGraw-Hill, 2002.

- [16] Gilmore. R. J. and Steer. M. B. Nonlinear circuit analysis using the method of harmonic balance—A review of the art. Part I. Introductory concepts. *Int. J. Microw. Mill.-Wave Comput.-Aided Eng.* 1991; 1: 22–37.
- [17] Nakhla. Michel S. and Vlach. Jiri. A piecewise harmonic balance technique for determination of periodic response of nonlinear systems. *IEEE Transactions on Circuits and Systems.* 1976; CAS-23: 85–91.
- [18] Drazin. P.G. Nonlinear systems, Cambridge University Press, 1992.

# CHAPTER 3. VERIFICATION OF FRICTION EQUIVALENT DROP THEORY

Here we demonstrate the feasibility of the friction equivalent drop theory in a set of preliminary and more extensive experiments.

## 3.1 Preliminary Verification

The simple corrugated sleeve mentioned in Section 2.2.1 typifies the majority of SCM cushions. Therefore, the initial verification experiment is conducted on a corrugated sleeve.

### 3.1.1 Test equipment and materials

The test equipment and materials were the same as those described in Section 2.2 and will not be reiterated here.

### 3.1.2 Test method

The test method is outlined below:

- I. Perform experiments.
  - i. Perform controlled shock tests and record the experimental data.
  - ii. Perform the traditional dynamic compression tests and record the experimental data.
  - iii. Using the correction condition (see Eq. (2.98)), correct  $V$  to  $V_{\text{new}}$ .
  - iv. Finally, repeat the dynamic compression test for  $V_{\text{new}}$  and measure the PRA obtained from the friction theory.
- II. Process and analyse experimental data.
- III. Compare test results and assess the friction theory.

### 3.1.3 Test conditions

To ensure adequate reliability and comparability of the experimental results, all test conditions described in Section 2.2 were maintained, except for condition 6—(data collection). For the tests in steps i and ii in the above section, data collection conformed to the test conditions of Section 2.2; whereas in step iv,  $V$  was altered from 3.43 m/s to  $V_{\text{new}}$  by Eq. (2.98).

### 3.1.4 Correcting method

As is evident from Section 3.1.2, the correction of  $V$  is an important step. Therefore, the correcting procedure is described in this section. The correcting method of  $V$  is shown as a flowchart in Figure 3-1. The process is divided into the following three steps<sup>[1]</sup>. (a) The calculation of  $u_{ff}$  and  $\mu_{ff}$  by simulation, (b) deduction of  $F_c$  to calculate  $V_F$  and (c) calculation of  $u_{cs}$  from traditional controlled shock test data. Finally,  $V_{\text{new}}$  is calculated by Eq. (2.98).

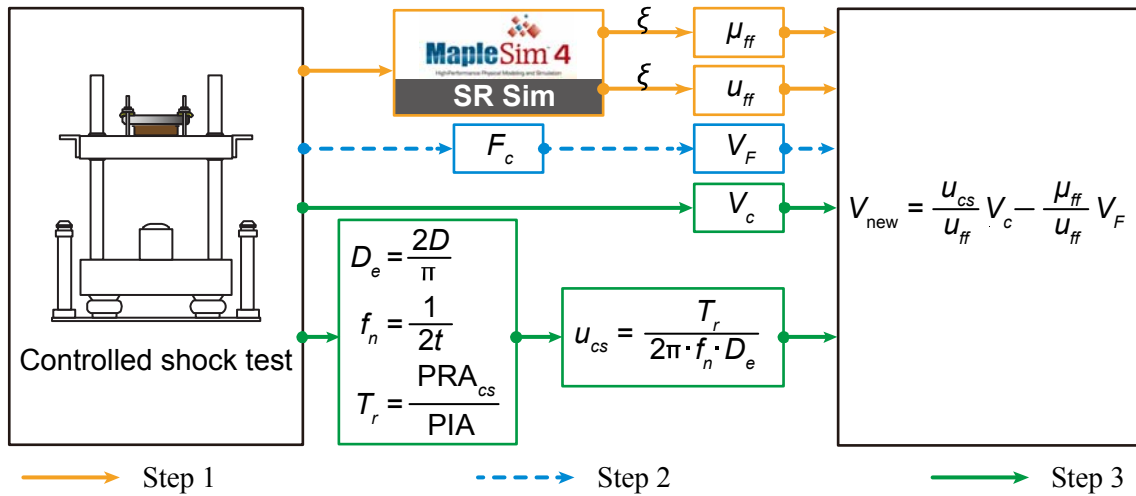


Figure 3-1 Flowchart for Correcting Method.

The parameters of velocity change  $V_c$ , impact duration of response  $D$ , impact duration of input pulse  $t$ , PIA and  $PRA_{cs}$  can be determined from experimental data;  $V_F$  can be calculated once  $F_c$  is known,  $u_{ff}$  and  $\mu_{ff}$  are functions of  $\xi$ .

$\xi$  and  $F_c$  are calculated as follows.

### A) Calculating $\xi$

In the damping theory,  $\xi$  is calculated using a method called SR analysis.<sup>[2]</sup> However, this method is not applicable to the friction theory because of friction. Therefore, in this study, a new method called ‘shock response simulation’ (SR Sim) was proposed and implemented in MapleSim.

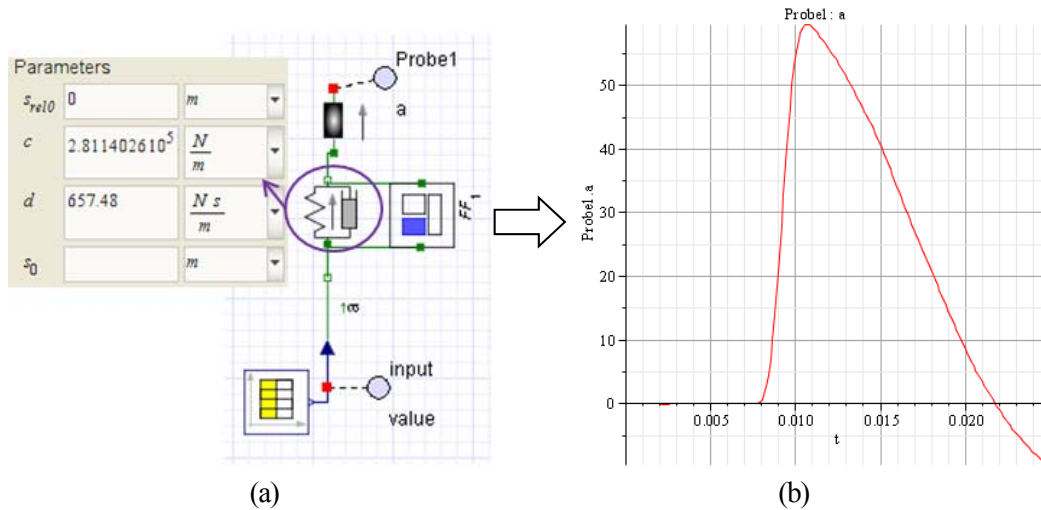


Figure 3-2 SR Sim for Controlled Shock Test.

(a) Simulation FVD model of the controlled shock test, (b) Simulation result.

- The FVD model for the controlled shock test (Figure 3-2(a)) was constructed in MapleSim. Here an extremely short duration input pulse was applied to the stationary FVD model.

- The corresponding parameters were input to the model, and simulations were conducted. The values of  $k$ ,  $m$  and  $F_c$  were calculated<sup>[3]</sup> and remained unchanged, while the value of  $c$  changed, yielding different response curves (Figure 3-2(b)).
- Comparing the peaks of the simulation curves, we record  $c$  when the maximum value best matched the nearest experimental data. Finally,  $\zeta$  was calculated as<sup>9</sup>

$$\xi = \frac{c}{2\sqrt{km}}. \quad (3.1)$$

The damping coefficients obtained from the aforementioned method are listed in Table 3-1.

Table 3-1 Calculation of Damping Coefficient  $\xi$ .

Order	$\omega_n$ (Hz)	$k$ (N/m)	$c$ (Ns/m)	$\xi$
1	272.00	295934.6	650	0.299
2	268.51	288395.2	645	0.300
3	273.18	298513.6	650	0.297
4	269.66	290876.0	647	0.300
5	272.00	295934.6	650	0.299
6	267.37	285946.0	635	0.297
7	266.24	283527.8	633	0.297
8	261.80	274155.7	630	0.301
9	262.89	276454.7	630	0.300
10	266.24	283527.8	634	0.298

## B) Calculating $F_c$

To simulate the shock response in the new model, the friction term must be allocated a specific value. Coulomb friction is usually calculated by the so-called positive pressure method; however, this approach is precluded here because of the structure of SCM. Therefore, on the basis of the principle of the conservation of energy, a hysteresis loop is applied to calculate friction in this study<sup>[4]</sup>.

Hysteresis is a phenomenon in which a system never return to its original state, even if the external force is totally conserve. Hysteresis occurs in many materials, e.g. a plastically deformable spring subjected to forces exceeding its deformation limits and SCMs made from corrugated board. If the displacement of a system with hysteresis is plotted as a function of applied force, then the resulting curve is in the form of a loop called a hysteresis loop.

The form of the hysteresis loop depends on the material's physical properties. For different cushioning materials, the loops can be divided into three mass–spring–attenuation models, as shown in Figure 3-3. In this figure, the  $x$ - and  $f$ -axes represent displacement and force, respectively. Hysteresis loops are shown for (a) VD model, (b) Coulomb damping model and (c) FVD model. The energy loss in each model is determined by the area enclosed by its hysteresis loop.

Therefore, the loss energy in the three models is:

For the VD model,

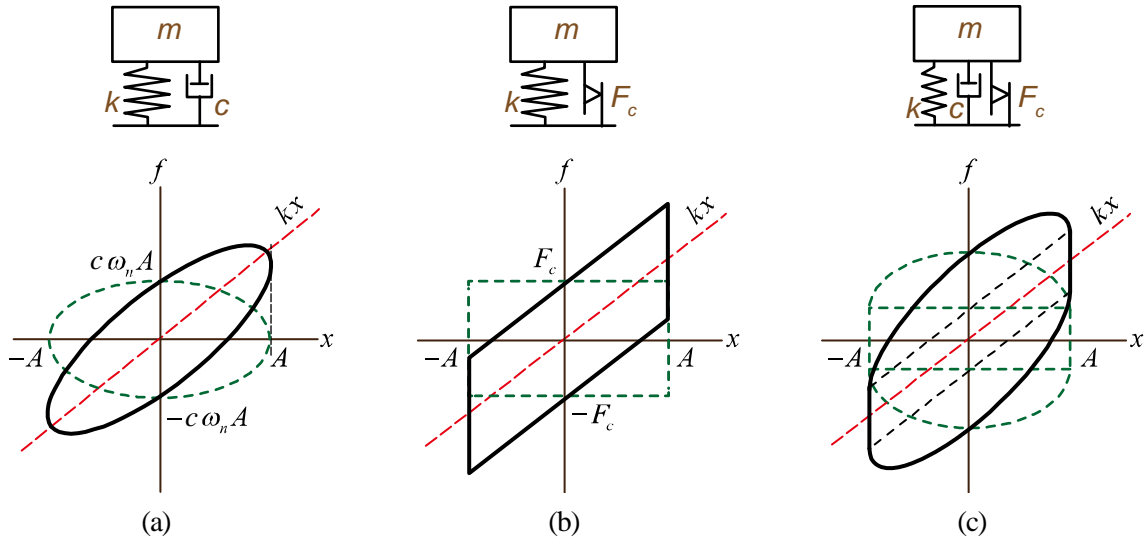


Figure 3-3 Hysteresis Loops of Three Damping Models.  
(a) VD model, (b) Coulomb damping model, (c) FVD model.

$$E_c = \pi c_0 \omega_n A^2; \quad (3.2)$$

for the Coulomb damping model,

$$E_F = 4F_c A; \quad (3.3)$$

and for the FVD model,

$$E_n = \pi c \omega_n A^2 + 4F_c A, \quad (3.4)$$

where  $A$  is the amplitude of the displacement equation of the system.

If the FVD model is equivalent to the VD model, the equivalent loss energy  $E_{eq}$  is expressed as

$$E_{eq} = \pi c_{eq} \omega_n A^2, \quad (3.5)$$

where  $c_{eq}$  is the equivalent damping coefficient due to the loss energy.

Setting Eq. (3.4) equal to Eq. (3.5), friction  $F_c$  is obtained as follows:

$$F_c = \frac{\pi}{4} (c_{eq} - c_0) \omega_n A. \quad (3.6)$$

Here  $c_{eq}$  can be calculated simulating the VD model in MapleSim using the experimental data.

The calculation process is detailed as follows.

Because friction is a form of attenuation, the FVD model (Figure 3-4(a)) is equivalent to the VD model (Figure 3-4(b)). This equivalent model was simulated in MapleSim, where the value of  $k$  was calculated and remained unchanged. Whereas,  $c$  was changed. The different curves obtained are shown in Figure 3-4(c). When the maximum of the curve was closest to the nearest experimental data  $c$  was recorded as the equivalent damping coefficient  $c_{eq}$ .  $F_c$  was then calculated as (for example):

$$F_c = \frac{\pi}{4} (c_{eq} - c_0) \omega_n A = \frac{\pi}{4} \times (537 - 509) \times 265 \times (12.6 \times 10^{-3}) = 74 \text{ (N)}.$$

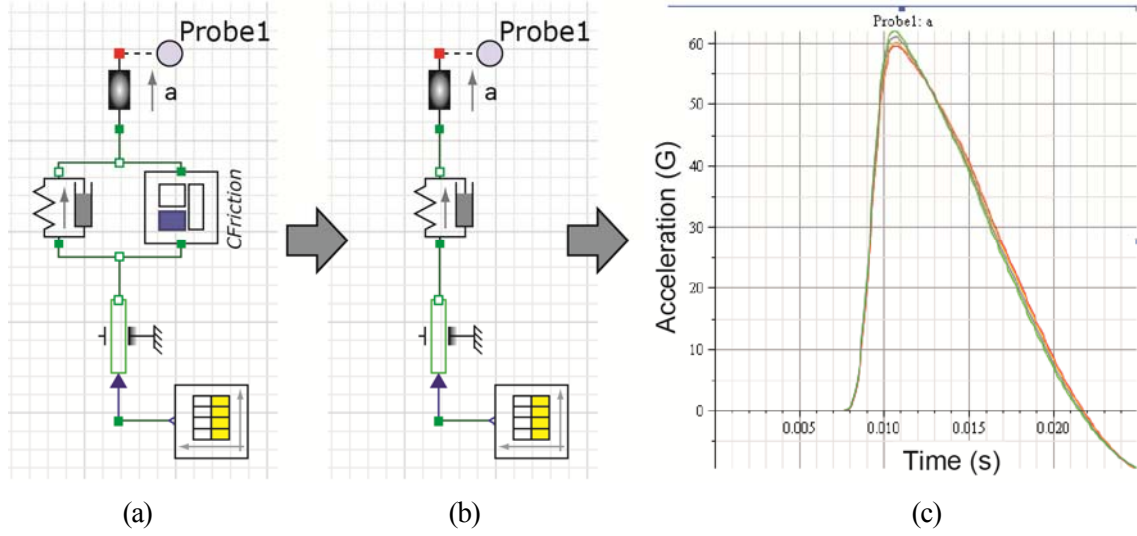


Figure 3-4 Procedure for Calculating Coulomb Friction.  
(a) FVD model, (b) Equivalent VD model, (c) Simulation result

The calculated friction forces are listed in Table 3-2.

Table 3-2 Calculation of Friction  $F_c$ .

order	$c_{eq}$ (Ns/m)	$c_0$ (Ns/m)	$\omega_n$ (Hz)	$A$ (mm)	$F_c$ (N)
1	705	733	306	11.5	78
2	690	716	299	11.6	70
3	680	710	291	11.4	78
4	650	676	286	11.6	68
5	615	643	288	11.6	74
6	730	758	310	11.8	79
7	710	735	296	11.7	68
8	660	689	288	11.9	79
9	655	684	295	11.5	78
10	695	722	311	11.6	75

### C) Calculating $V_{new}$

For convenience, we substitute Eqs. (2.37), (2.38), (2.40) and (2.94) into Eq. (2.36) to yield

$$V_{new} = \frac{2 u_{cs}}{\left| \frac{4\xi^2 - 1}{\xi} \right| \exp\left(-\frac{\xi\pi}{\sqrt{2-4\xi^2}}\right)} \cdot V_c - \frac{2\sqrt{2}(1-2\xi^2)}{\xi\pi \left| \frac{4\xi^2 - 1}{\xi} \right| \exp\left(-\frac{\xi\pi}{\sqrt{2-4\xi^2}}\right)} \cdot \frac{F_c}{m\omega_n} \quad (3.7)$$

Finally, inserting all parameters into Eq. (3.7), we obtain the corrected impact velocities  $V_{new}$ . The results are shown in Table 3-3.



Table 3-3 Corrected Impact Velocity  $V_{new}$ .

Order	$V_c$ (m/s)	$V_{new}$ (m/s)
1		3.55
2		3.62
3		3.53
4		3.70
5		3.50
6	3.43	3.50
7		3.66
8		3.87
9		3.54
10		3.41

### 3.1.5 Results and discussion

The results of the preliminary and verification experiments are shown in Table 3-4. All data are the PRAs of each test.

Table 3-4 Comparison of Experimental Results Analyzed by Traditional and Friction Theories.

Order	Traditional theory		Friction theory
	Controlled shock test <sup>a</sup>	Test at free fall <sup>b</sup>	Test at free fall <sup>c</sup>
1	63.30	58.70	59.10
2	62.80	60.00	59.70
3	57.40	56.50	59.90
4	60.50	56.90	60.30
5	62.20	60.00	61.10
6	61.60	57.40	61.20
7	56.90	60.70	61.30
8	61.20	57.90	63.10
9	63.20	57.60	58.10
10	63.70	56.80	58.30
Average	61.28	58.25	60.21
DiA		3.03	1.07

Unit: G.

The data in columns **a** and **b** are based on the traditional theory, while those in column **c** are based on the friction theory.

- For data in column **a**, according to the definition of the equivalent free-fall height,  $V_c$  should be equal to 3.43 m/s. Therefore, the response was recorded only when  $V_c = 3.43$  m/s.
- Similarly, the data in column **b** assume that  $V = 3.43$  m/s. Again, the response was recorded only when  $V = 3.43$  m/s.
- For data in column **c**, according to the verification experiment, the response was recorded only when  $V_{new}$  changes to corrected values.

Considering the uniqueness of the sleeve cushion, the correcting effect was evaluated from averages of three tests. The differences in average (DiA) were also compared. DiA is an important indicator of the error in the equivalent free-fall height, and it enables the correcting effect of the friction theory to be directly determined.

The DiA of two tests based on the traditional theory is 3.03, reflecting the significant errors in the traditional theory. On the other hand, the DiA between the corrected and uncorrected tests at free fall is 1.07. Comparing the two values, we note that the error in the friction equivalent drop theory is reduced to one-third of that in the standard equivalent drop theory.

## 3.2 Further Verification

In Section 3.1, we proved the feasibility of the friction theory using a corrugated sleeve as a test material. However, this conclusion was based on a single material (corrugated fiberboard) and design configuration (a corrugated sleeve with the same equivalent free-fall height and weight dummy). Therefore, to completely verify the model, we must consider other factors such as stress, test material and free fall height. The influence of these three factors can be investigated by varying the weight dummy, using pulp mould as the test material and changing the free fall height of the mass. To this end, we conducted further verification experiment, focusing on the influence of stress and materials.

### 3.2.1 Test equipment and materials

#### A) Test equipment

The test equipment was the same as that described in Section 2.2 and will not be reiterated here.

#### B) Test materials

The test materials comprised the following two cushions: a corrugated sleeve and pulp mould.

On the basis of previously gained knowledge <sup>[3]</sup> and the technical specifications of the test equipment <sup>[5], [6]</sup>, the corrugated sleeve was created by folding a corrugated fiberboard (A-flute, LB210/MC120/LB210, see Figure 3-5). The dimensions of the sleeve were 180 × 180 × 80 (mm). We also used a simplified pulp mould (208 × 208 (mm)), illustrated in Figure 3-6(a). To ensure a good response acceleration curve, the appropriate height of the pulp mould was set to 50 mm. The wall thickness of the pulp mould was 3 mm; the inside surface was very rough, whereas the outer was moderately smooth. The three-dimensional structure of the pulp mould is shown in Figure 3-6(a), and a cross-section is shown in Figure 3-6(b).

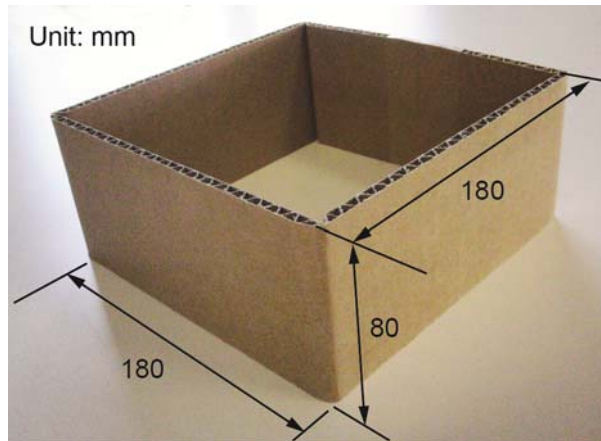


Figure 3-5 Structural Corrugated Sleeve in Verification Test.

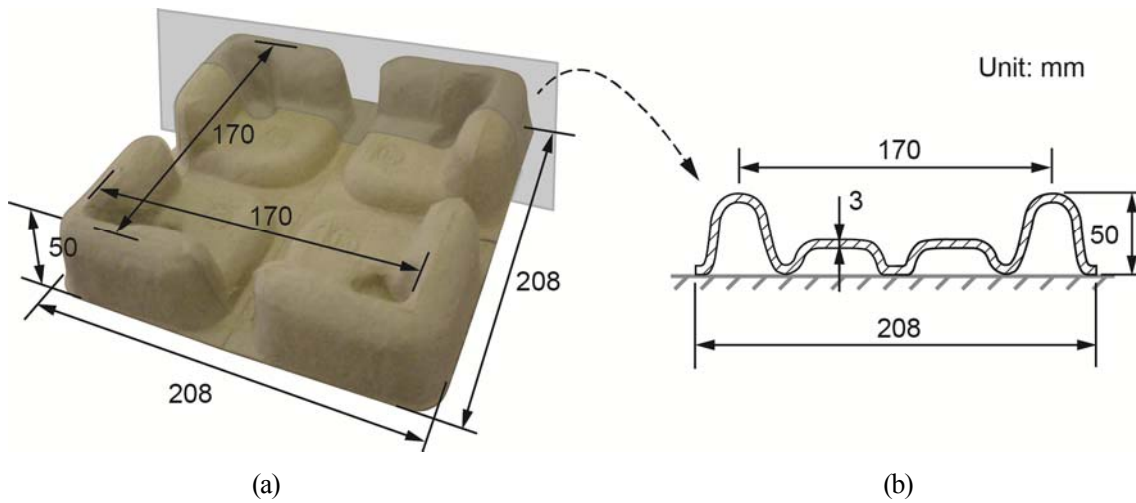


Figure 3-6 Pulp Mould.

(a) Three-dimensional structure, (b) Cross-section.

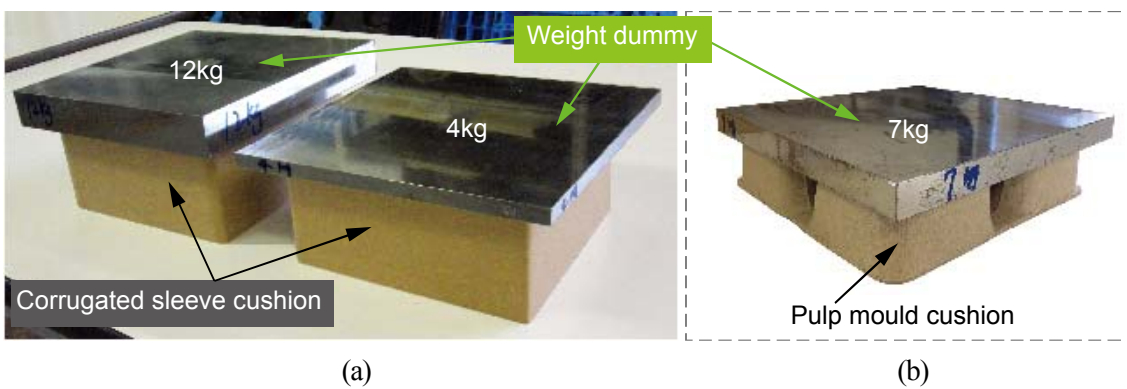


Figure 3-7 Weight Dummy.

(a) Coupled to the corrugated sleeve, (b) Coupled to the pulp mould.

### C) Weight dummy

Following NAKAGAWA<sup>[7]</sup>, we used nine weight dummies of 4–12 kg, in one kilogram increments. The length and width of the nine weight dummies were retained constant (i.e. 220 × 220 (mm), respectively), but their thicknesses varied. Figure 3-7 shows dummies of different weights coupled to the two test materials.

### 3.2.2 Test design

A flowchart of the test design is presented in Figure 3-8. The test is broadly divided into data acquisition and data analysis.

#### A) Data acquisition

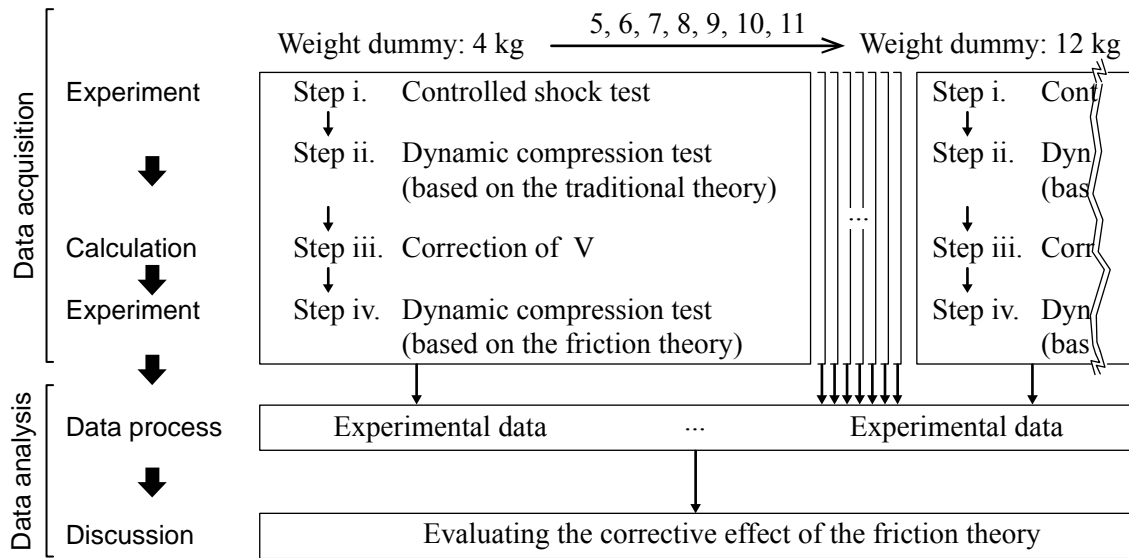


Figure 3-8 Flowchart of Extended Verification Test Procedures.

During the data acquisition stage, the experiment was repeated for nine test dummies of 4–12 kg. The test method was as follows:

- Step I: Perform the controlled shock test and record  $V_c$  and  $PRA_{cs}$ .
- Step II: Applying the impact pulse of the controlled shock test in Step I, perform the traditional dynamic compression test, record  $V$  and  $PRA_{df}$ .
- Step III: Following the correction method shown in Figure 3-1, use the data collected in Steps I and II to correct the impact velocity  $V$ . In some cases, result  $V_{new}$  lies outside  $3.43 \pm 0.10$  m/s.
- Step IV: If  $V_{new}$  is outside  $3.43 \pm 0.10$  m/s, then repeat the dynamic compression test to measure the new PRA corresponding to the  $V_{new}$ .

The JIS Z 0240 specifies 0.6 m as the usual drop height during transportation. Therefore,  $H$  was set to 0.6 m and retained constant in all experiments. The theoretical impact velocity of the mass  $V_{th}$  was calculated as 3.43 m/s using  $V_{th} = \sqrt{2gH}$ . According to the traditional theory,  $V_c = V_{th} = 3.43$  m/s.

In earlier studies <sup>[2],[3]</sup>, data were used only if  $V$  or  $V_c = 3.43$  m/s in both tests. In this study, to improve the accuracy of the test results, we relaxed the effective impact velocity  $V$  and effective velocity change  $V_c$  to  $3.43 \pm 0.10$  m/s. All data yielding impact velocities within this range were recorded.

## B) Data analysis

At the data analysis stage, all experimental data collected during data acquisition were processed. The corrective effect of the friction theory was evaluated on the two test materials. To ensure the reliability of the results, we collected 30 sets of data for each of the three tests (Steps I, II and IV) for each test material <sup>15</sup>.

### 3.2.3 Variance of friction

As mentioned in Section 3.1.4,  $F_c$  is expressed as Eq. (3.6), which can also be expressed as

$$F_c = \frac{1}{4} \frac{E_n}{A} - \frac{\pi}{4} c \omega_n A. \quad (3.8)$$

Furthermore, by substituting  $\omega_n = \sqrt{k/m}$  and  $c = 2\sqrt{km}$  into Eq. (3.8), we obtain

$$F_c = \frac{1}{4} \frac{E_n}{A} - \frac{\pi}{2} k A. \quad (3.9)$$

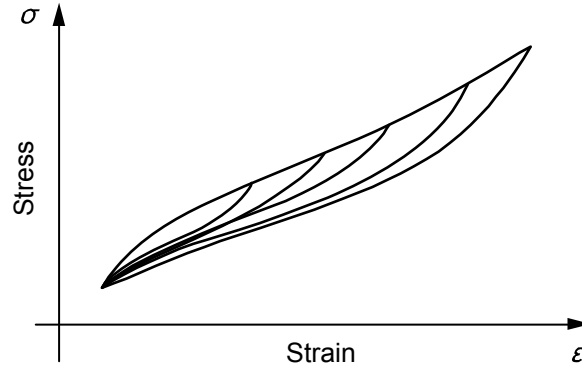


Figure 3-9 Complete Nested Hysteresis Loops.

According to the literature <sup>[4],[8]</sup>, the friction model yields complete nested hysteresis loops (Figure 3-9). Therefore, the term  $E_n/A$  in Eq. (3.9) is constant. Furthermore, because  $k$  is also constant, we can predict from Eq. (3.9) that if increasing the weight dummy causes a large change in  $A$ , then  $F_c$  will decrease.

From the experimental data of the dynamic compression test using weights of 4–12 kg, we can draw the hysteresis loops for the corrugated sleeve. the resulting hysteresis loops for 4 kg, 8 kg and 12 kg weight dummies are shown in Figure 3-10. From this figure, we observe the following:

1. The upper parts of the hysteresis loops are almost identical. The ratio  $E_n/A$  is independent of dummy weights from 4 kg to 12 kg and is approximately  $2 \times 10^3$  N.

2. The displacement values for the weight dummies are  $A_{4\text{kg}} \approx 7 \text{ mm}$ ,  $A_{8\text{kg}} \approx 16 \text{ mm}$  and  $A_{12\text{kg}} \approx 23 \text{ mm}$ . Hence, the parameter  $A$  increases with weight.

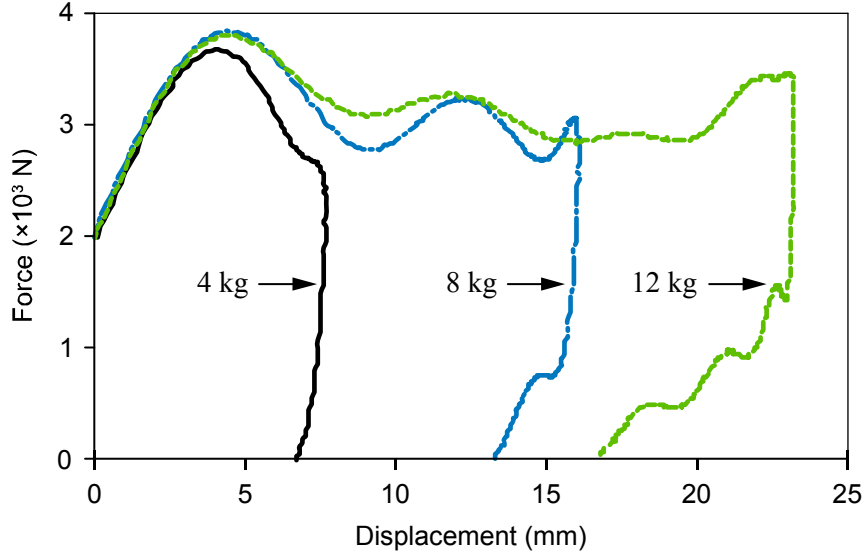


Figure 3-10 Hysteresis Loops of the Corrugated Sleeve for 4, 8 and 12 kg Weight Dummies.

### 3.2.4 Probability distributions of dGs

An important quantity in this study is the Difference in the PRAs of the two tests (dGs). The dGs provides a rough estimate of the correction effect in the friction theory, and given by

$$\text{dGs} = \text{PRA}_{cs}(V_c) - \text{PRA}_{ff}(V). \quad (3.10)$$

#### A) Calculation of dGs

Two types of  $\text{PRA}_{ff}(V)$  exist, corresponding to before and after the correction of  $V$ , denoted as  $\text{PRA}_{ff}(V_{\text{old}})$  and  $\text{PRA}_{ff}(V_{\text{new}})$ , respectively. Therefore, Eq. (3.10) has the following two cases:

$$\text{dGs} = \text{PRA}_{cs}(V_c) - \text{PRA}_{ff}(V_{\text{old}}); \quad (3.11)$$

$$\text{dGs} = \text{PRA}_{cs}(V_c) - \text{PRA}_{ff}(V_{\text{new}}). \quad (3.12)$$

The dGs values calculated from Eq. (3.11) are presented in Table 3-5. Since the experimental data are too numerous to display in their entirety, Table 3-5 lists only a representative portion of the data. First, the test results of both tests are listed in order of increasing  $V_c$  or  $V$ . Second, values of  $\text{PRA}_{cs}(V_c)$  and  $\text{PRA}_{ff}(V_{\text{old}})$  corresponding to the same value of  $V_c$  or  $V$  are grouped together (highlighted in blocks of the same colour). Third, dGs is calculated by Eq. (3.11) for all data within a specified group.

An example of the dGs calculation using Eq. (3.12) is presented in Table 3-6 (for a portion of the data). First, using the friction theory, we calculate  $V_{\text{new}}$  from the data of the controlled shock test (block ①). Block ② shows the results of the dynamic compression test. Listed are the old test results (when  $V_{\text{new}}$  is within  $3.43 \pm 0.1 \text{ m/s}$ ) and the new test results (when  $V_{\text{new}}$  lies outside  $3.43 \pm 0.1 \text{ m/s}$ ) of the dynamic compression test. Third,  $\text{PRA}_{cs}(V_c)$  corresponding to a special  $V_{\text{new}}$  and  $\text{PRA}_{ff}(V_{\text{new}})$ , for which  $V$

equals  $V_{new}$  are grouped together (blocks with the same colour) and are permuted and combined (block ③). Finally, dGs is calculated by Eq. (3.12) using all data in a group (block ④).

Table 3-5 Example of dGs Calculation.  $\Gamma_{before}$ , Pulp mould, Dummy: 6 kg.

Controlled shock test		Dynamic compression test (Traditional theory)		dGs	
$V_c$ (m/s)	$PRA_{cs}(V_c)$ (G)	$V$ (m/s)	$PRA_{ff}(V)$ (G)	$V$ (m/s)	$PRA_{cs}(V_c) - PRA_{ff}(V)$ (G)
3.39	80.6	3.39	73.3	3.39	7.3
3.40	79.1	3.39	73.8	3.39	6.8
3.40	80.1	3.40	73.9	3.40	5.2
3.41	77.4	3.41	72.8	3.40	6.2
3.42	82.2	3.42	72.9	3.41	4.6
3.43	79.9	3.42	73.0	3.42	9.3
3.43	80.0	3.43	76.8	3.42	9.2
3.44	80.4	3.43	76.9	3.43	3.1
⋮	⋮	⋮	⋮	⋮	⋮

group 1   
  group 2   
  group 3   
  group 4   
  group 5   
  group 6   
 ...

Table 3-6 Example of dGs Calculation.  $\Gamma_{after}$ , Corrugated Sleeve, Dummy: 6 kg.

①		②		③			④	
Controlled shock test	Corrected velocity	Dynamic compression test (Friction theory)		Data Arrangement			dGs	
$PRA_{cs}(V_c)$ (G)	$V_{new}$ (m/s)	$V_{new}$ (m/s)	$PRA_{ff}(V_{new})$ (G)	$PRA_{cs}(V_c)$ (G)	$V_{new}$ (m/s)	$PRA_{ff}(V_{new})$ (G)	Velocity (m/s)	dGs (G)
60.4	3.49	3.48	56.5	60.4	3.49	58.5	3.49	1.9
60.4	3.51	3.49	58.5			62.8	3.49	-2.4
64.2	3.51	3.49	62.8			59.5	3.49	0.9
62.5	3.43	3.47	59.5	60.4	3.51	60.7	3.51	-0.3
61.8	3.48	3.49	59.5	64.2		62.8	3.51	-2.4
62.4	3.43	3.43	57.2	61.8	3.48	56.5	3.51	3.5
63.1	3.52	3.55	59.3	62.5	3.43	57.2	3.51	1.4
60.3	3.50	3.50	56.0	62.4		58.0	3.48	5.3
⋮	⋮	⋮	⋮	⋮	⋮	⋮	⋮	⋮

Data of  $PRA_{ff}(V_{old})$  when  $V = 3.43$  m/s

## B) Graphics of probability distributions of dGs

The probability distribution of dGs was obtained by the following data process.

1. Once all dGs values are calculated, their number is counted and recorded as  $N$ .
2. The dGs is separated by 1 G increments. For example: if dGs is between 0 G and 3.4 G, it is separated into the following four bins:  $0 \leq dGs < 1$ ,  $1 \leq dGs < 2$ ,  $2 \leq dGs < 3$  and  $3 \leq dGs < 4$  (G).
3. Count and record the number of each dGs,  $n_i$ , in each bin.
4. Calculate the probability  $P = n_i/N$ .

The probability distributions of dGs before and after the correction of the two test materials are plotted in Figures 3-11 and 3-12. From these plots, we draw the following conclusions.

1. When a light weight dummy is used, dGs is large both before and after the correction.
2. By increasing the dummy weight, dGs reduces gradually.
3. dGs after the correction is more likely to reach 0 G than that before the correction. This behavior becomes more prominent as the dummy weight increases.

It should be noted that the bar numbers (horizontal axis) for aggregated data differ among the weight dummies because of the varied deviations under different dummies.

On the basis of the bar charts of the probability distribution of dGs, we can qualitatively conclude that the friction theory is applicable to SCM under different stresses. However, at this stage, we cannot quantify the corrective effect of the friction theory.

### 3.2.5 Chi-square test

A chi-square test is widely used to decide whether the distribution of a single variable conforms to an expected distribution such as the normal distribution. Among several versions of the chi-square test, Pearson's chi-squared test ( $\chi^2$ ) is well known. This test assesses goodness of fit, homogeneity and independence. The goodness of fit test establishes whether an observed frequency distribution differs from a theoretical distribution. The homogeneity test compares the distribution of counts in two or more groups on the same categorical variable, while independence test assesses whether paired observations on two variables, expressed in a contingency table, are independent. In this study, the homogeneity test was used as a qualitative measure of the corrective effect of the friction equivalent drop theory<sup>[9]</sup>.

The chi-square homogeneity test is calculated as follows:

1. State hypotheses ( $H_0$  and  $H_a$ ).
2. Find expected values for each cell ( $V_{exp}$ ).
3. Compute the chi-squared statistic ( $\chi^2$ ) given by Eq. (3.13).

$$\chi^2 = \sum_{\text{all cells}} \frac{(V_{obs} - V_{exp})^2}{V_{exp}} \quad (3.13)$$

where  $V_{obs}$  and  $V_{exp}$  are the observed and expected values, respectively.

4. Determine the critical value of  $\chi^2(\chi^2^*)$  from the  $\chi$ -table based on the degree of freedom ( $d_f$ ) and  $\alpha$  level.
5. Decision: if  $\chi^2 > \chi^2^*$ , then reject  $H_0$ ; otherwise accept it.

The calculation of chi-square homogeneity is demonstrated using the data from graphic 6 in Figure 3-12. The results are presented in Table 3-7. The observed values are shown in the left column of the table. Analyzing the experimental data, we found that dGs varies within 0–8 G. Therefore, the column 'dGs' is separated into eight rows. The 'Before correction' and 'After correction' entries are the dGs counts.



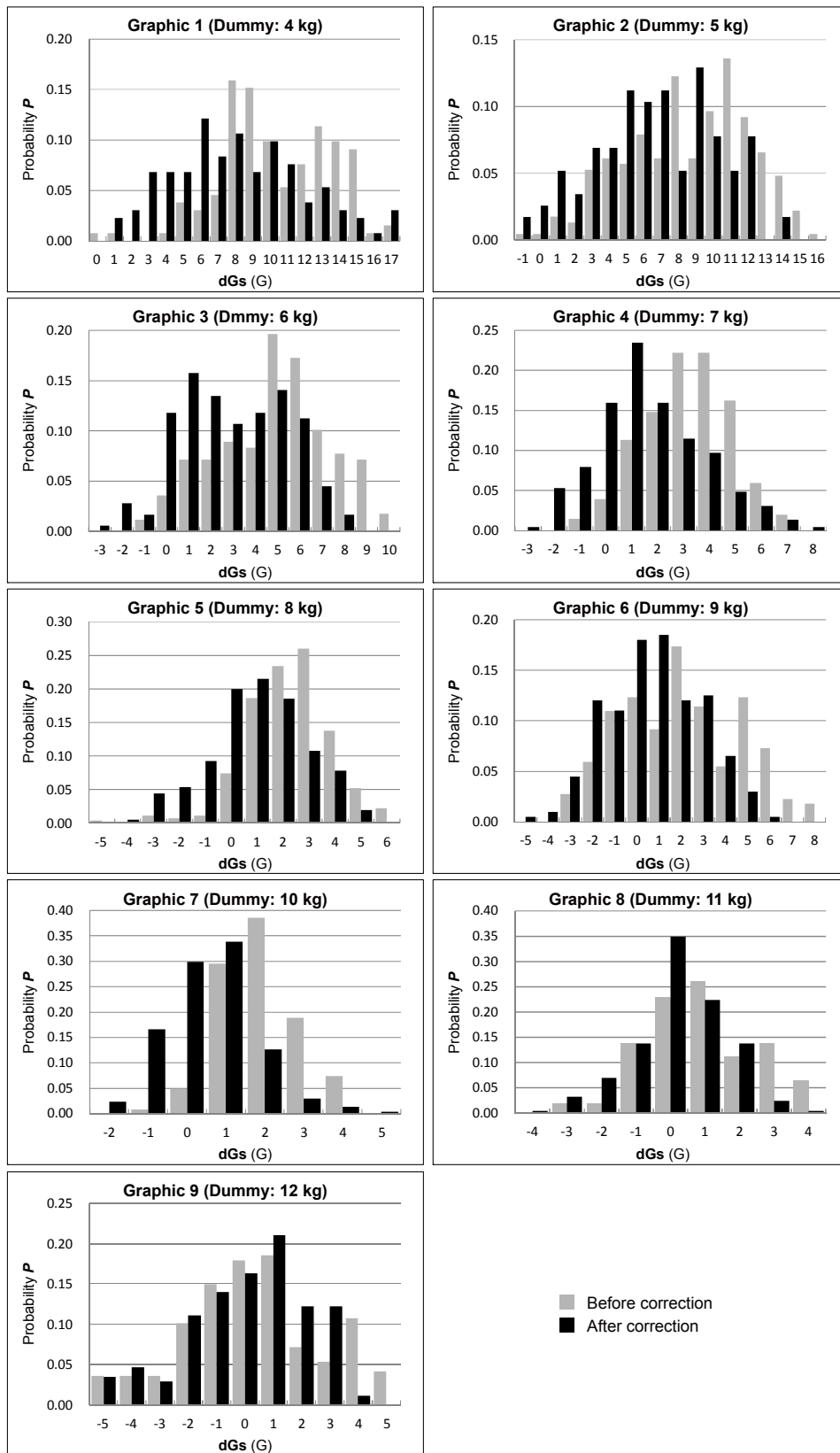


Figure 3-11 Probability Distribution of dGs of Corrugated Sleeve for Different Weight Dummies.

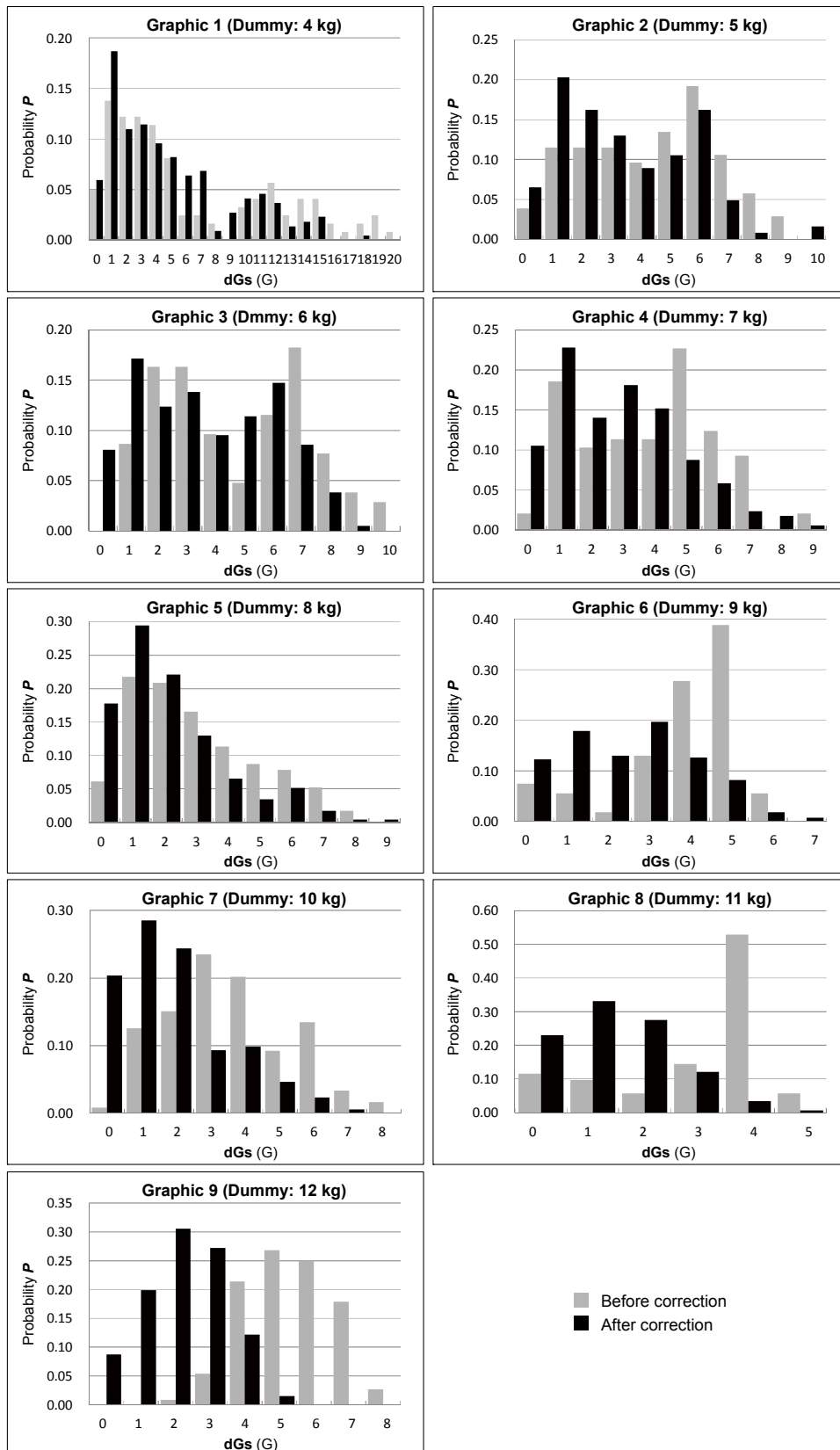


Figure 3-12 Probability Distributions of dGs of Pulp Mould for Different Weight Dummies.

There are five steps in the calculation process:

1. Determine the hypotheses. The variables are the dGs distribution and results of the friction theory (before and after correction). Therefore, the hypotheses are defined as  
 $H_0$ : the distribution of dGs is the same before and after correction;  
 $H_a$ : the distribution of dGs is different before and after correction.
2. Compute the expected counts before and after correction by multiplying the overall before and after correction proportions by the total counts in each category. For example,  $0 \leq dGs < 1$  (before correction) =  $19\% \times 37 \approx 7$ ;  $4 \leq dGs < 5$  (after correction) =  $81\% \times 49 \approx 40$ . The expected values are shown in the right columns of Table 3-7.
3. Substitute the observed and expected values into Eq. (3.14);  $\chi^2$  was calculated as 47.0.
4. Compute  $\chi^{2*}$ . The degree of freedom  $d_f = (\text{number of rows} - 1) \times (\text{number of columns} - 1) = (8 - 1) \times (2 - 1) = 7$ . The assumed  $\alpha$  level is 5%. From the  $\chi$ -table, we find that for  $d_f = 7$  and  $\alpha = 5\%$ ,  $\chi^{2*} = 14.1$ .
5. Because  $\chi^2$  is greater than  $\chi^{2*}$ , reject  $H_0$ . The distribution of dGs is different between the before and after correction values.

Similar chi-square tests were performed on the data of the remaining eight dummy weights. The results are presented in Table 3-8. Evidently,  $\chi^2 > \chi^{2*}$  in the tests involving dummies of 6–12 kg, but  $\chi^2 < \chi^{2*}$  in the tests involving dummies of 4 and 5 kg. Therefore, the dGs distribution is rendered more significant by the correction for impact velocity.

Table 3-7 Observed and Expected Values Used in an Example of Chi-square Test.

dGs (G)	Observed Value ( $V_{obs}$ )			Expected Value ( $V_{exp}$ )	
	Before correction	After correction	Total	Before correction	After correction
$0 \leq dGs < 1$	4	33	37	7	30
$1 \leq dGs < 2$	3	48	51	10	41
$2 \leq dGs < 3$	1	35	36	7	29
$3 \leq dGs < 4$	7	53	60	11	49
$4 \leq dGs < 5$	15	34	49	9	40
$5 \leq dGs < 6$	21	22	43	8	35
$6 \leq dGs < 7$	3	5	8	2	6
$7 \leq dGs < 8$	0	2	2	0	2
Total	54	232	286		
Observed distribution	19 %	81 %	100 %		

It should be noted that the chi-square tests only proved variations of dGs before and after the correction. They did not indicate whether the correction resulted in positive or negative changes or the degree to which the corrective effects change. Therefore, we cannot quantitatively evaluate the effects of the friction theory based only on the bar charts of the probability distribution of dGs.

Table 3-8 Results of Chi-square Tests of Homogeneity for Graphics 1–9 in Figure 3-12.

Dummy weight (kg)	4	5	6	7	8	9	10	11	12
$d_f$	20	10	10	9	9	7	8	5	8
$\chi^{2*}$	31.4	18.3	18.3	16.9	18.3	14.1	15.5	11.1	15.5
$\chi^2$	28.3	17.3	31.5	30.6	24.5	47.0	68.3	162.6	225.0

### 3.2.6 Evaluation of correction effect

#### A) Data normalization

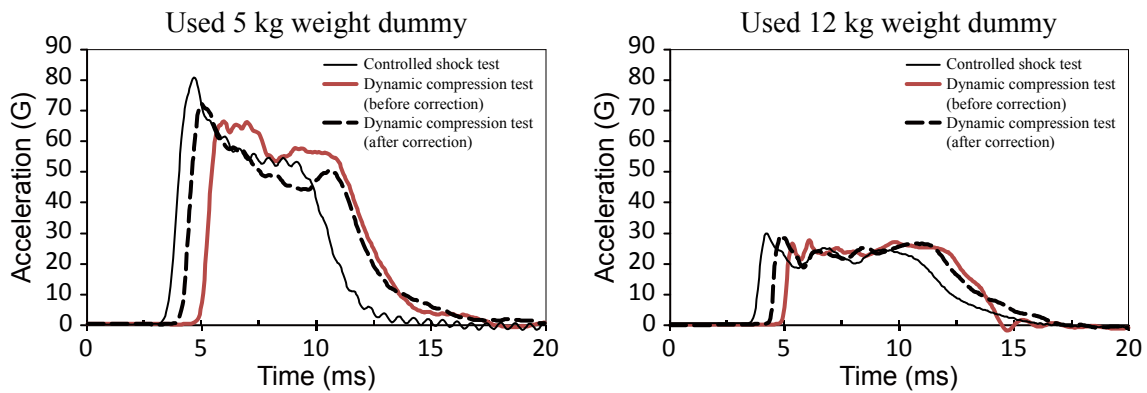


Figure 3-13 Response Accelerations of the Two Tests using 5 kg and 12 kg Weight Dummies.

Figure 3-13 shows response acceleration curves generated by the controlled shock and dynamic compression tests using 5 kg and 12 kg weight dummies. The PRAs of the same test under different stresses considerably differ. In other words, because the correction effect is being evaluated on varying datasets, the test results cannot be directly compared. To enable a direct comparison of the test results, the influence of varying comparison basis must be removed by data normalization.

To perform data normalization, we first require the true value of the PRA. To this end, we measure both  $PRA_{cs}(V_c)$  and  $PRA_{ff}(V)$  and determine which type represents the true value of the PRA. According to the aforementioned test method, when  $h = 0.6$  m,  $V_{th} = 3.43$  m/s. Therefore, the PRA when  $V = 3.43$  m/s under the dynamic compression test,  $PRA_{ff}(V_{=3.43})$ , must be the true value. In fact, several  $PRA_{ff}(V_{=3.43})$  measurements were obtained during the dynamic compression test. Therefore, for data normalization, we compute the average  $PRA_{ff}(V_{=3.43})$ .

The data normalization equation  $\Gamma$  is defined as

$$\Gamma = \frac{\sum_n (PRA_{cs}(V_c) - PRA_{ff}(V))}{PRA_{ff}(V_{=3.43})}. \quad (3.15)$$

To accommodate both types of  $A_{ff_{max}}(V)$ , Eq. (3.15) is divided into the following two equations:

$$\Gamma_{before} = \frac{\sum_n (PRA_{cs}(V_c) - PRA_{ff}(V_{old}))}{PRA_{ff}(V_{=3.43})}, \quad (3.16)$$

$$\Gamma_{\text{after}} = \frac{\sum_n (\text{PRA}_{cs}(V_c) - \text{PRA}_{ff}(V_{\text{new}}))}{\text{PRA}_{ff}(V_{=3.43})}. \quad (3.17)$$

Here  $\text{PRA}_{cs}(V_c)$  is the PRA of the controlled shock test for a specified  $V_c$  (e.g.  $V_c = 3.45$  m/s), While  $\text{PRA}_{ff}(V_{\text{old}})$  is the PRA of the dynamic compression test based on the traditional theory when  $V$  is equal to the aforementioned  $V_c$  (i.e.  $V = 3.45$  m/s). Similarly,  $\text{PRA}_{ff}(V_{\text{new}})$  is the PRA of the dynamic compression test based on the friction theory when  $V = V_{\text{new}}$  (i.e.  $V_{\text{new}}$  is calculated for  $V_c = 3.45$  m/s based on the friction theory, using the data obtained from the controlled shock test).

## B) Correction indicator

If the PRA data alone are considered in each test, Figure 3-13 can be generalized to Figure 3-14. After data normalization, Figure 3-14(b) is the result of applying data normalization on Figure 3-14(a). Using a parameter  $\Gamma$ , we can compare the correction effect under different stresses. However, the correction effect cannot be evaluated as  $\Gamma_{\text{before}} - \Gamma_{\text{after}}$ , because, as seen in Figure 3-14(b), the errors vary widely when different weight dummies are used.

Therefore, we propose a new correction indicator  $\Delta$ , defined as

$$\Delta = \frac{\Gamma_{\text{before}} - \Gamma_{\text{after}}}{\Gamma_{\text{before}}} \times 100\%. \quad (3.18)$$

This quantity represents the degree to which the friction theory can improve the equivalent precision of the two tests, compared to the uncorrected results. A larger value indicates a better corrective effect.

Figure 3-14(c) is the result of applying the correction indicator  $\Delta$  to Figure 3-14(b).

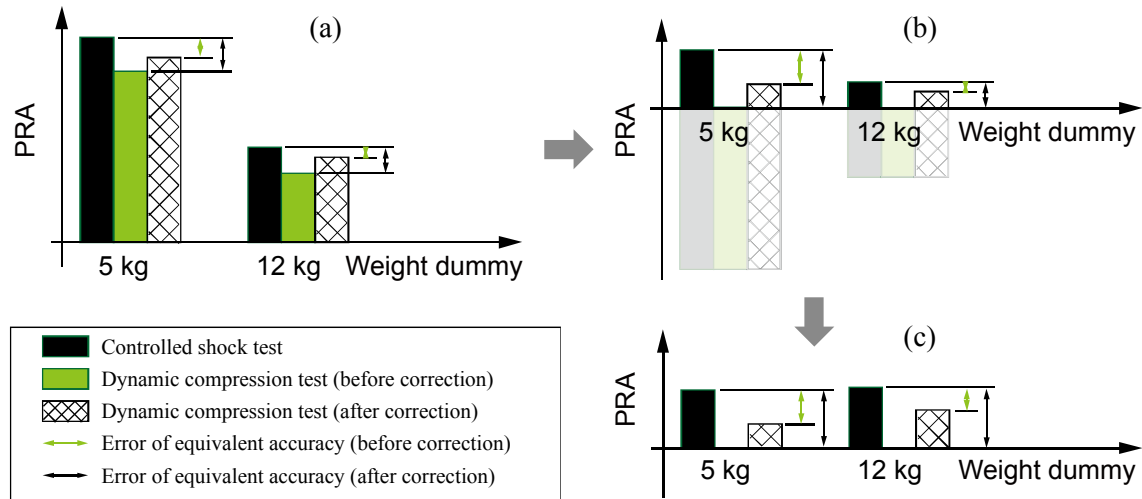


Figure 3-14 Schematic of Correction Indicator.

## 3.2.7 Discussion

The statistical analyses of the corrugated sleeve and pulp mould cushions are summarized in Table 3-9. Columns ① and ② contain the dummy weights and the average  $\text{PRA}_{ff}(V_{=3.43})$ , respectively. Column ③ shows the average dGs. The data in column ④ are the standard deviations of the dGs. The data in

column ⑤ are the correction indicator  $\Delta$ . Figures 3-15–3-22 provide an intuitive visual interpretation of the tabulated analyses.

On the basis of these data, we conclude the following conclusions:

1. The PRA of the dynamic compression test decreases as the dummy weight increases. From the equivalent drop theory, the same trend is expected in the controlled shock test.
2. For the corrugated sleeve, the standard deviations of dGs before and after the correction decrease with increasing dummy weight. Standard deviations of dGs are reduced after the correction. For the pulp mould, the standard deviations of the dGs trend to decrease with the increase of the weight dummy. For both cushions, the average deviation in the dGs behaves similarly to the standard deviation.
3. For the corrugated sleeve, the corrective effect imparted to weight dummies of 4 kg and 5 kg is approximately 20 %, increasing to approximately 80 % at a 12 kg dummy weight. For the pulp mould, a similar corrective effect (20 %) is imparted to the 4–6 kg dummies, increasing to 60 % at a 12 kg dummy weight. Together with the cushion curves (Figures 3-15 and 3-19), we conclude that the corrective effect becomes more significant toward to the lowest point of the cushion curve.

Table 3-9 Experimental Results of Corrugated Sleeve and Pulp Mould Cushions.

	① (kg)	② (G)	③ (G)		④ (G)		⑤
			before <sup>a</sup>	after <sup>b</sup>	before	after	
Corrugated sleeve	4	80.3	10.55	8.04	3.18	3.85	23.80 %
	5	67.0	8.76	6.62	3.57	3.55	24.41 %
	6	57.2	5.02	3.00	2.50	2.40	40.34 %
	7	50.0	3.33	1.64	1.66	2.08	50.77 %
	8	45.0	2.37	1.00	1.64	1.85	57.89 %
	9	40.5	2.20	0.68	2.75	2.10	69.01 %
	10	36.8	1.96	0.53	0.98	1.12	72.81 %
	11	34.5	0.84	0.17	1.87	1.54	80.30 %
12	30.4	0.40	0.06	2.46	2.14	84.73 %	
Pulp mould	4	106.5	6.27	4.91	5.46	4.10	21.82 %
	5	86.1	4.38	3.37	2.37	2.36	23.17 %
	6	78.0	4.82	3.66	2.53	2.31	23.97 %
	7	65.8	3.96	2.81	2.18	1.96	29.07 %
	8	58.2	3.04	2.12	2.02	1.78	30.16 %
	9	52.4	3.04	2.48	1.49	1.63	36.88 %
	10	47.4	3.63	1.93	1.80	1.56	46.74 %
	11	44.5	3.04	1.47	1.43	1.05	51.59 %
12	38.7	5.42	2.26	1.26	1.14	58.27 %	

① Dummy weights.

② Average PRA of the dynamic compression test when  $V=3.43$  m/s.

③ Average dGs.

④ Standard deviations of dGs.

⑤ Correction indicator  $\Delta$  (a larger value indicates better corrective effect).

<sup>a</sup> Before correction using the friction theory.

<sup>b</sup> After correction using the friction theory.

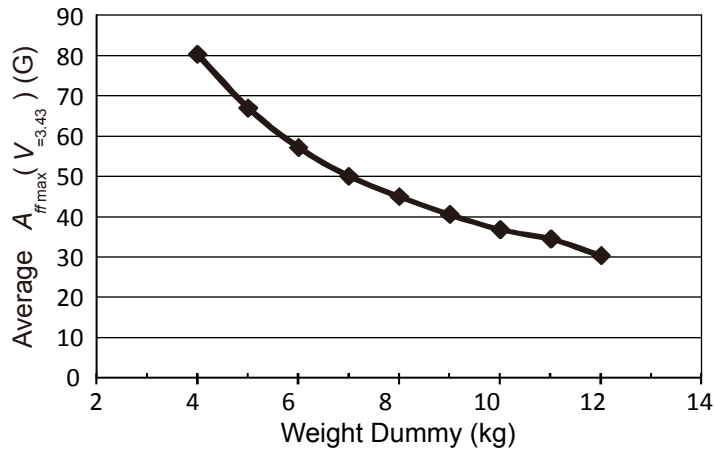


Figure 3-15 Cushion Curve for Corrugated Sleeve.

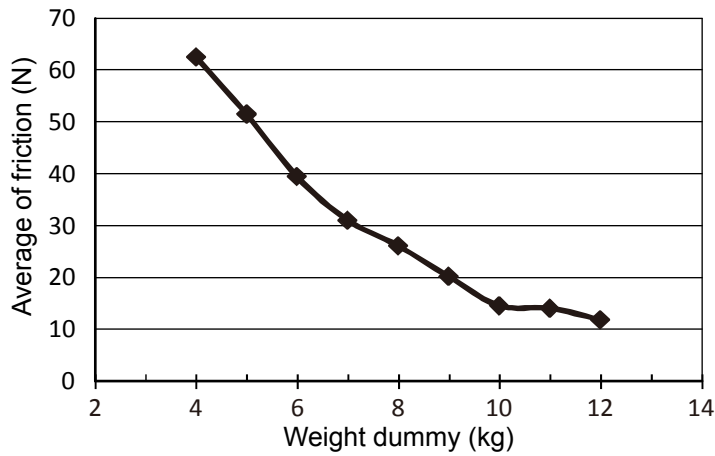


Figure 3-16 Friction Curve for Corrugated Sleeve.

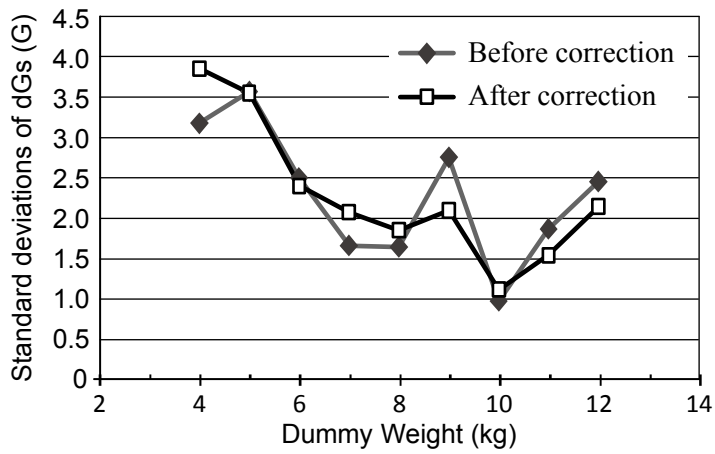


Figure 3-17 Standard Deviations of dGs Curves for Corrugated Sleeve.

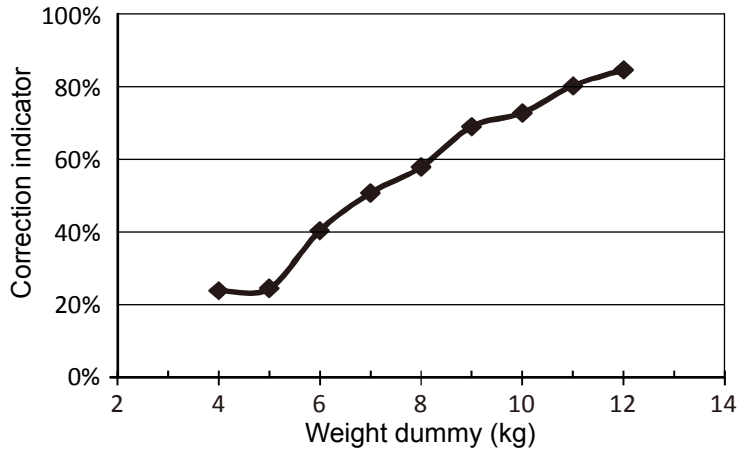


Figure 3-18 Correction Indicator Curve for Corrugated Sleeve.

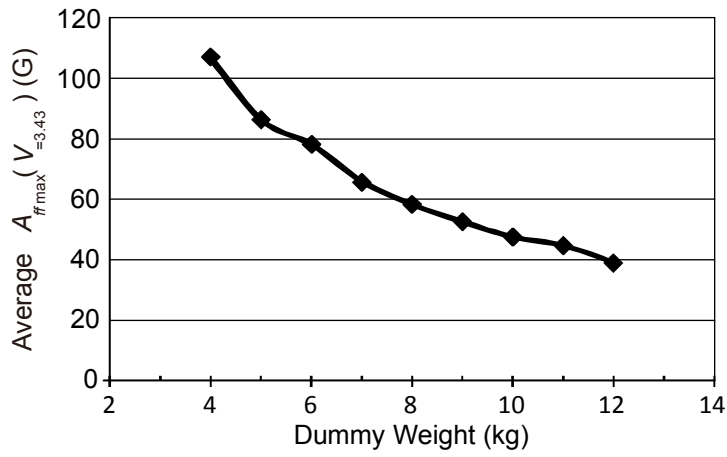


Figure 3-19 Cushion Curve for Pulp Mould.

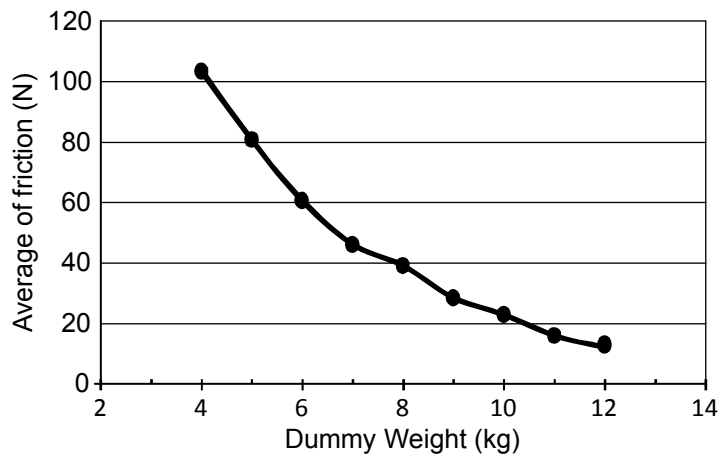


Figure 3-20 Friction Curve for Pulp Mould.



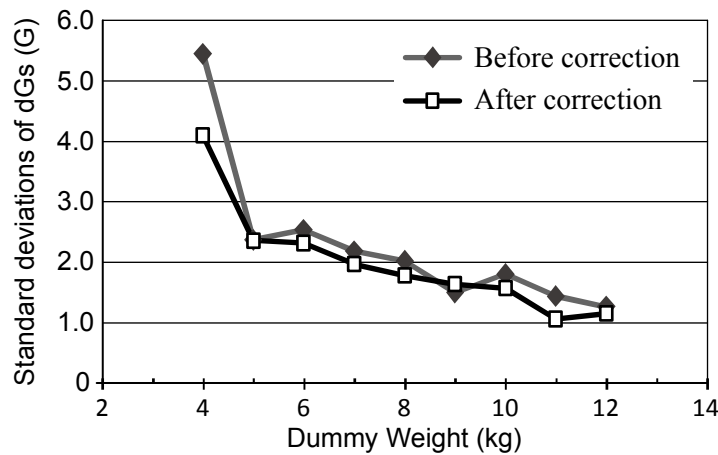


Figure 3-21 Standard Deviations of dGs Curves for Pulp Mould.

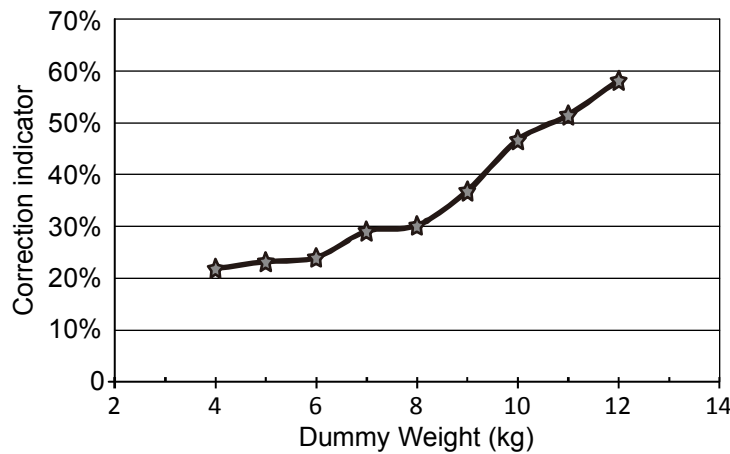


Figure 3-22 Correction Indicator Curve for Pulp Mould.

### 3.3 References

- [1] Chen ZHONG, Katsuhiko SAITO and Kazuaki KAWAGUCHI. Improvement of Equivalent Drop Theory for Transport Packaging. *International Journal of Packaging Technology and Science*. 2013; 26(2): 67–81.
- [2] Katsuhiko SAITO and Chen ZHONG. Modified Simulated Drop Test for Transmitted Shock Characteristics of Structural Plastic Foam Cushioning Materials. *17th IAPRI World conference on Packaging*, 2009.
- [3] Chen ZHONG and Katsuhiko SAITO. Modified Simulated Drop Test for Transmitted Shock Characteristics of Structural Corrugated Fiberboard. *Journal of Applied Packaging Research*. 2010; 4(4): 189–201.
- [4] Cyril M. Harris and Allan G. Piersol. *Harris' Shock and Vibration Handbook (Fifth Edition)*, McGraw-Hill, 2002.
- [5] Yoshida Seiki Co., Ltd. *Dynamic Compression Tester User's Guide (in Japanese)*. ACST-200 serial.
- [6] Yoshida Seiki Co., Ltd. *Shock Machine User's Guide (in Japanese)*. ASQ-700 serial.

- [7] Yukiomi NAKAGAWA. Study on Packaging Design by Paper Cushioning Materials (in Japanese). *Doctoral dissertation*, 2008.
- [8] S. Bran, D. Ewins and S. S Rao. Encyclopedia of Vibration, Academic Press, 2002.
- [9] Robert V. Hogg and Allen T. Craig. Introduction to Mathematical Statistics, Prentice Hall, 1994.

This page is intentionally left blank

# CHAPTER 4. THE HYBRID DROP TEST

## 4.1 Introduction

During transit from manufacturers to consumers, products are vulnerable to shock and vibration hazards. Shock hazards are greatly reduced by cushion packaging. Several technical assessments can be used to verify the cushioning performance of a package (e.g. the cushion curve or damage boundary curve)<sup>[1]</sup>. Generally, a drop test is indispensable to achieve technical assessments. Traditionally, a well-known free fall test and a controlled shock test methods are used, as mentioned in Sections 1.4 and 1.5.

Generally, traditional drop testing methods are applied to determine whether the PRA is within the desired range and product is likely to be damaged (i.e. whether the cushioning provides sufficient protection). However, the test dummy will be damaged with high probability under traditional testing methods. Damage must be avoided when the product is very valuable or in limited supply. For example, Figure 4-1 shows a printer encased in a cushioning package. Unrestrained traditional drop tests on such a valuable product should never be attempted.

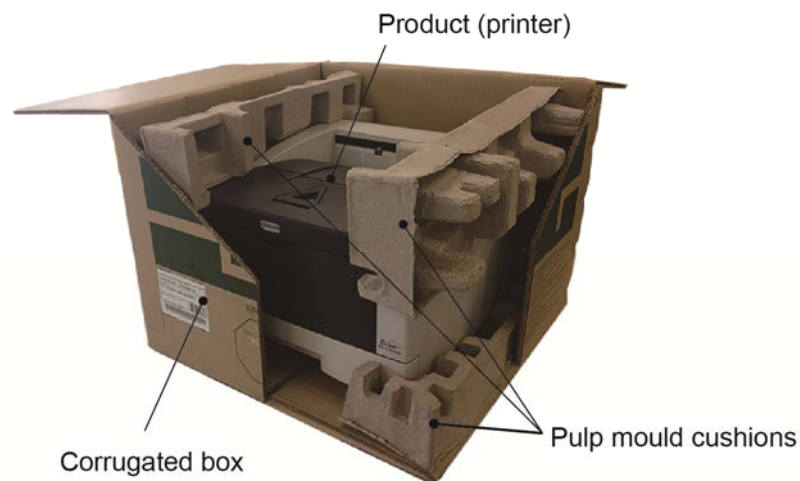


Figure 4-1 Example of a High-value Package.

In addition to physical test methods, such as the free fall and controlled shock tests, a number of widely used simulation methods, such as ANSYS<sup>®</sup><sup>[2]</sup>, LS-DYNA<sup>®</sup><sup>[3]</sup> and MSC Nastran<sup>™</sup><sup>[4]</sup>, are available. In general, a digital simulation proceeds as follows. First, the physical characteristics of the cushioning material are evaluated in preliminary tests. The data derived from these tests are converted to native parameters that can be used by the simulation software, and the simulation is run. Although the cushioning performance of the transport packaging can often be verified without repeated testing, digital simulation is particularly advantageous if repeat tests are necessary.

Simulation methods are perfectly adequate in many engineering applications, but they are insufficient for transport packaging because of the physical characteristics of the cushioning materials. Two common cushioning materials in packaging construction are paper and plastic, both of which exhibit nonlinear characteristics. The physical characteristics of such nonlinear materials are difficult to determine with sufficient accuracy to satisfy the requirements of a simulation method.

Packaging design and testing regulations are often specified. On the basis of the design requirements, the drop height is established as 80 cm. At this height, however, the damage boundary of the product is approached. Since our product must absolutely not be damaged during the verification test, the traditional free fall and controlled shock test methods are precluded, and an alternative evaluation method is sought.

## 4.2 Concept of New Testing Method

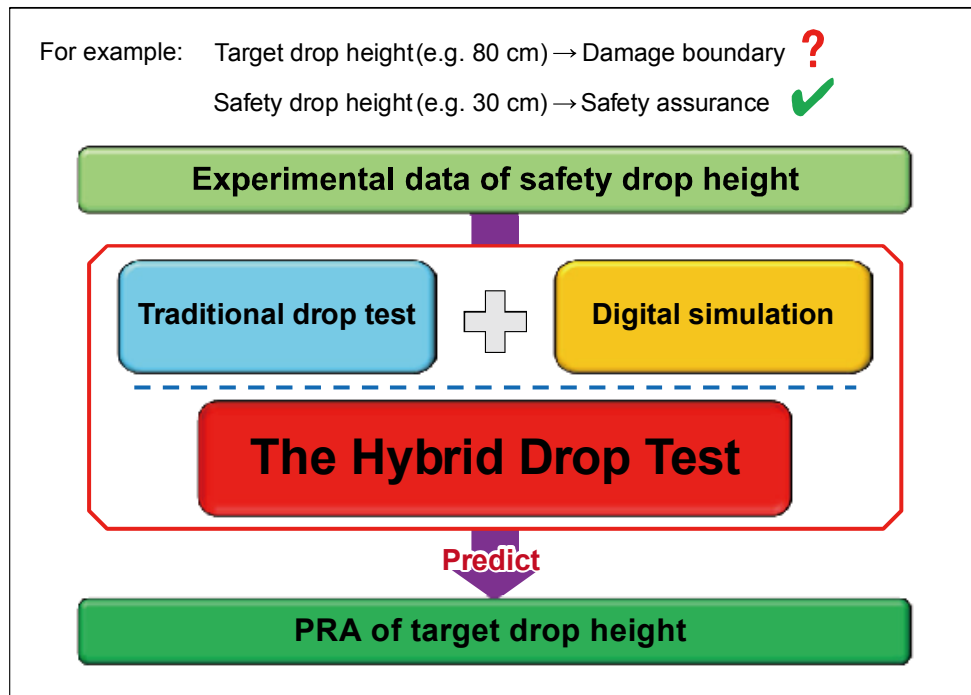


Figure 4-2 Conceptual Graphic of Proposed Testing Method.

The proposed method will protect fragile products as follows. First, we assume that a drop height  $H$  of 30 cm is safe on the basis of experience. Second, given that an 80 cm target drop height is dangerous, a drop test is performed at the safer drop height of 30 cm. Finally, using a digital simulation, we try to predict results for an 80 cm target drop height on the basis of data from a 30 cm safety drop height. If the attempt is successful, the issues outlined in the previous section are circumvented. A conceptual graphic of the new testing method is shown in Figure 4-2.

## 4.3 Hybrid Drop Test

As explained above, the proposed method combines traditional drop testing and simulation methods. By contrast to the free fall and controlled shock testing methods, this new method is called 'the hybrid drop testing method'. The hybrid drop testing method predicts the PRA generated by the designed conditions or higher drop heights from the results of a single low-height drop test. This method provides packaging researchers with an alternative means of testing their design, ensures the safety of the test product and improves test efficiency.

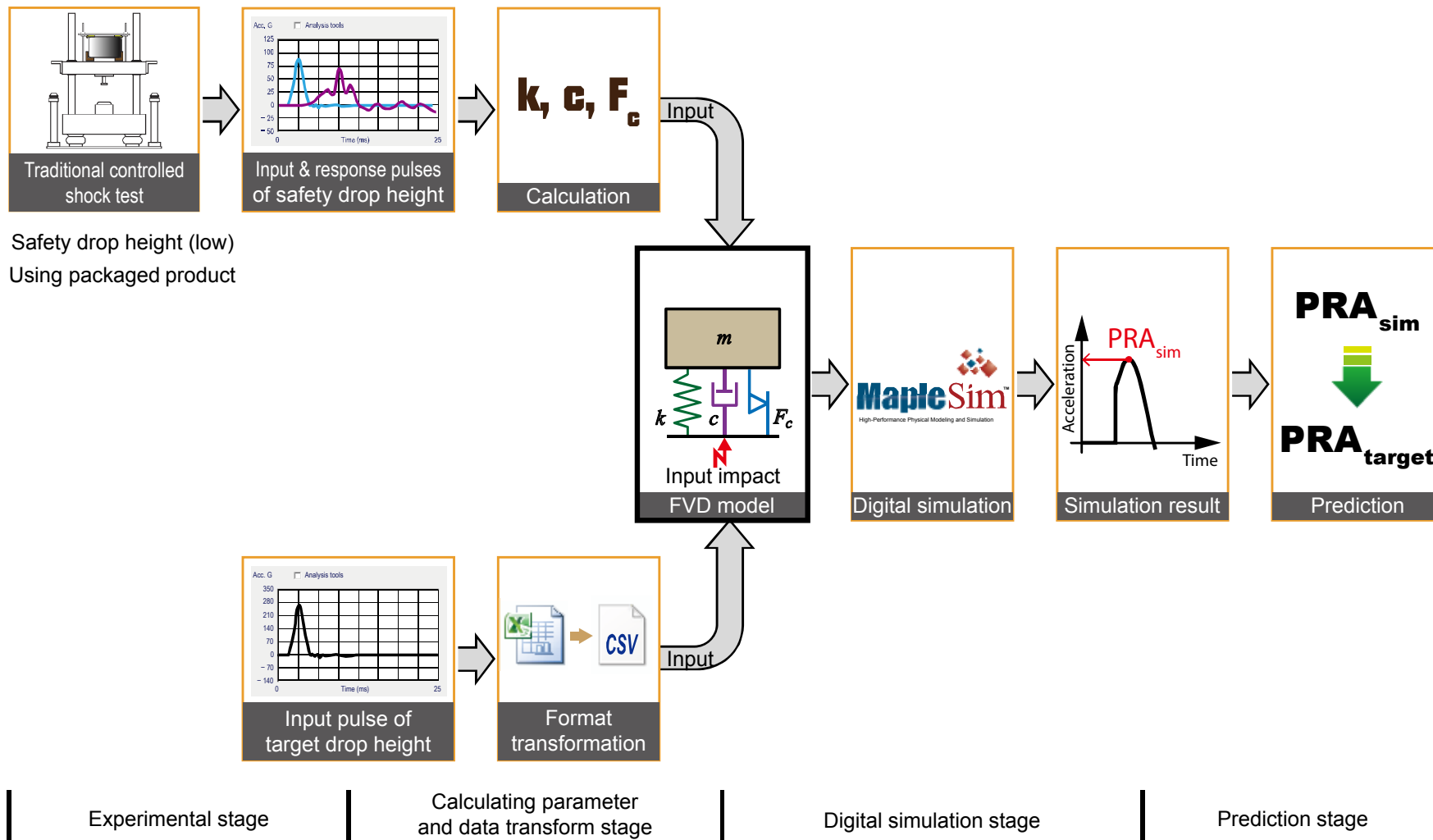


Figure 4-3 The Hybrid Drop Testing Method.

The hybrid drop test is illustrated in Figure 4-3. Centered on the FVD model, the method has the following four stages.

- Stage I: Experimental stage.
  - i. Determine the target and safety drop heights according to the design requirements.
  - ii. Using a packaged product, implement the controlled shock test at the safety drop height. Record input and response pulse data.
  - iii. Perform the controlled shock test to obtain an input pulse for the target drop height.
- Stage II: Parameter calculation and data transform stage.
  - i. Calculate parameters  $m$ ,  $k$ ,  $F_c$  and  $c$  of the FVD model from the experimental data.
- Stage III: Digital simulation stage.
  - i. Build a simulation FVD model in the simulation software.
  - ii. Input parameters  $m$ ,  $k$ ,  $F_c$  and  $c$  and the input pulse of the target drop height to the simulation FVD model. Run the simulation.
- Stage IV: Prediction stage.
  - i. From the PRA of the simulation results  $PRA_{sim}$ , predict the PRA for the target drop height  $PRA_{target}$ .

The details of each stage in the hybrid drop testing method are given in the following subsection.

## 4.4 Experimental Stage

Two controlled shock tests are required at the experimental stage. The two tests differ in drop height, whether they involve packaged product and recorded data.

### 4.4.1 First controlled shock test

The first controlled shock test is performed at the safety drop height. This test obtains data for calculating the parameters of the FVD model. In the first controlled shock test, the product is safe because the safety drop height is assured. The test method is conducted in the following steps.

- 1 Determine the safety drop height and raise the shock table to this level.
- 2 Fix the packaged product to the shock table.
- 3 Simultaneously release the package and shock table, and record the experimental data (e.g. input acceleration, response acceleration and impact duration).

### 4.4.2 Second controlled shock test

The second controlled shock test is performed at the target drop height. This test obtains the input pulse at the target drop height without requiring the product. The test method is conducted as follows.

- 1 Determine the target drop height and raise the shock table to this level.
- 2 Release the shock table and record the input pulse.

## 4.5 Calculating Parameters and Data Transform Stage

Calculation of the parameters  $m$ ,  $k$ ,  $F_c$  and  $c$  is a key step in the hybrid drop test. The calculations of  $k$ ,  $F_c$  and  $c$  are complicated and shown in Figure 4-4.

### 4.5.1 Calculating $m$

Mass  $m$  is weighed directly.

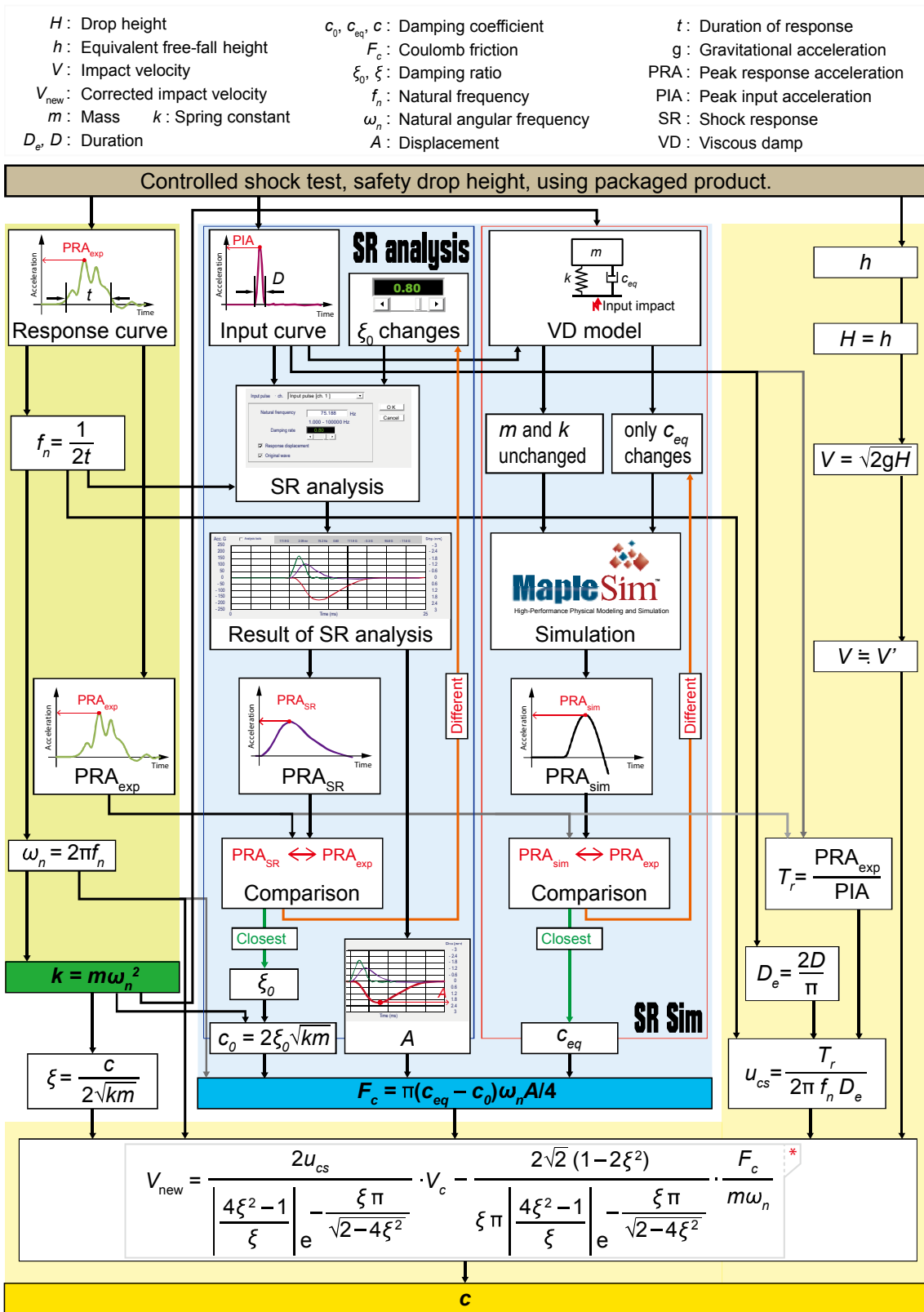


Figure 4-4 Schematic of Calculation of  $k$ ,  $F_c$  and  $c$ .



### 4.5.2 Calculating $k$

From the vibrational theory<sup>[5]</sup>,  $k$  is expressed as  $\omega_n = \sqrt{k/m}$ . The FVD model is the damping system, whose natural angular frequency  $\omega_d$  is given by<sup>[6]</sup>

$$\omega_d = \omega_n \sqrt{1 - \zeta^2}. \quad (4.1)$$

Since the value of  $\zeta$  is unknown,  $k$  cannot be explicitly determined from  $\omega_d$ . However, Eq. (4.1) can be rewritten as

$$\Omega_{\text{error}} = \frac{\omega_d}{\omega_n} = \sqrt{1 - \zeta^2}. \quad (4.2)$$

The relationship between  $\Omega_{\text{error}}$  and  $\zeta$  is shown in Table 4-1.

Table 4-1 Relationship between  $\Omega_{\text{error}}$  and  $\xi$ .

$\xi$	$\Omega_{\text{error}}$
0.1	0.9950
0.2	0.9798
0.3	0.9539
0.4	0.9165
0.5	0.8660

We observe that  $\Omega_{\text{error}}$  is smaller than 0.9 when  $\zeta$  is smaller than 0.4. That is,  $\omega_n$  approximates  $\omega_d$  when  $\zeta < 0.4$ . In this study,  $\zeta$  was calculated as  $0.2 \pm 0.03$ . Thus,  $k$  can be approximated in terms of substituting  $\omega_n$  for  $\omega_d$ . The method is described as follows. From the experimental data, we obtain the response curve of the product and read the duration of the response  $t$ . We then calculate  $f_n$  from  $f_n = 1/(2t)$  to yield  $\omega_n = 2\pi f_n$  and  $k = m\omega_n^2$ .

### 4.5.3 Calculating $F_c$

As mentioned in Section 3.1.4, friction  $F_c$  is given by Eq. (3.6).

#### A) Calculating $c_0$ and $A$

The input pulse on the shock table is determined from the experimental data. The input pulse curve is used in the SR analysis. Here the damping rate  $\zeta$  is varied from 0 to 1 while  $f_n$  is fixed at its calculated value. From the varying SR analysis results, we directly obtain the PRA of the SR analysis ( $\text{PRA}_{\text{SR}}$ ) and the value of  $A$  (Figure 4-5). The experimental PRA ( $\text{PRA}_{\text{exp}}$ ) is known from the experimental data. Next, we compare  $\text{PRA}_{\text{SR}}$  with  $\text{PRA}_{\text{exp}}$  and record the  $\zeta$  and  $A$  when  $\text{PRA}_{\text{SR}}$  is closest to  $\text{PRA}_{\text{exp}}$ . The damping coefficient  $c_0$  is then calculated as  $c_0 = 2\zeta\sqrt{km}$ .

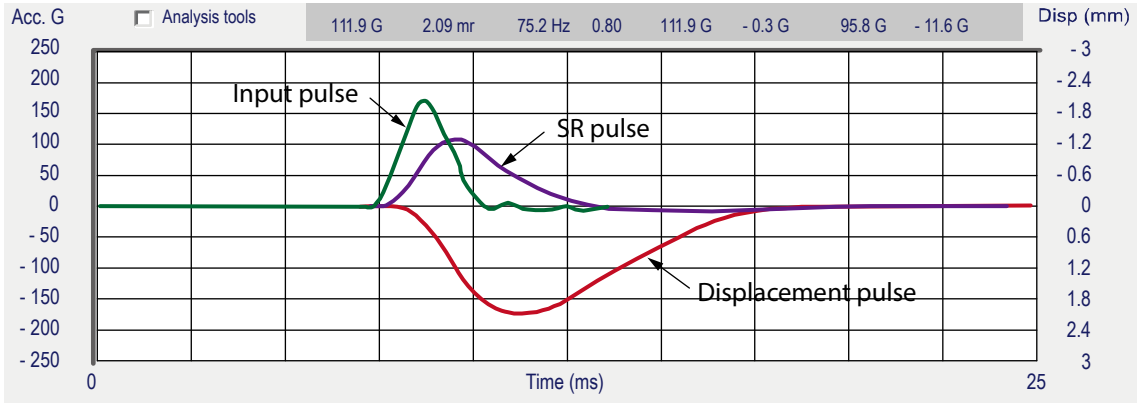


Figure 4-5 Screenshot of SR Analysis Results.

## B) Calculating $c_{eq}$

The equivalent damping coefficient  $c_{eq}$  is determined by the SR Sim method [6]. The VD model is constructed in MapleSim. The corresponding parameters are input, and the simulations are run. The values of  $m$  and  $k$  are calculated beforehand and remain fixed, while  $c$  is varied, yielding a range of curves. When the  $PRA_{sim}$  of a curve is closest to  $PRA_{exp}$ ,  $c_{eq}$  is recorded.

### 4.5.4 Calculating $c$

Table 4-2 Comparison between  $V$  and  $V_{new}$ .

No.	$h$ (cm)	$c$ (Ns/m) <sup>1</sup>	$V$ (m/s) <sup>2</sup>	$V_{new}$ (m/s) <sup>3</sup>	$V_{new} - V$ (m/s)
1	10	1150	1.40	1.24	-0.16
2		1200		1.64	0.24
3		1100		1.26	-0.14
4		1200		1.70	0.30
5		1150		1.54	0.14
1	20	1200	1.97	1.65	-0.33
2		1250		2.25	0.27
3		1200		2.18	0.20
4		1200		2.25	0.27
5		1150		1.98	0.00
1	30	1300	2.42	2.83	0.41
2		1250		2.77	0.34
3		1250		2.71	0.29
4		1300		2.79	0.37
5		1250		2.63	0.21

<sup>1</sup> Using SR Sim method mentioned in Section 3.1.4.

<sup>2</sup> Calculated by  $V = \sqrt{2gh}$ .

<sup>3</sup> Calculated by Eq. (2.98).

Applying the friction theory,  $c$  is initially calculated using the SR Sim method mentioned in Section 3.1.4 (see ‘calculating  $\zeta$ ’). However, this process is time consuming, because many iterations of the simulations may be required to find a suitable value of  $c$ . Table 4-2 shows how  $V_{\text{new}}$  compares with  $V$ . Here  $V$  is a theoretical velocity calculated by  $V = \sqrt{2gh}$ ,  $c$  is calculated using aforementioned SR Sim method and  $V_{\text{new}}$  is calculated by Eq. (2.98). According to Table 4-2, after a large number of experiments, the error between  $V$  and  $V_{\text{new}}$  is within  $\pm 0.5$  m/s. Therefore,  $V_{\text{new}}$  is approximately equal to the impact velocity  $V$ . Therefore, we propose an approximation method that calculates  $c$  more efficiently than the SR Sim method. The approximation method is outlined below.

1. Calculate  $V$  by  $V = \sqrt{2gh}$ .
2. Let  $V = \text{Eq. (2.98)}$ .
3. Importing all parameters into the equation obtained in the above step,  $c$  is readily calculated using common mathematical software (such as Excel).

#### 4.5.5 Data transformation

Data transformation is presented in Figure 1-29 of Section 1.8.3 and will not be reiterated here.

### 4.6 Digital Simulation Stage

#### 4.6.1 Simulation method

Once all parameters are calculated and the data are reformatted, digital simulation is performed in MapleSim. The simulation method is as follows<sup>[7]</sup>.

- 1 Construct a simulation FVD model in MapleSim.
- 2 Input parameters of the FVD model and the input pulse of the target drop height, obtained as described in Section 4.5, into the simulation FVD model.
- 3 Run the simulation.

#### 4.6.2 Simulation FVD model

The mathematical FVD model shown in Figure 2-4 (Section 2.3) is constructed in MapleSim. The simulation FVD model is presented in Figure 4-6. The parameters for the model are calculated as described in Sections 4.5.1, 4.5.2, 4.5.3 and 4.5.4, and they are input to components 1, 2 and 3. The input pulse data, transformed as described in Section 4.5.5, are input to component 5. The parameter settings for all components are shown at the top of Figure 4-6.

Notice that the spring constant  $k = k'/2$  is applied because the simulation FVD model treat the two-spring mathematical FVD model as a single spring for simplicity (Please refer to Section 2.3.1).

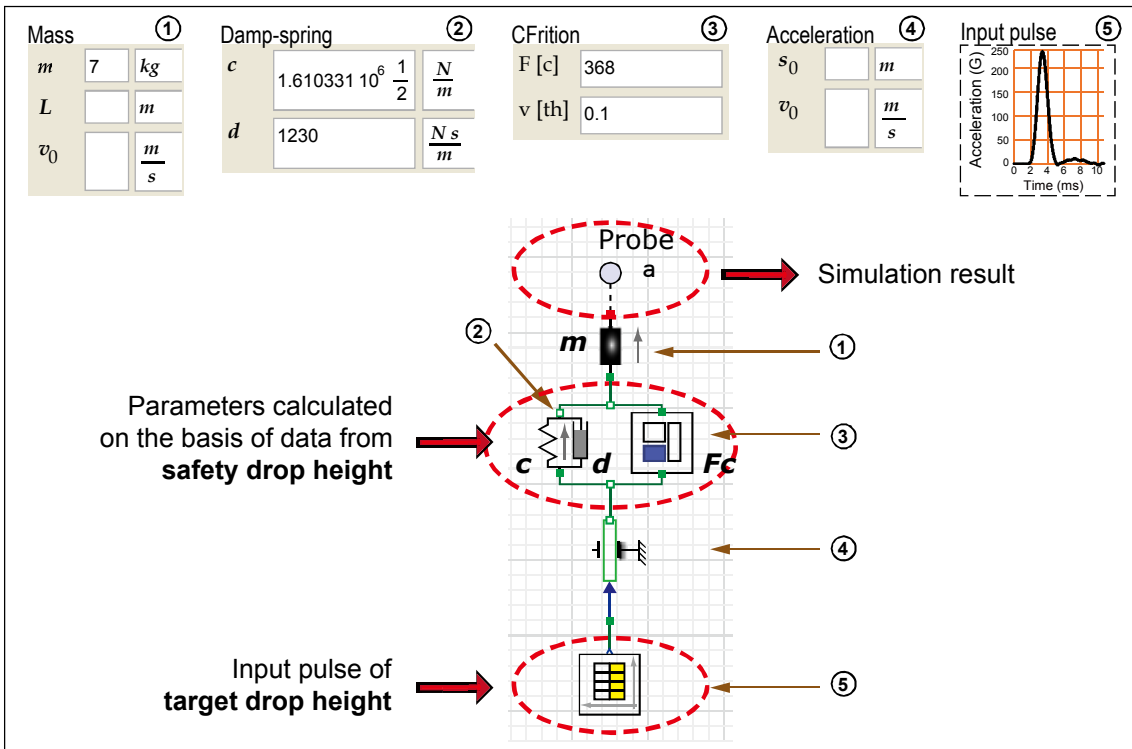


Figure 4-6 Simulation FVD Model and Its Parameters.  
(In MapleSim, spring constant ' $k$ ' and damping coefficient ' $c$ ' are represented by ' $c$ ' and ' $d$ ', respectively).

### 4.6.3 Simulation result

The simulation is run after clicking the 'Simulate the model' button (Figure 1-25(a)). A simulation result, measured by the 'probe' component shown in Figure 4-6, is provided in Figure 4-7. This figure is an acceleration–time curve, from which the peak of the simulation result  $PRA_{sim}$  is easily obtained.

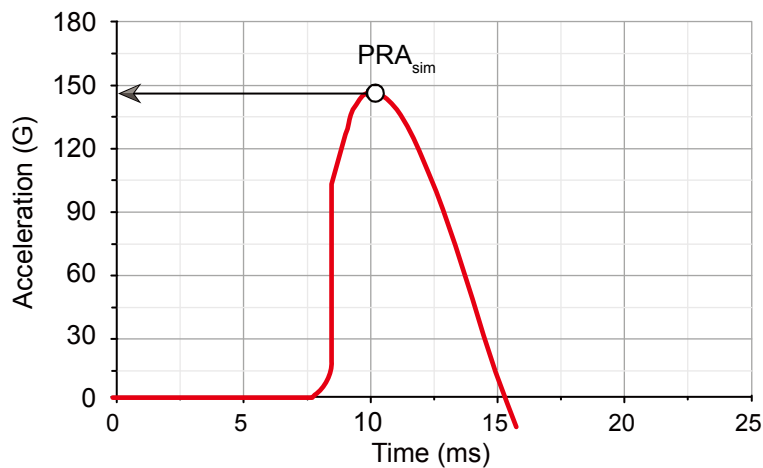


Figure 4-7 Screenshot of Simulation Result.

## 4.7 Prediction Stage

The final purpose of the hybrid drop test is to predict the PRA of the target drop height  $PRA_{\text{target}}$ . Once  $PRA_{\text{sim}}$  is known,  $PRA_{\text{target}}$  is immediately determined from the definition  $PRA_{\text{target}} = PRA_{\text{sim}}$  in the hybrid drop testing method.

## 4.8 References

- [1] Daniel Goodwin and Dennis Young. Protective Packaging for Distribution. DEStech Publications Inc., 2011.
- [2] Abdelmajid Lajmi, Henri Champlaud and Van Ngan Lê. Computation of the Maximum Torque of a Cap Liner Using a Power-Law Friction and Finite Element Analysis. *International Journal of Packaging Technology and Science*. 2011; 24: 103–121.
- [3] N. J. Mills and Y. Masso-Moreu. Finite Element Analysis (FEA) Applied to Polyethylene Foam Cushions in Package Drop Tests. *International Journal of Packaging Technology and Science*. 2005; 18: 29–38.
- [4] M. E. Biancolini and C. Brutti. Numerical and Experimental Investigation of the Strength of Corrugated Board Packages. *International Journal of Packaging Technology and Science*. 2003; 16: 47–60.
- [5] Cyril M. Harris, Allan G. Piersol. Harris' Shock and Vibration Handbook (Fifth Edition), McGraw-Hill, 2002.
- [6] Chen ZHONG, Katsuhiko SAITO and Kazuaki KAWAGUCHI. Improvement of Equivalent Drop Theory for Transport Packaging. *International Journal of Packaging Technology and Science*. 2013; 26(2): 67–81.
- [7] Maplesoft Co. Ltd. MapleSim User's Guide, MapleSim Ver. 4.5.

# CHAPTER 5. VERIFICATION OF THE HYBRID DROP TEST

## 5.1 Test Equipment and Dummy

### 5.1.1 Test equipment

The shock machine for performing the controlled shock test, and the shock manager for measuring the experimental data, have been described in Sections 1.5.2 and 1.3, respectively, and will not be reiterated here.

### 5.1.2 Test dummy

The verification test product was a printer shown in Figure 5-1. Its dimension and weight are  $358 \times 262 \times 238$  (mm) and 7.0 kg (unevenly distributed), respectively.



Figure 5-1 Real product Used in Verification Test.

We constructed a mockup that conformed to the printer specifications (Figure 5-2(a)). The cushioning material was an edge-coupling pulp mould <sup>[1], [2]</sup> (Figure 5-2(b)). The pulp mould cushions were designed such that the PRA of the printer was smaller than 150 G at a drop height of 80 cm.

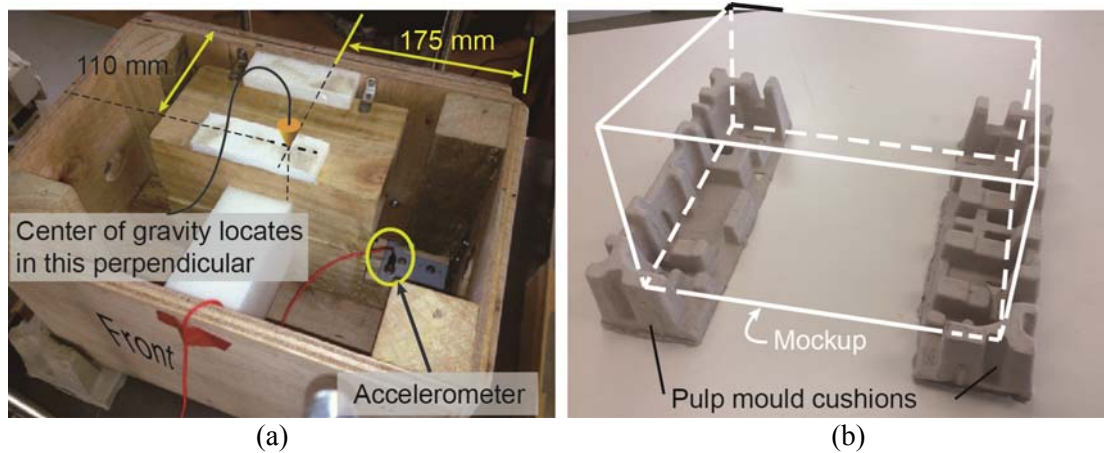


Figure 5-2 Mockup and Cushions.  
(a) Inner structure of mockup, (b) Edge-coupling pulp mould cushions.

The mockup and the pulp mould cushions comprised the test dummy in this study. Figure 5-3 shows the test dummy affixed to the shock table.

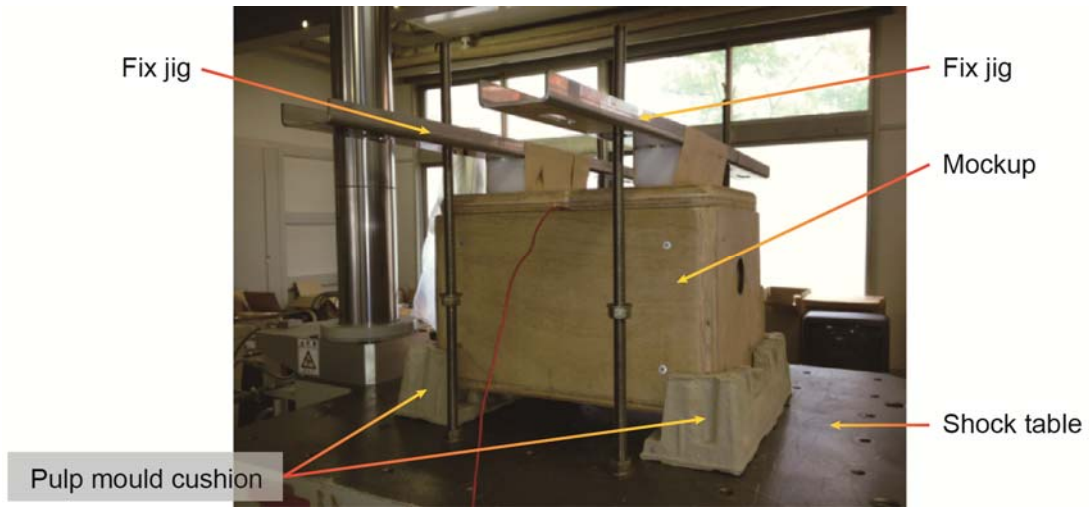


Figure 5-3 Test Dummy Affixed on the Shock Table.

## 5.2 Test Method

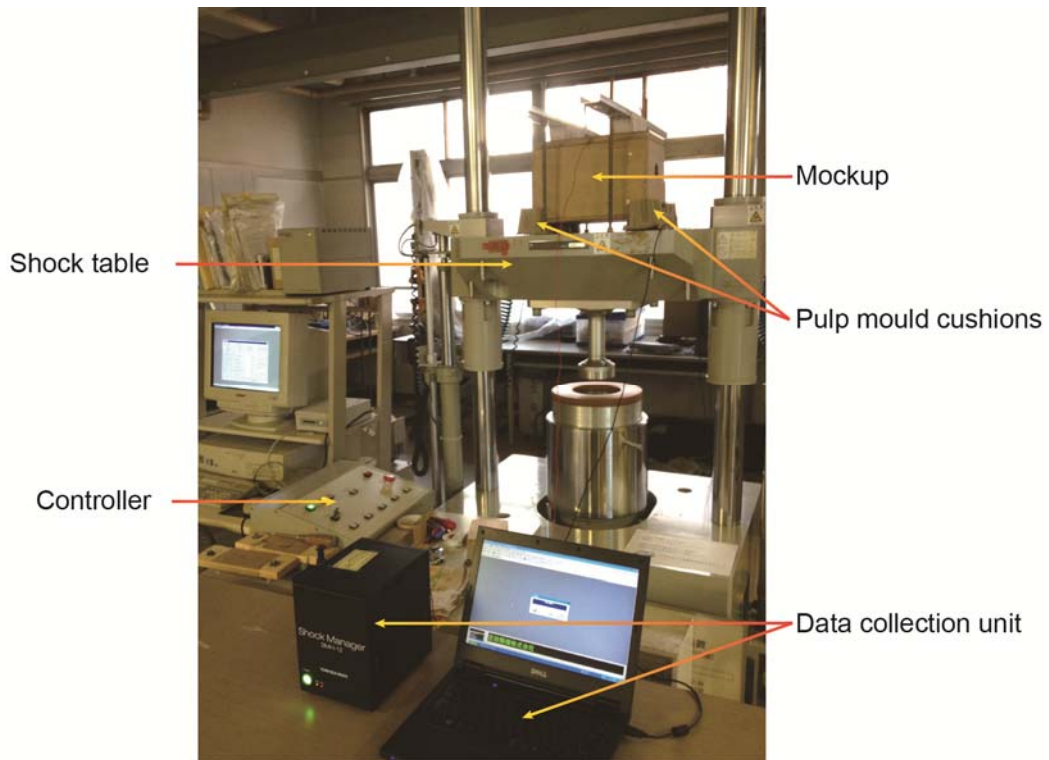


Figure 5-4 Controlled Shock Test for Verification.

Figure 5-4 illustrates the verification test. Experiments were performed as follows.

1. A traditional controlled shock test was performed.
2. The equivalent free-fall height  $h$  was set to 10, 20, 30, 40, 50, 60, 70 and 80 (cm).
3. Five consecutive experiments were performed at each equivalent free-fall height. Input and response pulse data were recorded.
4. New pulp mould cushions were used for each test.
5. The response data of the mockup was measured by an accelerometer, fixed to an iron plate near the centre of gravity of the mockup (Figure 5-2(a)).

### 5.3 Test Results

Figure 5-5(a) displays the input and response curves of the mockup, and Figure 5-5(b) is a photograph of a single pulp mould cushion. The several wavelets in the response curve are due to the varying height structure of the cushions. Each wavelet in the response curve results from the mockup impacting the buffer facets at different levels. Therefore, the response curve of Figure 5-5(a) is obtained as the mockup gradually impacts all buffer facets at different heights.

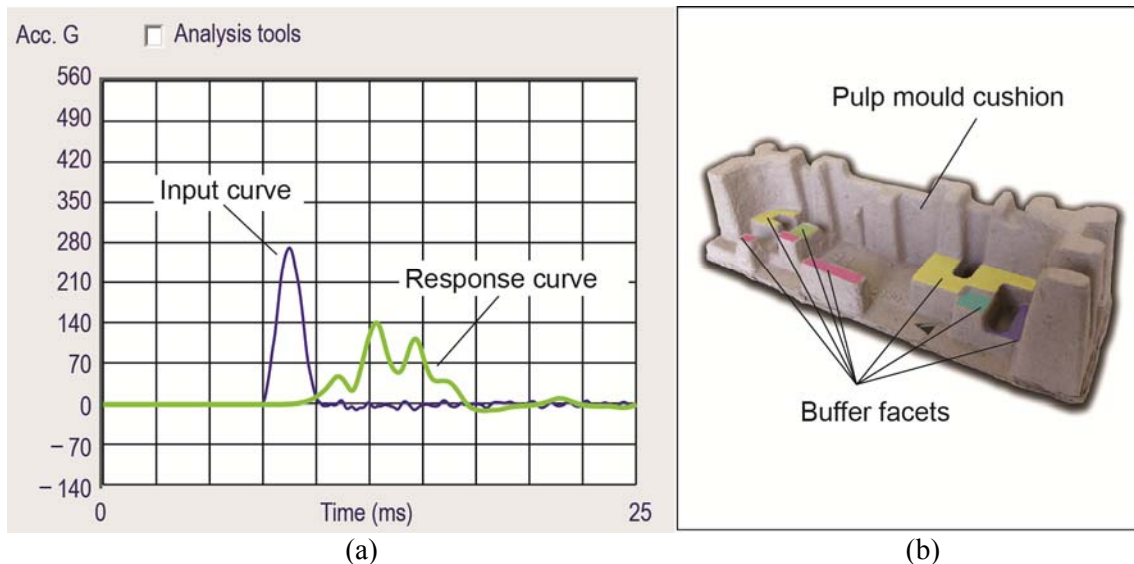


Figure 5-5 Verification Test Results.  
 (a) Screenshot of test result, (b) Buffer facets of a single pulp mould cushion.

All experimental data are summarized in Table 5-1. In each controlled shock test, we recorded  $V_c$ , PIA,  $PRA_{cs}$  and duration times of input and response pulses ( $D_{in}$  and  $D_{out}$ , respectively). Since five consecutive experiments were performed at each equivalent free-fall height, 40 sets of results are listed in Table 5-1.

From the data of column ' $PRA_{cs}$  (G)' in Table 5-1, we computed the average  $PRA_{cs}$  at each equivalent free-fall height. The average  $PRA_{cs}$  versus equivalent free-fall height is plotted in Figure 5-6. Here the PRA value is the average  $PRA_{cs}$ . As mentioned in Section 5.1.2, the pulp mould cushions were designed to ensure that the PRA of the printer was below 150 G at  $H = 80$  cm. From Figure 5-6, we observe that this design requirement is met.



Table 5-1 Results of Verification Experiments.

$h$ (cm)	No.	$V_c$ (m/s)	$PRA_{cs}$ (G)	PIA (G)	$D_{in}$ (ms)	$D_{out}$ (ms)
10	1	1.50	70.2	87.6	3.00	6.90
	2	1.50	72.6	88.5	3.00	7.15
	3	1.40	63.4	81.1	3.00	7.35
	4	1.43	65.7	84.0	3.00	7.50
	5	1.44	65.2	83.8	3.05	7.60
20	1	2.00	88.5	134.0	2.65	6.55
	2	2.02	92.3	135.4	2.60	6.80
	3	2.05	99.6	138.2	2.60	6.80
	4	1.97	92.5	131.9	2.60	7.00
	5	2.04	80.9	137.8	2.60	7.30
30	1	2.42	111.7	170.7	2.50	6.65
	2	2.42	115.7	170.9	2.50	6.70
	3	2.41	112.4	168.9	2.50	6.70
	4	2.47	113.2	173.3	2.55	6.60
	5	2.44	104.2	171.3	2.50	6.85
40	1	2.81	129.1	207.1	2.35	6.45
	2	2.79	114.7	206.3	2.35	6.55
	3	2.84	119.1	210.8	2.35	6.55
	4	2.77	122.0	204.1	2.35	6.60
	5	2.85	130.7	211.5	2.35	6.60
50	1	3.13	132.3	237.3	2.25	6.55
	2	3.14	131.8	241.6	2.20	6.55
	3	3.15	130.7	240.7	2.25	6.55
	4	3.15	130.4	244.7	2.20	6.55
	5	3.12	134.8	238.2	2.25	6.60
60	1	3.47	140.7	269.1	2.20	6.50
	2	3.45	135.7	267.1	2.20	6.95
	3	3.42	134.4	263.7	2.20	6.55
	4	3.43	138.2	267.1	2.20	6.60
	5	3.42	133.4	265.7	2.20	6.65
70	1	3.71	143.2	292.7	2.20	6.65
	2	3.78	139.2	298.5	2.15	6.75
	3	3.69	141.5	287.9	2.15	6.75
	4	3.76	140.3	295.6	2.15	7.00
	5	3.71	138.8	289.9	2.15	6.90
80	1	3.96	138.7	317.3	2.15	6.70
	2	4.01	146.5	322.3	2.10	6.75
	3	3.97	142.7	318.6	2.10	6.80
	4	4.01	145.0	319.8	2.10	6.80
	5	3.97	146.1	319.3	2.10	6.80

$h$  : Equivalent free-fall height  
 No. : Experimental order  
 $V_c$  : Velocity change  
 $D_{in}$  : Duration of input pulse  
 $D_{out}$  : Duration of response pulse

$PRA_{cs}$  : Peak response acceleration of the controlled shock test  
 PIA : Peak input acceleration of the controlled shock test

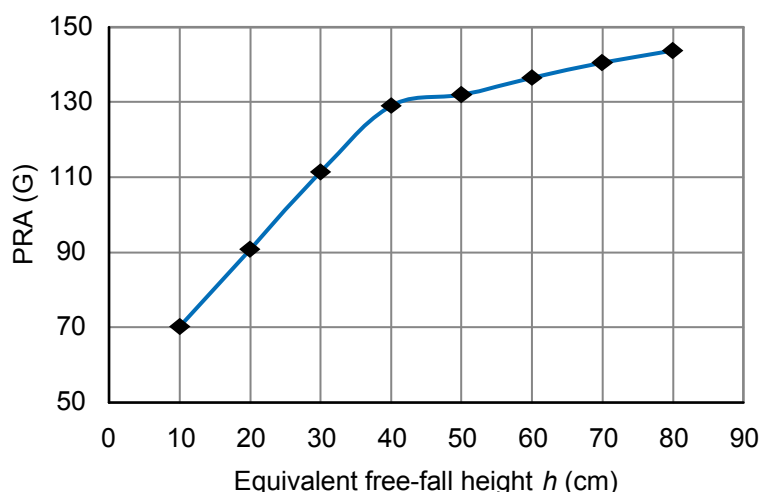


Figure 5-6 PRA- $h$  Curve.

## 5.4 Data Analysis flow

For convenience, we here denote the data used to calculate the four parameters of the simulation FVD model and input as the input pulse as  $DATA_{\text{safety}}$  and  $DATA_{\text{target}}$ , respectively.

Because  $h$  varied from 10 cm to 80 cm in 10 cm increments, eight experimental datasets were collected. In the hybrid drop test,  $DATA_{\text{safety}} < DATA_{\text{target}}$ . Therefore, the data obtained when  $h = 10\text{--}70$  cm can comprise  $DATA_{\text{safety}}$ , while the data obtained when  $h = 20\text{--}80$  cm can form  $DATA_{\text{target}}$ .

The experimental data were analyzed as shown in Figure 5-7. Data were analyzed in the following five steps.

1. Parameters  $k$ ,  $F_c$  and  $c$  in the FVD model were calculated from  $DATA_{\text{safety}}$ .
2. The input pulse to the FVD model was derived from  $DATA_{\text{target}}$ .
3. The input pulse and parameters  $m$ ,  $k$ ,  $c$  and  $F_c$  were input to the simulation FVD model, and simulations were run. The  $PRA_{\text{sim}}$  was recorded.
4. Using the input pulse as  $DATA_{\text{target}}$ , the  $PRA_{\text{exp}}$  was recorded from the experimental data.
5. The  $PRA_{\text{exp}}$  was directly read from  $DATA_{\text{target}}$ .

This flowchart is similar to Figure 4-3, except that, in Figure 5-7,  $DATA_{\text{target}}$  are used only in the hybrid drop test and the final steps of the analysis are different.

## 5.5 Parameter Calculation and Comparison of $PRA_{\text{exp}}$ and $PRA_{\text{sim}}$

Before running the simulation, we must calculate the three parameters  $k$ ,  $F_c$  and  $c$  of the FVD model.

The calculation of the above three parameters and the digital simulation method have been described in Sections 4.5 and 4.6, respectively, and will not be elaborated here. The calculated  $F_c$  and  $c$  are shown in Tables 5-2 and 5-3, respectively.

Once all parameters of the simulation FVD model were calculated, simulations were run and the  $PRA_{\text{sim}}$  were recorded. Finally,  $PRA_{\text{sim}}$  was compared with  $PRA_{\text{exp}}$ . For each set of  $DATA_{\text{safety}}$  or  $DATA_{\text{target}}$ , five tests were performed, and five sets of results were recorded. Therefore, 25  $PRA_{\text{exp}}$  vs.  $PRA_{\text{sim}}$  comparisons were obtained (Figure 5-8). For detail of the comparisons at varied drop heights, please refer to APPENDIX.

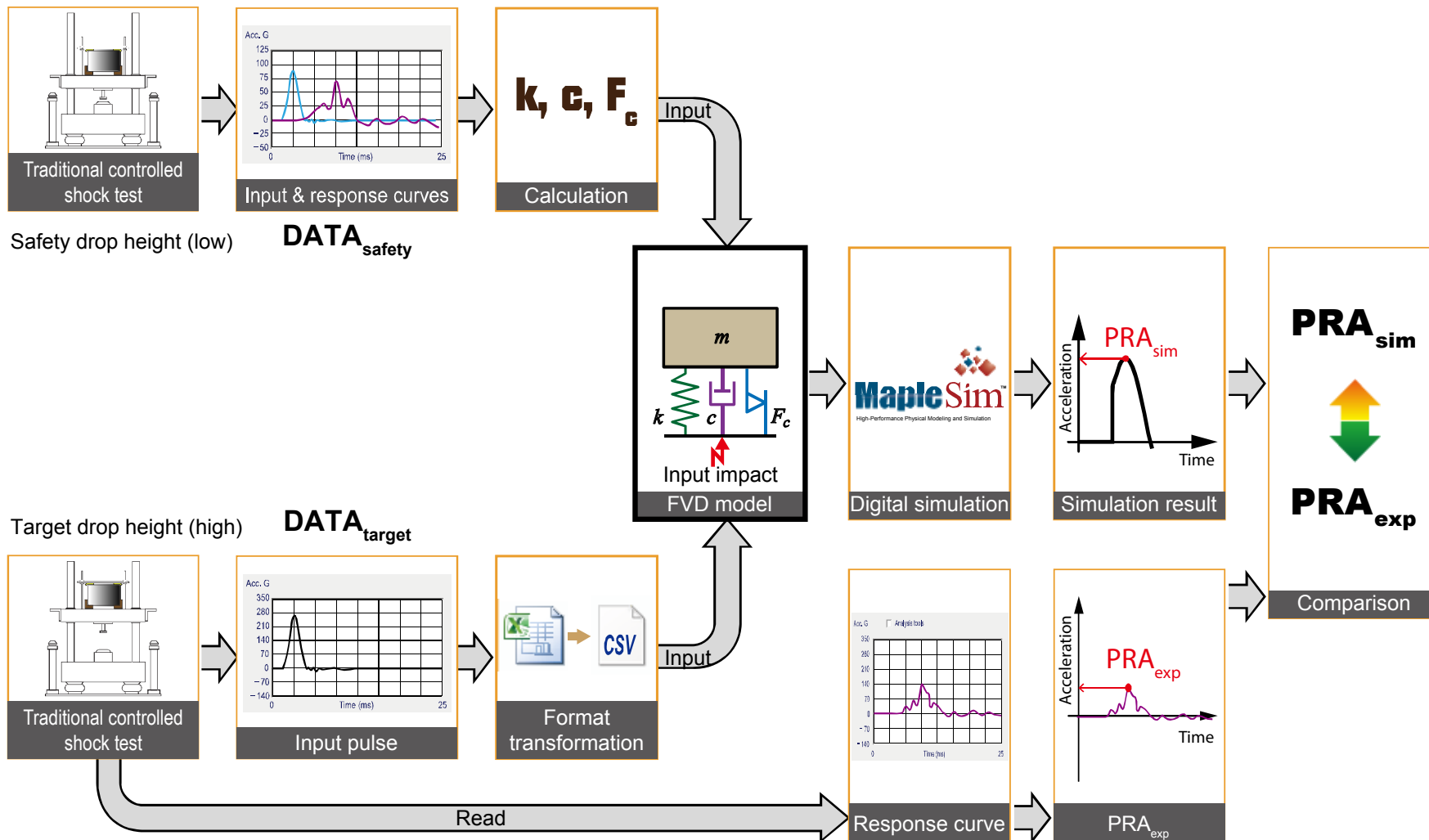


Figure 5-7 Data Analysis Flowchart.

Table 5-2 Calculation of  $F_c$ .

$h$ (cm)	No.	$\omega_n$ (Hz)	$k$ (N/m)	$\xi_0$	$c_0$ (Ns/m)	$c_{eq}$ (Ns/m)	$A$ (mm)	$F_c$ (N)
10	1	455.3	1451108	0.99	6311	7700	1.1	547
	2	439.4	1351406	0.99	6090	7500	1.2	584
	3	427.4	1278860	0.99	5924	7300	1.1	508
	4	418.9	1228217	0.99	5806	7400	1.2	629
	5	413.4	1196109	0.99	5729	7200	1.3	621
20	1	479.6	1610331	0.70	4700	4100	1.9	430
	2	462.0	1494101	0.85	5498	6200	1.8	459
	3	462.0	1494101	0.99	6403	7150	1.7	461
	4	448.8	1409943	0.99	6220	5400	1.6	463
	5	430.4	1296439	0.61	3675	4250	2.3	447
30	1	472.4	1562264	0.80	5291	4700	2.2	483
	2	468.9	1539034	0.80	5252	4700	2.1	427
	3	468.9	1539034	0.84	5514	5000	2.2	417
	4	476.0	1586025	0.77	5131	4600	2.2	437
	5	458.6	1472369	0.64	4109	3600	2.6	477
40	1	487.1	1660651	0.68	4637	5050	2.6	411
	2	479.6	1610331	0.46	3089	3450	3.2	435
	3	479.6	1610331	0.50	3357	3700	3.1	400
	4	476.0	1586025	0.62	4132	4500	2.8	386
	5	476.0	1586025	0.72	4798	5200	2.7	406
50	1	479.6	1610331	0.58	3895	4250	3.2	428
	2	479.6	1610331	0.57	3827	4150	3.3	401
	3	479.6	1610331	0.59	3962	4300	3.2	408
	4	479.6	1610331	0.59	3962	4300	3.3	420
	5	476.0	1586025	0.55	3665	4000	3.3	413
60	1	483.3	1635201	0.47	3180	3400	4.0	334
	2	452.0	1430303	0.45	2848	3100	4.3	385
	3	479.6	1610331	0.48	3223	3450	3.9	333
	4	476.0	1586025	0.41	2732	2500	4.3	373
	5	472.4	1562264	0.36	2381	2600	4.4	358
70	1	472.4	1562264	0.34	2249	2450	4.9	366
	2	465.4	1516318	0.26	1694	1900	5.7	429
	3	465.4	1516318	0.35	2281	2500	5.0	401
	4	448.8	1409943	0.36	2262	2500	5.0	420
	5	455.3	1451108	0.34	2167	2400	5.1	424
80	1	468.9	1539034	0.27	1772	2000	5.8	486
	2	465.4	1516318	0.27	1759	1950	5.9	411
	3	462.0	1494101	0.26	1682	1900	5.9	467
	4	462.0	1494101	0.26	1682	1900	6.0	475
	5	462.0	1494101	0.26	1682	1900	5.9	467

$h$  : Equivalent free-fall height  
 No. : Experimental order  
 $\omega_n$  : Natural angular frequency  
 $k$  : Spring constant  
 $\xi_0$  : Damping rate

$c_0$  : Damping coefficient  
 $c_{eq}$  : Equivalent damping coefficient  
 $A$  : Displacement  
 $F_c$  : Friction calculated by Eq. (3.6)  
 $m = 7$  kg

Table 5-3 Calculation of  $c$ .

$h$ (cm)	No.	$V$ (m/s)	$k$ (N/m)	$F_c$ (N)	$u_{cs}$	$\xi$	$c$ (Ns/m)
10	1	1.40	1451108	547	0.92158	0.188	1196
	2		1351406	584	0.97757	0.185	1140
	3		1278860	508	0.95764	0.190	1138
	4		1228217	629	0.97768	0.193	1130
	5		1196109	621	0.96936	0.193	1118
20	1	1.98	1610331	430	0.81621	0.191	1280
	2		1494101	459	0.89143	0.184	1190
	3		1494101	461	0.94245	0.179	1156
	4		1409943	463	0.94404	0.182	1146
	5		1296439	447	0.82417	0.191	1150
30	1	2.42	1562264	483	0.87030	0.186	1229
	2		1539034	427	0.90719	0.181	1188
	3		1539034	417	0.89175	0.182	1198
	4		1586025	437	0.84532	0.185	1235
	5		1472369	477	0.83336	0.189	1213
40	1	2.80	1660651	411	0.85548	0.183	1250
	2		1610331	435	0.77483	0.192	1292
	3		1610331	400	0.78738	0.189	1269
	4		1586025	386	0.83939	0.186	1237
	5		1586025	406	0.86778	0.181	1207
50	1	3.13	1610331	428	0.81150	0.187	1258
	2		1610331	401	0.81210	0.186	1251
	3		1610331	408	0.79037	0.188	1265
	4		1610331	420	0.79329	0.188	1265
	5		1586025	413	0.83000	0.185	1236
60	1	3.43	1635201	334	0.77240	0.188	1269
	2		1430303	385	0.80249	0.186	1180
	3		1610331	333	0.75871	0.190	1277
	4		1586025	373	0.77611	0.189	1259
	5		1562264	358	0.75881	0.191	1261
70	1	3.70	1562264	366	0.73942	0.192	1269
	2		1516318	429	0.73203	0.193	1255
	3		1516318	401	0.77153	0.190	1237
	4		1409943	420	0.77265	0.189	1186
	5		1451108	424	0.76828	0.190	1213
80	1	3.96	1539034	486	0.68110	0.200	1314
	2		1516318	411	0.73052	0.193	1255
	3		1494101	467	0.72517	0.195	1261
	4		1494101	475	0.73409	0.193	1250
	5		1494101	467	0.74082	0.193	1250

$h$  : Equivalent free-fall height  
 No. : Experimental order  
 $k$  : Spring constant (see Table 5-2)  
 $\xi$  : Damping rate (see Figure 4-4)

$V$  : Impact velocity calculated by  $V = \sqrt{2gh}$   
 $u_{cs}$  : Coefficient (see Figure 4-4)  
 $F_c$  : Friction (see Table 5-2)  
 $m = 7$  kg

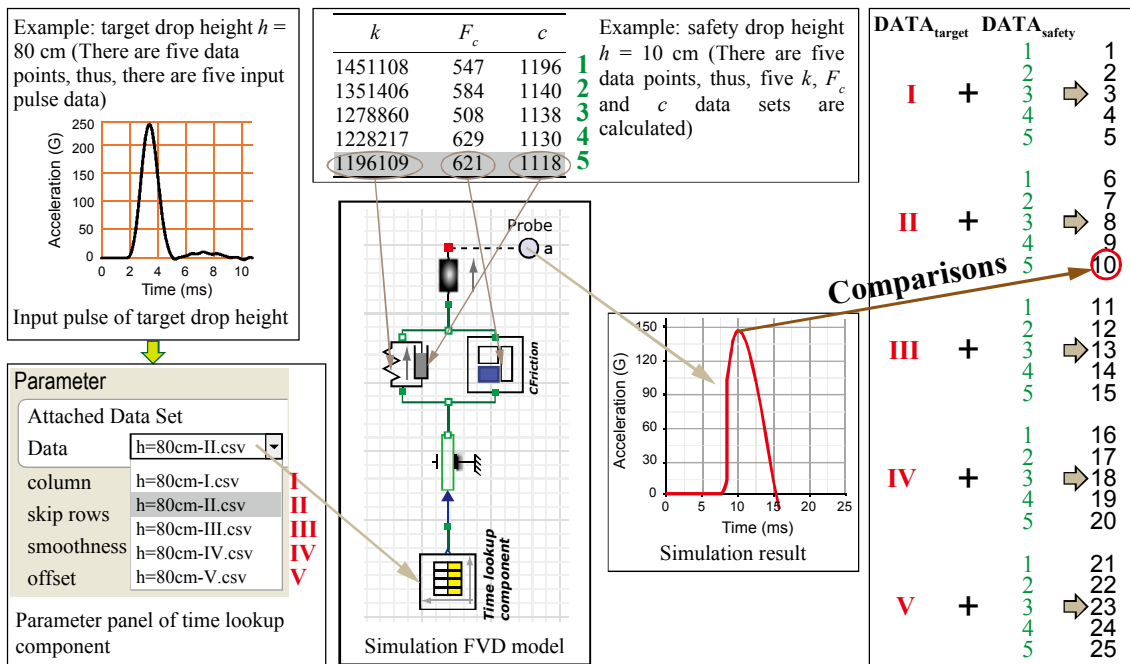


Figure 5-8 Schematic of 25  $PRA_{exp}$  vs.  $PRA_{sim}$  comparisons.

For convenience,  $DATA_{safety}$  and  $DATA_{target}$  are labeled by the equivalent free-fall height at which the experimental data were obtained. For example,  $DATA_{safety}$  (collected at  $h = 20$  cm) are denoted as  $DATA_{safety}(20)$ ;  $DATA_{target}$  (collected at  $h = 40-80$  cm) are denoted as  $DATA_{target}(40-80)$ .

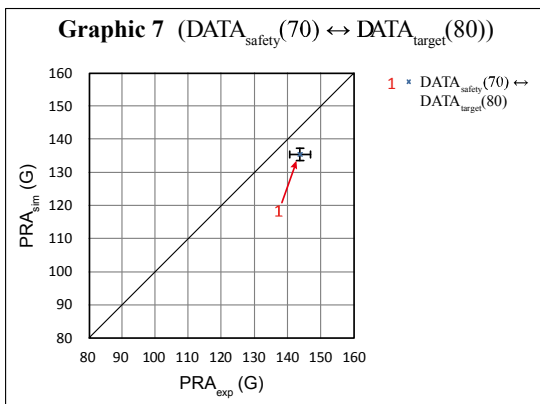
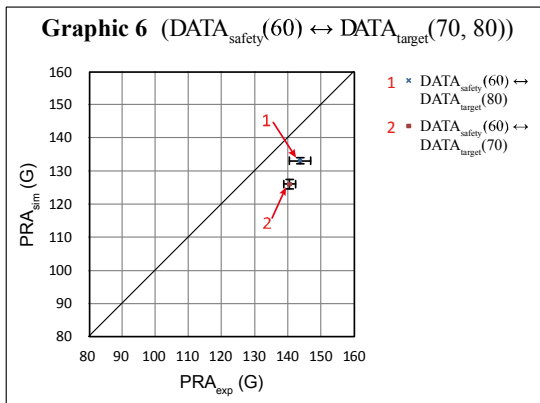
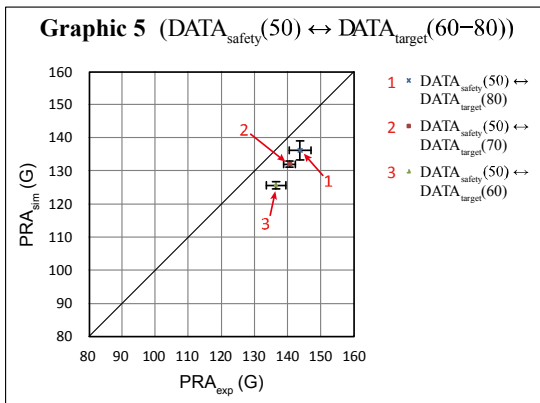
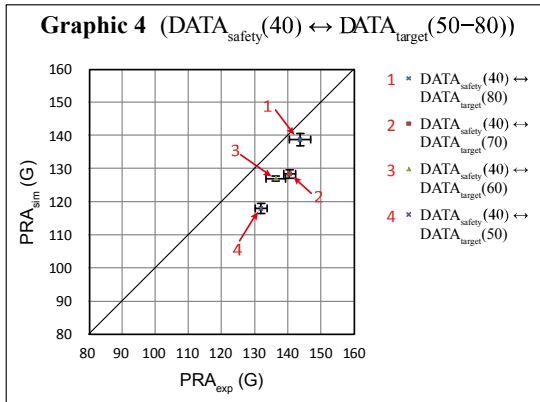
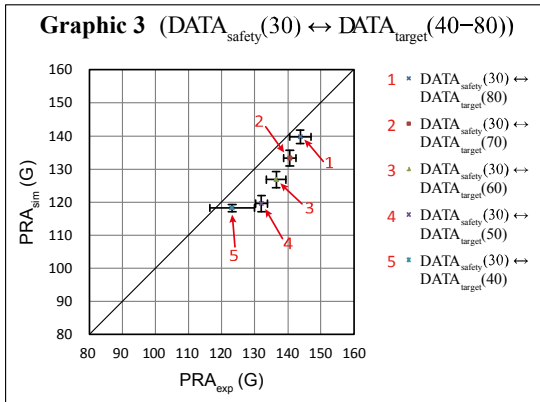
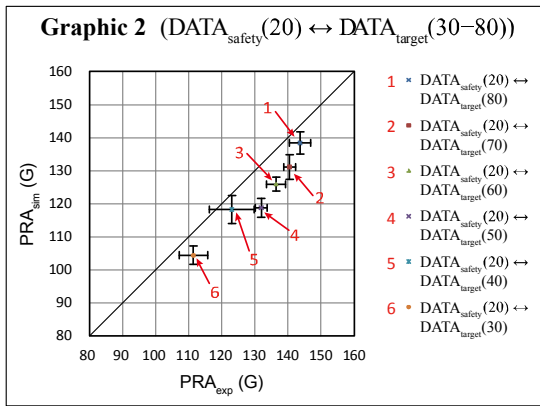
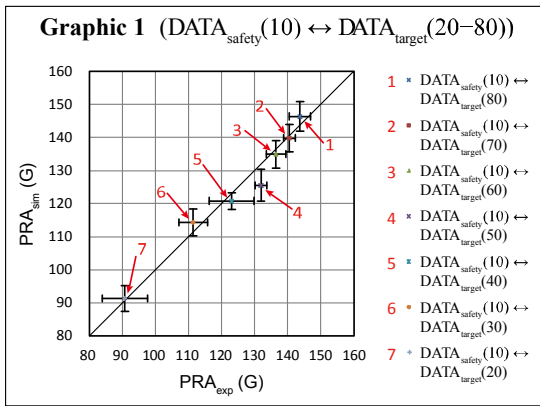
## 5.6 Discussion

On the basis of data in Section 6.4 of the APPENDIX, The comparisons between  $PRA_{exp}$  and  $PRA_{sim}$  are displayed graphically in Figure 5-9.  $PRA_{exp}$  and  $PRA_{sim}$  are plotted along the horizontal and vertical axes, respectively. From this figure, we observe that the comparisons cluster around  $PRA_{exp} = PRA_{sim}$ . Therefore, the hybrid drop test provides a qualitative prediction of the PRA of the target drop height. That is, the hybrid drop test is feasible for practical application.

For an intuitive interpretation of the difference between  $PRA_{sim}$  and  $PRA_{exp}$ , we introduce an indicator, the predictive error  $P$ , expressed as follows:

$$P = \frac{PRA_{sim} - PRA_{exp}}{PRA_{exp}} \times 100\% \quad (5.1)$$

From the data given in Section 6.4 of the APPENDIX, we obtain the values of  $P$  and their standard deviations and compare the results for different equivalent free-fall heights. The results are presented in Table 5-4.



Standard deviation

Figure 5-9  $PRA_{sim}$  vs.  $PRA_{exp}$ .

Table 5-4 Predictive Error and Standard Deviation at Different Equivalent Free-fall Heights.

DATA <sub>safety</sub> (h) (cm)	DATA <sub>target</sub> (h) (cm)						
	80	70	60	50	40	30	20
10	1.9 (3.7)*	-0.4 (3.3)	-1.0 (3.6)	-5.1 (3.7)	-1.5 (5.1)	2.8 (5.1)	1.3 (8.1)
20	-3.7 (3.0)	-6.8 (2.9)	-7.7 (2.3)	-10.1 (2.3)	-3.7 (5.6)	-6.2 (4.2)	
30	-2.8 (2.5)	-5.2 (2.0)	-7.1 (2.5)	-9.4 (2.1)	-3.8 (4.5)		
40	-3.5 (2.4)	-8.7 (1.2)	-6.9 (2.0)	-10.7 (1.6)			
50	-5.2 (3.0)	-6.1 (1.3)	-7.9 (2.0)				
60	-7.4 (2.1)	-10.4 (1.4)					
70	-5.9 (2.4)						

\* Predictive error (standard deviation). The unit of all data is %.

The data in Table 5-4 are presented graphically in Figure 5-10. From that figure, we conclude the following:

1. All  $P$  values are within  $\pm 15\%$ .
2.  $P$  values for DATA<sub>safety</sub>(10) versus DATA<sub>target</sub>(80) and DATA<sub>safety</sub>(20) versus DATA<sub>target</sub>(80) are within  $|\pm 10\%|$ . These two cases are of practical significance; they essentially indicate that the hybrid drop test is sufficiently accurate for practical applications.
3. Most of the  $P$  values are located in the dangerous zone. Therefore, the hybrid drop test should be applied at the predicted value + standard deviation.

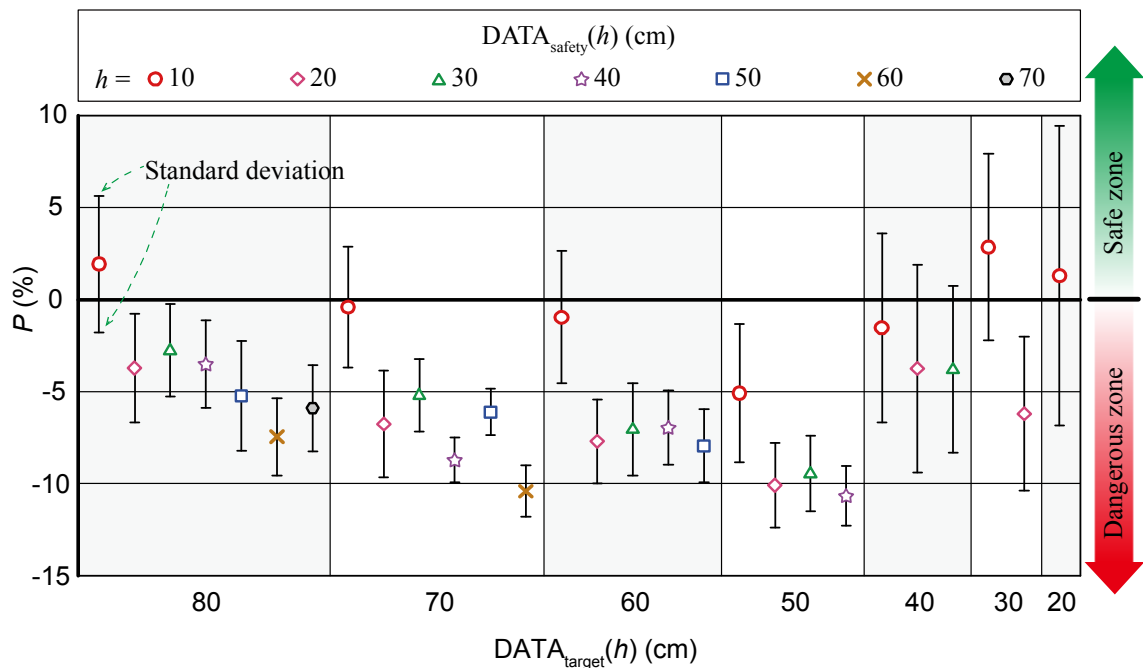


Figure 5-10 Predictive Error  $P$  at Different Equivalent Free-fall Heights.



## 5.7 References

- [1] John Hoffmann. Compression and Cushioning Characteristics of Moulded Pulp Packaging. *International Journal of Packaging Technology and Science*. 2000; 13: 211–220.
- [2] X. Ma, A.K. Soh and B.Wang. A Design Database for Moulded Pulp Packaging Structure. *International Journal of Packaging Technology and Science*. 2004; 17: 193–204.

## CHAPTER 6. SUMMARY

With the acceleration of cross-border movement of goods in recent years, national economies worldwide have become increasingly interdependent. The relationship between goods distribution and economic globalization has rendered packaging of goods more important than ever.

Packaging is the science, art and technology of enclosing or protecting products for distribution, storage, sale and use. It also refers to design, evaluation and production of packages. Packaging can be regarded as a coordinated system of preparing goods for transport, warehousing, logistics, sale and end use. During distribution, products are vulnerable to two main physical distribution hazards: shock and vibration. To ensure their safe delivery from manufacturers to consumers, packages must be buffered by appropriate and sufficient cushioning packages.

Numerous cushioning materials can be used in packaging, and many packaging methods are available. Therefore, engineers have many choices when designing a package for a given product. However, finding the optimal package design poses a more challenging problem. In particular, if the package cannot make up the difference between the product ruggedness and environmental inputs, ‘under packaging’ occurs and product damage will most likely result. Conversely, if the package is provided too much protection, ‘over package’ happens and cost and materials are wasted on protection that is not required. To achieve the desirable ‘optimal package’, the performance of the cushioning materials must be tested prior to their inclusion in the packaging design. In addition, the entire cushioning package must be tested to confirm that it provides sufficient protection to the products.

The traditional design procedure for a cushioning package is as follows. Step 1: Define the distribution environment. Step 2: Define product fragility. Step 3: Design the cushioning package. In this step, designer may need to undertake and plot the data as shock cushioning and vibration transmissibility curves. Step 4: Perform verification tests to confirm whether the package design has been optimized. This step confirms whether the package design is optimally designed, insufficient to protect the product, or over-protective.

The traditional package design procedure ensures that, provided that all design requirements are met under verification testing, the package design is successful. However, if the packaging fails the verification test, designers must return to Step 3 and repeat this procedure. In the worst-case scenario, if the cushioning material is of the wrong type, then large quantities of labor and material resources are undoubtedly required.

Therefore, verification testing is an important component of packaging design. Among the common methods for assessing package performance are free fall, shock and vibration tests. To determine product safety and PRA is within the desired range, designers generally apply traditional drop tests, which expose the test dummy to a high probability of damage.

In addition to physical testing methods, simulation methods are widely used in package design. However, these are not applicable to cushioning packages because of the nonlinear physical characteristics of the cushioning materials.

On the other hand, an equivalent drop theory is an important theoretical basis of package. The traditional equivalent drop theory is useful because the free fall and controlled shock tests should yield identical test results at a specified drop height, but it is limited to perfectly elastic materials. To correct these flaws, we have proposed a damping equivalent drop theory based on a viscous damping model. However, the damping equivalent drop theory cannot exactly replicate the test results of structure cushioning materials, although it can improve the precision of equivalent tests on quasi-linear cushions. The problem with the viscous damping model is that only viscous damping and linear spring factors are considered.

To resolve the issues above, the following four achievements were obtained in this dissertation.

- I. We proposed a new physical model that embodies both friction and viscous damping. The new model is called the FVD model. Mathematical equations of the shock responses to the test at free fall and controlled shock test were deduced using Maple and MapleSim, respectively. From these mathematical equations, we proposed a new equivalent drop theory called the ‘friction equivalent drop theory’.
- II. The feasibility of the friction equivalent drop theory was demonstrated in a series of verification tests. A preliminary verification experiment based on a single material (a corrugated sleeve) and design configuration (equivalent free-fall height and weight dummy) was performed. In the preliminary verification, the error of the test at free fall was reduced to one-third that of the original equivalent drop theory. To confirm this result, further verification experiments were performed for a range of stresses and materials. The test was broadly divided into data acquisition and data analysis. To qualitatively assess the corrective effect in the friction equivalent drop theory, the probability distributions of the differences in the peak response accelerations of the two tests were plotted as bar charts. Next, the corrective effect was quantitated by a correction indicator. The friction equivalent drop theory was successfully applied to both structural corrugated sleeve and pulp mould cushions. The corrective effects vary with stress but become more prominent toward the lowest point of the cushion curve.
- III. To address the flaws in traditional testing and digital simulation methods, we use the FVD model and friction equivalent drop theory to develop a new, high-efficiency verification testing method. This proposed method combines traditional drop testing and digital simulation methods; therefore, it is called ‘the hybrid drop testing method’. Centering on the FVD model, the hybrid drop test involves the following four stages: experimental, parameter calculation and data transformation, digital simulation and prediction. The key step is parameter calculation, which applies the friction equivalent drop theory.
- IV. Similar to the friction equivalent drop theory, the feasibility of the hybrid drop testing method was proven through experiments. Numerous shock tests were performed on a mockup of a real printer as the test dummy. The corresponding parameters of FVD model were calculated from the experimental data, and the simulations were based on the hybrid drop test. Finally, the simulated and experimental results were compared. The results show that the hybrid drop test is sufficiently accurate for practical applications. However, in practice, the method should be applied at the upper limit of the predicted value, i.e. the predicted value + standard deviation.

Using the hybrid drop testing method, we can predict the PRA for a specified package design at higher drop heights by performing a single, low-height drop test. The hybrid drop testing method provides packaging researchers with an alternative testing choice. It also ensures the safety of the test product and improves test efficiency. We expect that this new testing method will become of valuable assistance in future packaging design.

# ACKNOWLEDGEMENTS

My dissertation would not have been possible without the support of various people to whom I would like to express my sincere gratitude.

My deepest gratitude goes first and foremost to Prof. Katsuhiko SAITO, my supervisor, for his constant guidance and encouragement at both an academic and a personal level. I cannot find words to express my gratitude to him, because my master's and doctoral course would never have been completed without his assistance throughout the past five years. Under his guidance, I have gained not only professional knowledge but also the thinking skills required for higher-level research. I was extremely fortunate to meet Prof. SAITO at the right stage of my career. The Transport Packaging Laboratory at Kobe University has provided me with experiences and skill that will last a lifetime. Prof. SAITO has substantially enhanced my ability to complete the research contained in this dissertation. He has walked me through all writing stages of the dissertation. This dissertation would have remained a dream without his consistent and illuminating instruction.

High tribute shall be paid to Prof. Akihisa ABE and Prof. Nobuyoshi KOGUCHI. Without the lesson entitled 'Transportation Impact Science', given by Prof. ABE, the mathematical calculations in this dissertation could not have been accomplished. Prof. ABE has provided me with valuable questions and suggestions since this study began. I would like to thank Prof. KOGUCHI for his time and support. Without the valuable advice of both professors, this dissertation could not have reached its present form.

I am extremely grateful to Dr. Kazuaki KAWAGUCHI at Shinyei Technology Co. Ltd. His previous valuable research provided the keystone for the friction equivalent drop theory proposed in this dissertation. Many useful references and suggestions were supplied by him throughout the period of this study. His interest in the dissertation is sincerely appreciated.

I would like to acknowledge Mr. Akira HIGASHIYAMA and Mr. Eiji YAMAHARA at Rengo Co. Ltd., for providing me with adequate quantities of corrugated board test materials; Mr. Hiroshi SETOUE and Mr. Masakazu TAKEUCHI at Kyocera Document Solutions Co. Ltd., for supplying the mockup for the final verification test. Their help and support over the past five years have also ensured the successful completion of this study.

Particular thanks are given to my previous classmates, Ms. Aya IWAIHARA, currently employed at Mitsubishi Electric Logistics Co.; Mr. Fumiaki ANDO, currently employed at Japan Tobacco Inc.; Ms. Ayaka OHYAMA, currently employed at The Pack Corporation; Mr. Qi ZHANG, who is currently employed with TSK Corporation; and my classmate, Mr. Akinari TAKAHASHI, who will be employed at Kyocera Document Solutions Co. Ltd. after graduation; Mr. Akira HOSOYAMA at Technology Research Institute of Osaka Prefecture. Thanks for their kindness, friendship, assistance in my overseas life and for teaching me a lot about Japanese culture.

Finally, very special thanks to my parents, my father Weisheng ZHONG and my mother Wenyun LIU, whose unwavering faith and confidence in my attributes has shaped me into the person I am today. Thank you for everything. My thanks also extend to my wife Li ZHU. Her loving care has enabled me to concentrate my energy on research. Thank you for always accompanying me during the past six challenging but ultimately rewarding years in Japan.

This page is intentionally left blank

# APPENDIX

## Data of PRA<sub>exp</sub> vs. PRA<sub>sim</sub>

Table 7-1 DATA<sub>safety</sub>(10)↔DATA<sub>target</sub>(20-80).

Unit: G	Group 1				Group 2				Group 3				Group 4				Group 5			
	PRA <sub>exp</sub>	PRA <sub>sim</sub>	Diff	<i>P</i>	PRA <sub>exp</sub>	PRA <sub>sim</sub>	Diff	<i>P</i>	PRA <sub>exp</sub>	PRA <sub>sim</sub>	Diff	<i>P</i>	PRA <sub>exp</sub>	PRA <sub>sim</sub>	Diff	<i>P</i>	PRA <sub>exp</sub>	PRA <sub>sim</sub>	Diff	<i>P</i>
Data <sub>safety</sub> (10) ↓ Data <sub>target</sub> (80)	138.7	147	8.3	6.0%	146.5	147	0.5	0.3%	142.7	148	5.3	3.7%	145.0	147	2	1.4%	146.1	148	1.9	1.3%
		148	9.3	6.7%		149	2.5	1.7%		150	7.3	5.1%		149	4	2.8%		150	3.9	2.7%
		138	-0.7	-0.5%		137	-9.5	-6.5%		139	-3.7	-2.6%		138	-7	-4.8%		138	-8.1	-5.5%
		149	10.3	7.4%		150	3.5	2.4%		150	7.3	5.1%		150	5	3.4%		150	3.9	2.7%
		148	9.3	6.7%		148	1.5	1.0%		149	6.3	4.4%		148	3	2.1%		148	1.9	1.3%
Data <sub>safety</sub> (10) ↓ Data <sub>target</sub> (70)	143.2	141	-2.2	-1.5%	139.2	141	1.8	1.3%	141.5	139	-2.5	-1.8%	140.3	140	-0.3	-0.2%	138.8	141	2.2	1.6%
		142	-1.2	-0.8%		142	2.8	2.0%		139	-2.5	-1.8%		141	0.7	0.5%		142	3.2	2.3%
		133	-10.2	-7.1%		133	-6.2	-4.5%		131	-10.5	-7.4%		132	-8.3	-5.9%		133	-5.8	-4.2%
		145	1.8	1.3%		145	5.8	4.2%		144	2.5	1.8%		145	4.7	3.3%		145	6.2	4.5%
		142	-1.2	-0.8%		142	2.8	2.0%		140	-1.5	-1.1%		141	0.7	0.5%		141	2.2	1.6%
Data <sub>safety</sub> (10) ↓ Data <sub>target</sub> (60)	140.7	136	-4.7	-3.3%	135.7	136	0.3	0.2%	134.4	136	1.6	1.2%	138.2	135	-3.2	-2.3%	133.4	135	1.6	1.2%
		137	-3.7	-2.6%		137	1.3	1.0%		136	1.6	1.2%		138	-0.2	-0.1%		138	4.6	3.4%
		128	-12.7	-9.0%		128	-7.7	-5.7%		126	-8.4	-6.3%		127	-11.2	-8.1%		127	-6.4	-4.8%
		139	-1.7	-1.2%		139	3.3	2.4%		138	3.6	2.7%		140	1.8	1.3%		139	5.6	4.2%
		137	-3.7	-2.6%		137	1.3	1.0%		135	0.6	0.4%		137	-1.2	-0.9%		137	3.6	2.7%

Data <sub>safety</sub> (10) ↓ Data <sub>target</sub> (50)	132.3	128	-4.3	-3.3%	131.8	127	-4.8	-3.6%	130.7	126	-4.7	-3.6%	130.4	128	-2.4	-1.8%	134.8	129	-5.8	-4.3%
		129	-3.3	-2.5%		128	-3.8	-2.9%		127	-3.7	-2.8%		129	-1.4	-1.1%		130	-4.8	-3.6%
		121	-11.3	-8.5%		120	-11.8	-9.0%		120	-10.7	-8.2%		121	-9.4	-7.2%		122	-12.8	-9.5%
		119	-13.3	-10.1%		118	-13.8	-10.5%		117	-13.7	-10.5%		119	-11.4	-8.7%		120	-14.8	-11.0%
		131	-1.3	-1.0%		130	-1.8	-1.4%		130	-0.7	-0.5%		131	0.6	0.5%		132	-2.8	-2.1%
Data <sub>safety</sub> (10) ↓ Data <sub>target</sub> (40)	129.1	121	-8.1	-6.3%	114.7	118	3.3	2.9%	119.1	118	-1.1	-0.9%	122.0	117	-5	-4.1%	130.7	118	-12.7	-9.7%
		123	-6.1	-4.7%		124	9.3	8.1%		123	3.9	3.3%		123	1	0.8%		123	-7.7	-5.9%
		124	-5.1	-4.0%		119	4.3	3.7%		119	-0.1	-0.1%		119	-3	-2.5%		119	-11.7	-9.0%
		124	-5.1	-4.0%		124	9.3	8.1%		124	4.9	4.1%		124	2	1.6%		123	-7.7	-5.9%
		122	-7.1	-5.5%		119	4.3	3.7%		119	-0.1	-0.1%		119	-3	-2.5%		118	-12.7	-9.7%
Data <sub>safety</sub> (10) ↓ Data <sub>target</sub> (30)	111.7	113	1.3	1.2%	115.7	114	-1.7	-1.5%	112.4	114	1.6	1.4%	113.2	113	-0.2	-0.2%	104.2	113	8.8	8.4%
		115	3.3	3.0%		116	0.3	0.3%		115	2.6	2.3%		115	1.8	1.6%		115	10.8	10.4%
		107	-4.7	-4.2%		108	-7.7	-6.7%		108	-4.4	-3.9%		108	-5.2	-4.6%		107	2.8	2.7%
		118	6.3	5.6%		119	3.3	2.9%		119	6.6	5.9%		118	4.8	4.2%		118	13.8	13.2%
		117	5.3	4.7%		118	2.3	2.0%		118	5.6	5.0%		118	4.8	4.2%		118	13.8	13.2%
Data <sub>safety</sub> (10) ↓ Data <sub>target</sub> (20)	88.5	89	0.5	0.6%	92.3	89	-3.3	-3.6%	99.6	90	-9.6	-9.6%	92.5	89	-3.5	-3.8%	80.9	89	8.1	10.0%
		92	3.5	4.0%		92	-0.3	-0.3%		92	-7.6	-7.6%		92	-0.5	-0.5%		91	10.1	12.5%
		85	-3.5	-4.0%		86	-6.3	-6.8%		86	-13.6	-13.7%		86	-6.5	-7.0%		85	4.1	5.1%
		96	7.5	8.5%		96	3.7	4.0%		96	-3.6	-3.6%		96	3.5	3.8%		96	15.1	18.7%
		95	6.5	7.3%		95	2.7	2.9%		95	-4.6	-4.6%		95	2.5	2.7%		95	14.1	17.4%

Table 7-2 DATA<sub>safety</sub>(20)↔DATA<sub>target</sub>(30-80)

Unit: G	Group 1				Group 2				Group 3				Group 4				Group 5			
	PRA <sub>exp</sub>	PRA <sub>sim</sub>	Diff	P	PRA <sub>exp</sub>	PRA <sub>sim</sub>	Diff	P	PRA <sub>exp</sub>	PRA <sub>sim</sub>	Diff	P	PRA <sub>exp</sub>	PRA <sub>sim</sub>	Diff	P	PRA <sub>exp</sub>	PRA <sub>sim</sub>	Diff	P
Data <sub>safety</sub> (20) ↓ Data <sub>target</sub> (80)	138.7	142	3.3	2.4%	146.5	144	-2.5	-1.7%	142.7	144	1.3	0.9%	145.0	144	-1	-0.7%	146.1	144	-2.1	-1.4%
		139	0.3	0.2%		139	-7.5	-5.1%		139	-3.7	-2.6%		139	-6	-4.1%		139	-7.1	-4.9%
		138	-0.7	-0.5%		138	-8.5	-5.8%		139	-3.7	-2.6%		138	-7	-4.8%		138	-8.1	-5.5%
		137	-1.7	-1.2%		138	-8.5	-5.8%		138	-4.7	-3.3%		138	-7	-4.8%		138	-8.1	-5.5%
		133	-5.7	-4.1%		133	-13.5	-9.2%		134	-8.7	-6.1%		133	-12	-8.3%		134	-12.1	-8.3%
Data <sub>safety</sub> (20) ↓ Data <sub>target</sub> (70)	143.2	136	-7.2	-5.0%	139.2	137	-2.2	-1.6%	141.5	135	-6.5	-4.6%	140.3	137	-3.3	-2.4%	138.8	137	-1.8	-1.3%
		133	-10.2	-7.1%		133	-6.2	-4.5%		130	-11.5	-8.1%		132	-8.3	-5.9%		132	-6.8	-4.9%
		133	-10.2	-7.1%		133	-6.2	-4.5%		130	-11.5	-8.1%		131	-9.3	-6.6%		132	-6.8	-4.9%
		130	-13.2	-9.2%		130	-9.2	-6.6%		129	-12.5	-8.8%		129	-11.3	-8.1%		130	-8.8	-6.3%
		127	-16.2	-11.3%		126	-13.2	-9.5%		124	-17.5	-12.4%		125	-15.3	-10.9%		126	-12.8	-9.2%
Data <sub>safety</sub> (20) ↓ Data <sub>target</sub> (60)	140.7	129	-11.7	-8.3%	135.7	129	-6.7	-4.9%	134.4	128	-6.4	-4.8%	138.2	129	-9.2	-6.7%	133.4	129	-4.4	-3.3%
		127	-13.7	-9.7%		127	-8.7	-6.4%		125	-9.4	-7.0%		127	-11.2	-8.1%		127	-6.4	-4.8%
		127	-13.7	-9.7%		127	-8.7	-6.4%		125	-9.4	-7.0%		127	-11.2	-8.1%		126	-7.4	-5.5%
		125	-15.7	-11.2%		125	-10.7	-7.9%		124	-10.4	-7.7%		125	-13.2	-9.6%		125	-8.4	-6.3%
		122	-18.7	-13.3%		122	-13.7	-10.1%		123	-11.4	-8.5%		124	-14.2	-10.3%		124	-9.4	-7.0%
Data <sub>safety</sub> (20) ↓ Data <sub>target</sub> (50)	132.3	123	-9.3	-7.0%	131.8	123	-8.8	-6.7%	130.7	122	-8.7	-6.7%	130.4	123	-7.4	-5.7%	134.8	125	-9.8	-7.3%
		119	-13.3	-10.1%		118	-13.8	-10.5%		118	-12.7	-9.7%		119	-11.4	-8.7%		119	-15.8	-11.7%
		120	-12.3	-9.3%		118	-13.8	-10.5%		118	-12.7	-9.7%		119	-11.4	-8.7%		120	-14.8	-11.0%
		118	-14.3	-10.8%		118	-13.8	-10.5%		118	-12.7	-9.7%		118	-12.4	-9.5%		118	-16.8	-12.5%
		115	-17.3	-13.1%		114	-17.8	-13.5%		114	-16.7	-12.8%		115	-15.4	-11.8%		115	-19.8	-14.7%



Data <sub>safety</sub> (20) ↓ Data <sub>target</sub> (40)	129.1	120	-9.1	-7.0%	114.7	116	1.3	1.1%	119.1	116	-3.1	-2.6%	122.0	116	-6	-4.9%	130.7	122	-8.7	-6.7%
		112	-17.1	-13.2%		120	5.3	4.6%		120	0.9	0.8%		120	-2	-1.6%		120	-10.7	-8.2%
		123	-6.1	-4.7%		123	8.3	7.2%		122	2.9	2.4%		122	0	0.0%		123	-7.7	-5.9%
		113	-16.1	-12.5%		111	-3.7	-3.2%		111	-8.1	-6.8%		112	-10	-8.2%		112	-18.7	-14.3%
		121	-8.1	-6.3%		120	5.3	4.6%		120	0.9	0.8%		120	-2	-1.6%		121	-9.7	-7.4%
Data <sub>safety</sub> (20) ↓ Data <sub>target</sub> (30)	111.7	108	-3.7	-3.3%	115.7	109	-6.7	-5.8%	112.4	109	-3.4	-3.0%	113.2	110	-3.2	-2.8%	104.2	109	4.8	4.6%
		104	-7.7	-6.9%		105	-10.7	-9.2%		105	-7.4	-6.6%		105	-8.2	-7.2%		104	-0.2	-0.2%
		104	-7.7	-6.9%		105	-10.7	-9.2%		105	-7.4	-6.6%		105	-8.2	-7.2%		105	0.8	0.8%
		103	-8.7	-7.8%		103	-12.7	-11.0%		103	-9.4	-8.4%		103	-10.2	-9.0%		103	-1.2	-1.2%
		100	-11.7	-10.5%		101	-14.7	-12.7%		101	-11.4	-10.1%		101	-12.2	-10.8%		100	-4.2	-4.0%

Table 7-3 DATA<sub>safety</sub>(30)↔DATA<sub>target</sub>(40–80).

Unit: G	Group 1				Group 2				Group 3				Group 4				Group 5			
	PRA <sub>exp</sub>	PRA <sub>sim</sub>	Diff	<i>P</i>	PRA <sub>exp</sub>	PRA <sub>sim</sub>	Diff	<i>P</i>	PRA <sub>exp</sub>	PRA <sub>sim</sub>	Diff	<i>P</i>	PRA <sub>exp</sub>	PRA <sub>sim</sub>	Diff	<i>P</i>	PRA <sub>exp</sub>	PRA <sub>sim</sub>	Diff	<i>P</i>
Data <sub>safety</sub> (30) ↓ Data <sub>target</sub> (80)	138.7	143	4.3	3.1%	146.5	143	-3.5	-2.4%	142.7	143	0.3	0.2%	145.0	143	-2	-1.4%	146.1	143	-3.1	-2.1%
		138	-0.7	-0.5%		138	-8.5	-5.8%		139	-3.7	-2.6%		138	-7	-4.8%		138	-8.1	-5.5%
		137	-1.7	-1.2%		137	-9.5	-6.5%		138	-4.7	-3.3%		137	-8	-5.5%		137	-9.1	-6.2%
		140	1.3	0.9%		140	-6.5	-4.4%		141	-1.7	-1.2%		140	-5	-3.4%		140	-6.1	-4.2%
		140	1.3	0.9%		140	-6.5	-4.4%		141	-1.7	-1.2%		140	-5	-3.4%		140	-6.1	-4.2%
Data <sub>safety</sub> (30) ↓ Data <sub>target</sub> (70)	143.2	137	-6.2	-4.3%	139.2	137	-2.2	-1.6%	141.5	135	-6.5	-4.6%	140.3	136	-4.3	-3.1%	138.8	137	-1.8	-1.3%
		132	-11.2	-7.8%		133	-6.2	-4.5%		131	-10.5	-7.4%		132	-8.3	-5.9%		132	-6.8	-4.9%
		131	-12.2	-8.5%		131	-8.2	-5.9%		129	-12.5	-8.8%		130	-10.3	-7.3%		130	-8.8	-6.3%
		134	-9.2	-6.4%		133	-6.2	-4.5%		132	-9.5	-6.7%		133	-7.3	-5.2%		133	-5.8	-4.2%
		135	-8.2	-5.7%		135	-4.2	-3.0%		135	-6.5	-4.6%		135	-5.3	-3.8%		134	-4.8	-3.5%
Data <sub>safety</sub> (30) ↓ Data <sub>target</sub> (60)	140.7	131	-9.7	-6.9%	135.7	131	-4.7	-3.5%	134.4	130	-4.4	-3.3%	138.2	131	-7.2	-5.2%	133.4	131	-2.4	-1.8%
		125	-15.7	-11.2%		125	-10.7	-7.9%		125	-9.4	-7.0%		125	-13.2	-9.6%		124	-9.4	-7.0%
		124	-16.7	-11.9%		124	-11.7	-8.6%		124	-10.4	-7.7%		124	-14.2	-10.3%		123	-10.4	-7.8%
		127	-13.7	-9.7%		127	-8.7	-6.4%		126	-8.4	-6.3%		127	-11.2	-8.1%		127	-6.4	-4.8%
		128	-12.7	-9.0%		128	-7.7	-5.7%		127	-7.4	-5.5%		128	-10.2	-7.4%		128	-5.4	-4.0%
Data <sub>safety</sub> (30) ↓ Data <sub>target</sub> (50)	132.3	124	-8.3	-6.3%	131.8	124	-7.8	-5.9%	130.7	122	-8.7	-6.7%	130.4	123	-7.4	-5.7%	134.8	124	-10.8	-8.0%
		117	-15.3	-11.6%		117	-14.8	-11.2%		117	-13.7	-10.5%		118	-12.4	-9.5%		118	-16.8	-12.5%
		117	-15.3	-11.6%		117	-14.8	-11.2%		117	-13.7	-10.5%		118	-12.4	-9.5%		118	-16.8	-12.5%
		119	-13.3	-10.1%		119	-12.8	-9.7%		117	-13.7	-10.5%		118	-12.4	-9.5%		119	-15.8	-11.7%
		121	-11.3	-8.5%		121	-10.8	-8.2%		121	-9.7	-7.4%		121	-9.4	-7.2%		121	-13.8	-10.2%

Data <sub>safety</sub> (30) ↓ Data <sub>target</sub> (40)	129.1	119	-10.1	-7.8%	114.7	117	2.3	2.0%	119.1	118	-1.1	-0.9%	122.0	118	-4	-3.3%	130.7	117	-13.7	-10.5%
		120	-9.1	-7.0%		117	2.3	2.0%		117	-2.1	-1.8%		117	-5	-4.1%		117	-13.7	-10.5%
		119	-10.1	-7.8%		117	2.3	2.0%		117	-2.1	-1.8%		118	-4	-3.3%		118	-12.7	-9.7%
		120	-9.1	-7.0%		118	3.3	2.9%		118	-1.1	-0.9%		118	-4	-3.3%		118	-12.7	-9.7%
		121	-8.1	-6.3%		119	4.3	3.7%		119	-0.1	-0.1%		119	-3	-2.5%		119	-11.7	-9.0%

Table 7-4 DATA<sub>safety</sub>(40)↔DATA<sub>target</sub>(50–80).

Unit: G	Group 1				Group 2				Group 3				Group 4				Group 5			
	PRA <sub>exp</sub>	PRA <sub>sim</sub>	Diff	<i>P</i>	PRA <sub>exp</sub>	PRA <sub>sim</sub>	Diff	<i>P</i>	PRA <sub>exp</sub>	PRA <sub>sim</sub>	Diff	<i>P</i>	PRA <sub>exp</sub>	PRA <sub>sim</sub>	Diff	<i>P</i>	PRA <sub>exp</sub>	PRA <sub>sim</sub>	Diff	<i>P</i>
Data <sub>safety</sub> (40) ↓ Data <sub>target</sub> (80)	138.7	139	0.3	0.2%	146.5	139	-7.5	-5.1%	142.7	140	-2.7	-1.9%	145.0	139	-6	-4.1%	146.1	139	-7.1	-4.9%
		141	2.3	1.7%		141	-5.5	-3.8%		141	-1.7	-1.2%		141	-4	-2.8%		141	-5.1	-3.5%
		140	1.3	0.9%		140	-6.5	-4.4%		140	-2.7	-1.9%		140	-5	-3.4%		141	-5.1	-3.5%
		136	-2.7	-1.9%		136	-10.5	-7.2%		136	-6.7	-4.7%		137	-8	-5.5%		136	-10.1	-6.9%
		137	-1.7	-1.2%		137	-9.5	-6.5%		137	-5.7	-4.0%		137	-8	-5.5%		137	-9.1	-6.2%
Data <sub>safety</sub> (40) ↓ Data <sub>target</sub> (70)	143.2	129	-14.2	-9.9%	139.2	129	-10.2	-7.3%	141.5	128	-13.5	-9.5%	140.3	128	-12.3	-8.8%	138.8	128	-10.8	-7.8%
		130	-13.2	-9.2%		128	-11.2	-8.0%		130	-11.5	-8.1%		130	-10.3	-7.3%		130	-8.8	-6.3%
		129	-14.2	-9.9%		125	-14.2	-10.2%		129	-12.5	-8.8%		129	-11.3	-8.1%		129	-9.8	-7.1%
		128	-15.2	-10.6%		125	-14.2	-10.2%		128	-13.5	-9.5%		129	-11.3	-8.1%		129	-9.8	-7.1%
		128	-15.2	-10.6%		127	-12.2	-8.8%		128	-13.5	-9.5%		128	-12.3	-8.8%		128	-10.8	-7.8%
Data <sub>safety</sub> (40) ↓ Data <sub>target</sub> (60)	140.7	126	-14.7	-10.4%	135.7	126	-9.7	-7.1%	134.4	127	-7.4	-5.5%	138.2	127	-11.2	-8.1%	133.4	127	-6.4	-4.8%
		128	-12.7	-9.0%		128	-7.7	-5.7%		128	-6.4	-4.8%		128	-10.2	-7.4%		128	-5.4	-4.0%
		127	-13.7	-9.7%		127	-8.7	-6.4%		127	-7.4	-5.5%		128	-10.2	-7.4%		128	-5.4	-4.0%
		126	-14.7	-10.4%		127	-8.7	-6.4%		127	-7.4	-5.5%		127	-11.2	-8.1%		127	-6.4	-4.8%
		126	-14.7	-10.4%		126	-9.7	-7.1%		126	-8.4	-6.3%		126	-12.2	-8.8%		126	-7.4	-5.5%
Data <sub>safety</sub> (40) ↓ Data <sub>target</sub> (50)	132.3	117	-15.3	-11.6%	131.8	117	-14.8	-11.2%	130.7	118	-12.7	-9.7%	130.4	118	-12.4	-9.5%	134.8	117	-17.8	-13.2%
		120	-12.3	-9.3%		120	-11.8	-9.0%		120	-10.7	-8.2%		120	-10.4	-8.0%		120	-14.8	-11.0%
		119	-13.3	-10.1%		120	-11.8	-9.0%		119	-11.7	-9.0%		119	-11.4	-8.7%		119	-15.8	-11.7%
		117	-15.3	-11.6%		117	-14.8	-11.2%		117	-13.7	-10.5%		117	-13.4	-10.3%		117	-17.8	-13.2%
		116	-16.3	-12.3%		116	-15.8	-12.0%		116	-14.7	-11.2%		116	-14.4	-11.0%		116	-18.8	-13.9%

Table 7-5 DATA<sub>safety</sub>(50)↔DATA<sub>target</sub>(60–80).

Unit: G	Group 1				Group 2				Group 3				Group 4				Group 5			
	PRA <sub>exp</sub>	PRA <sub>sim</sub>	Diff	<i>P</i>	PRA <sub>exp</sub>	PRA <sub>sim</sub>	Diff	<i>P</i>	PRA <sub>exp</sub>	PRA <sub>sim</sub>	Diff	<i>P</i>	PRA <sub>exp</sub>	PRA <sub>sim</sub>	Diff	<i>P</i>	PRA <sub>exp</sub>	PRA <sub>sim</sub>	Diff	<i>P</i>
Data <sub>safety</sub> (50) ↓ Data <sub>target</sub> (80)	138.7	140	1.3	0.9%	146.5	135	-11.5	-7.8%	142.7	140	-2.7	-1.9%	145.0	140	-5	-3.4%	146.1	139	-7.1	-4.9%
		138	-0.7	-0.5%		133	-13.5	-9.2%		138	-4.7	-3.3%		137	-8	-5.5%		136	-10.1	-6.9%
		135	-3.7	-2.7%		130	-16.5	-11.3%		135	-7.7	-5.4%		138	-7	-4.8%		137	-9.1	-6.2%
		135	-3.7	-2.7%		130	-16.5	-11.3%		135	-7.7	-5.4%		139	-6	-4.1%		138	-8.1	-5.5%
		134	-4.7	-3.4%		133	-13.5	-9.2%		134	-8.7	-6.1%		138	-7	-4.8%		138	-8.1	-5.5%
Data <sub>safety</sub> (50) ↓ Data <sub>target</sub> (70)	143.2	133	-10.2	-7.1%	139.2	133	-6.2	-4.5%	141.5	133	-8.5	-6.0%	140.3	133	-7.3	-5.2%	138.8	133	-5.8	-4.2%
		131	-12.2	-8.5%		131	-8.2	-5.9%		131	-10.5	-7.4%		131	-9.3	-6.6%		131	-7.8	-5.6%
		131	-12.2	-8.5%		131	-8.2	-5.9%		131	-10.5	-7.4%		131	-9.3	-6.6%		131	-7.8	-5.6%
		133	-10.2	-7.1%		133	-6.2	-4.5%		133	-8.5	-6.0%		133	-7.3	-5.2%		133	-5.8	-4.2%
		132	-11.2	-7.8%		132	-7.2	-5.2%		132	-9.5	-6.7%		132	-8.3	-5.9%		132	-6.8	-4.9%
Data <sub>safety</sub> (50) ↓ Data <sub>target</sub> (60)	140.7	127	-13.7	-9.7%	135.7	127	-8.7	-6.4%	134.4	127	-7.4	-5.5%	138.2	127	-11.2	-8.1%	133.4	127	-6.4	-4.8%
		124	-16.7	-11.9%		124	-11.7	-8.6%		124	-10.4	-7.7%		124	-14.2	-10.3%		124	-9.4	-7.0%
		125	-15.7	-11.2%		125	-10.7	-7.9%		125	-9.4	-7.0%		125	-13.2	-9.6%		125	-8.4	-6.3%
		126	-14.7	-10.4%		126	-9.7	-7.1%		126	-8.4	-6.3%		126	-12.2	-8.8%		126	-7.4	-5.5%
		126	-14.7	-10.4%		126	-9.7	-7.1%		126	-8.4	-6.3%		126	-12.2	-8.8%		126	-7.4	-5.5%

Table 7-6 DATA<sub>safety</sub>(60)↔DATA<sub>target</sub>(70, 80).

Unit: G	Group 1				Group 2				Group 3				Group 4				Group 5			
	PRA <sub>exp</sub>	PRA <sub>sim</sub>	Diff	<i>P</i>	PRA <sub>exp</sub>	PRA <sub>sim</sub>	Diff	<i>P</i>	PRA <sub>exp</sub>	PRA <sub>sim</sub>	Diff	<i>P</i>	PRA <sub>exp</sub>	PRA <sub>sim</sub>	Diff	<i>P</i>	PRA <sub>exp</sub>	PRA <sub>sim</sub>	Diff	<i>P</i>
Data <sub>safety</sub> (60) ↓ Data <sub>target</sub> (80)	138.7	132	-6.7	-4.8%	146.5	132	-14.5	-9.9%	142.7	133	-9.7	-6.8%	145.0	132	-13	-9.0%	146.1	132	-14.1	-9.7%
		133	-5.7	-4.1%		133	-13.5	-9.2%		134	-8.7	-6.1%		133	-12	-8.3%		133	-13.1	-9.0%
		132	-6.7	-4.8%		132	-14.5	-9.9%		133	-9.7	-6.8%		132	-13	-9.0%		132	-14.1	-9.7%
		135	-3.7	-2.7%		135	-11.5	-7.8%		135	-7.7	-5.4%		134	-11	-7.6%		134	-12.1	-8.3%
		133	-5.7	-4.1%		133	-13.5	-9.2%		133	-9.7	-6.8%		133	-12	-8.3%		133	-13.1	-9.0%
Data <sub>safety</sub> (60) ↓ Data <sub>target</sub> (70)	143.2	126	-17.2	-12.0%	139.2	126	-13.2	-9.5%	141.5	123	-18.5	-13.1%	140.3	125	-15.3	-10.9%	138.8	126	-12.8	-9.2%
		125	-18.2	-12.7%		125	-14.2	-10.2%		125	-16.5	-11.7%		124	-16.3	-11.6%		125	-13.8	-9.9%
		128	-15.2	-10.6%		128	-11.2	-8.0%		128	-13.5	-9.5%		128	-12.3	-8.8%		128	-10.8	-7.8%
		127	-16.2	-11.3%		127	-12.2	-8.8%		127	-14.5	-10.2%		126	-14.3	-10.2%		125	-13.8	-9.9%
		126	-17.2	-12.0%		125	-14.2	-10.2%		125	-16.5	-11.7%		125	-15.3	-10.9%		126	-12.8	-9.2%

Table 7-7 DATA<sub>safety</sub>(70)↔DATA<sub>target</sub>(80).

Unit: G	Group 1				Group 2				Group 3				Group 4				Group 5			
	PRA <sub>exp</sub>	PRA <sub>sim</sub>	Diff	<i>P</i>	PRA <sub>exp</sub>	PRA <sub>sim</sub>	Diff	<i>P</i>	PRA <sub>exp</sub>	PRA <sub>sim</sub>	Diff	<i>P</i>	PRA <sub>exp</sub>	PRA <sub>sim</sub>	Diff	<i>P</i>	PRA <sub>exp</sub>	PRA <sub>sim</sub>	Diff	<i>P</i>
Data <sub>safety</sub> (70) ↓ Data <sub>target</sub> (80)	138.7	134	-4.7	-3.4%	146.5	134	-12.5	-8.5%	142.7	134	-8.7	-6.1%	145.0	134	-11	-7.6%	146.1	134	-12.1	-8.3%
		138	-0.7	-0.5%		138	-8.5	-5.8%		139	-3.7	-2.6%		138	-7	-4.8%		138	-8.1	-5.5%
		135	-3.7	-2.7%		135	-11.5	-7.8%		136	-6.7	-4.7%		135	-10	-6.9%		135	-11.1	-7.6%
		133	-5.7	-4.1%		133	-13.5	-9.2%		133	-9.7	-6.8%		133	-12	-8.3%		133	-13.1	-9.0%
		136	-2.7	-1.9%		136	-10.5	-7.2%		136	-6.7	-4.7%		136	-9	-6.2%		136	-10.1	-6.9%

## List of Symbols

Symbol	Meaning
$A_F$	$F_c/m$
$A_{in}$	Input acceleration
$a(t)$	Acceleration function
$A$	Displacement
$B$	Coefficients relating to $F_c$ for the controlled shock test
$b$	$F_c/k$
$c$	Damping constant
$c_e$	Equivalent damping coefficient
$c_{eq}$	Equivalent damping coefficient under the loss energy
$D$	Duration
$D_e$	Effective impact duration
$E$	Coefficients relating to $F_c$ for the controlled shock test
$E_{eq}$	Equivalent loss energy
$f_n$	Undamped natural frequency
$F$	Force
$F_c$	Coulomb friction
$g$	Acceleration of gravity
$H$	Drop height
$h$	Equivalent free-fall height
$J$	Evaluation function of equivalent linearization method
$k$	Spring constant
$k_e$	Equivalent spring constant
$m$	Mass
$n_{cs}$	Correction coefficient of the controlled shock test
$n_{ff}$	Correction coefficient of the test at free fall
$P$	Load
$Q$	Coefficients relating to $F_c$ for the controlled shock test
$S$	Compression area
$t$	Time
$T_0$	Initial impact duration
$T_d$	Shock period
$T_r$	Shock transmissibility
$u_{cs}$	Correcting coefficient of the controlled shock test using FVD model
$u_{ff}$	Correcting coefficient of the test at free fall using FVD model
$v$	Velocity

---

$v_0$	Initial velocity
$v(t)$	Velocity function
$V$	Impact velocity of the weight dummy
$V_{\text{new}}$	Corrected impact velocity
$V_c$	Velocity change on the shock table
$x$	Strain of the spring
$\dot{x}$	Velocity
$\ddot{x}$	Acceleration
$x(t)$	Displacement function
$\ddot{x}(t)_{\text{max}}$	PRA function of the controlled shock test
$\gamma$	Half-duration from 0 to RPA of shock pulse
$\epsilon$	$c/(2m)$
$\theta$	Phase angle
$\mu_{\text{ff}}$	Correcting coefficient of the test at free fall using FVD model
$\xi$	Damping ratio
$\rho$	Sample correlation coefficient
$\sigma$	Static stress
$\tau$	Time
$\phi$	Phase angle
$\omega_n$	Undamped natural angular frequency
$\omega_d$	$\omega_n \sqrt{1 - \xi^2}$
$\chi^2$	Chi-squared test

---



## List of Acronyms

Acronym	Meaning
ASTM	American Society for Testing and Material
CEN	European Committee for Standardization
DC test	Dynamic compression test
Damping theory	Damping equivalent drop theory
dGs	Difference in the peak response accelerations of the test at free fall and the controlled shock tests
DiA	Differences in average
FVD model	Frictional-viscous damping mass–spring model
Friction theory	Friction equivalent drop theory
ISO	International Organization for Standard
ISTA	International Safe Transit Association
JIS	Japanese Industrial Standards
PRA	Peak response acceleration
$PRA_{cs}$	Peak response acceleration of the controlled shock test
$PRA_{ff}$	Peak response acceleration of the test at free fall
PIA	Peak input acceleration
SCB	Structural corrugated board
SCM	Structural corrugated material
SRS	Shock response spectrum
SR analysis	Shock response analysis
SR curve	Shock response curve
Traditional theory	Traditional equivalent drop theory
TAPPI	Technical Association of the Pulp and Paper Industry
VD model	Viscous damping mass–spring model

## List of Figure Captions

Figure 1-1	Cushioning Package Concept.....	1
Figure 1-2	Cushioning Package Design Procedure.....	2
Figure 1-3	Generic Packaged Product and Acceleration–Time Curves.....	5
Figure 1-4	Shock Manager.....	5
Figure 1-5	Screenshot for Acceleration–Time Curves of Input and Response Pulses.....	6
Figure 1-6	Dynamic Compression Tester.....	7
Figure 1-7	Schematic of the Dynamic Compression Test for Cushioning Materials.....	8
Figure 1-8	Screenshot of the Dynamic Compression Test Results.....	8
Figure 1-9	Shock Machine.....	9
Figure 1-10	Schematic of the Controlled Shock Test for Cushioning Materials.....	9
Figure 1-11	Free Fall Tester.....	10
Figure 1-12	Schematic of the Free Fall Test for Packaged Product.....	11
Figure 1-13	Scene of the Controlled Shock Test for Packaged Product.....	12
Figure 1-14	Schematic of the Controlled Shock Test for Packaged Product.....	12
Figure 1-15	Settings Screenshot of the Controlled Shock Test for Packaged Product.....	13
Figure 1-16	Modeling of Packaged Product.....	14
Figure 1-17	Section of JIS Z 0240: 2002 Standard.....	15
Figure 1-18	Linear Model.....	16
Figure 1-19	SRS for Linear model.....	17
Figure 1-20	Schematic of Equivalent Free-fall Height.....	17
Figure 1-21	Schematic of the Traditional Equivalent Drop Theory.....	18
Figure 1-22	VD Model.....	18
Figure 1-23	SRS for VD Model.....	19
Figure 1-24	Schematic of the Damping Equivalent Drop Theory.....	20
Figure 1-25	MapleSim Window and Simulation Results.....	22
Figure 1-26	Linear Model in MapleSim.....	24
Figure 1-27	Simulation Result of Linear Model.....	24
Figure 1-28	VD Model in MapleSim.....	25
Figure 1-29	Flowchart for Importing Actual Waveform into MapleSim.....	25
Figure 1-30	Comparison between Simulated and Experimental SR Results in the VD Model.....	26
Figure 2-1	Example of a Common Cushioning Package.....	34
Figure 2-2	Structural Corrugated Sleeve in Preliminary Test.....	35
Figure 2-3	Results of Preliminary Experiments.....	36
Figure 2-4	Frictional-viscous Damping (FVD) Models.....	36
Figure 2-5	Interpretation of $k/2$ .....	37
Figure 2-6	Definition of Friction Component in Maple.....	38
Figure 2-7	Period of FVD Model.....	39
Figure 2-8	Deduction Flowchart for SR Equation of Controlled Shock Test.....	44
Figure 2-9	Step Function.....	46
Figure 2-10	Schematic of the Friction Equivalent Drop Theory.....	55
Figure 3-1	Flowchart for Correcting Method.....	58
Figure 3-2	SR Sim for Controlled Shock Test.....	58
Figure 3-3	Hysteresis Loops of Three Damping Models.....	60
Figure 3-4	Procedure for Calculating Coulomb Friction.....	61
Figure 3-5	Structural Corrugated Sleeve in Verification Test.....	64
Figure 3-6	Pulp Mould.....	64

Figure 3-7	Weight Dummy.....	64
Figure 3-8	Flowchart of Extended Verification Test Procedures.....	65
Figure 3-9	Complete Nested Hysteresis Loops.....	66
Figure 3-10	Hysteresis Loops of the Corrugated Sleeve for 4, 8 and 12 kg Weight Dummies.....	67
Figure 3-11	Probability Distribution of dGs of Corrugated Sleeve for Different Weight Dummies.....	70
Figure 3-12	Probability Distributions of dGs of Pulp Mould for Different Weight Dummies.....	71
Figure 3-13	Response Accelerations of the Two Tests using 5 kg and 12 kg Weight Dummies. ...	73
Figure 3-14	Schematic of Correction Indicator.....	74
Figure 3-15	Cushion Curve for Corrugated Sleeve.....	76
Figure 3-16	Friction Curve for Corrugated Sleeve.....	76
Figure 3-17	Standard Deviations of dGs Curves for Corrugated Sleeve.....	76
Figure 3-18	Correction Indicator Curve for Corrugated Sleeve.....	77
Figure 3-19	Cushion Curve for Pulp Mould.....	77
Figure 3-20	Friction Curve for Pulp Mould.....	77
Figure 3-21	Standard Deviations of dGs Curves for Pulp Mould.....	78
Figure 3-22	Correction Indicator Curve for Pulp Mould.....	78
Figure 4-1	Example of a High-value Package.....	81
Figure 4-2	Conceptual Graphic of Proposed Testing Method.....	82
Figure 4-3	The Hybrid Drop Testing Method.....	83
Figure 4-4	Schematic of Calculation of $k$ , $F_c$ and $c$ .....	85
Figure 4-5	Screenshot of SR Analysis Results.....	87
Figure 4-6	Simulation FVD Model and Its Parameters.....	89
Figure 4-7	Screenshot of Simulation Result.....	89
Figure 5-1	Real product Used in Verification Test.....	91
Figure 5-2	Mockup and Cushions.....	91
Figure 5-3	Test Dummy Affixed on the Shock Table.....	92
Figure 5-4	Controlled Shock Test for Verification.....	92
Figure 5-5	Verification Test Results.....	93
Figure 5-6	PRA- $h$ Curve.....	95
Figure 5-7	Data Analysis Flowchart.....	96
Figure 5-8	Schematic of 25 PRA <sub>exp</sub> vs. PRA <sub>sim</sub> comparisons.....	99
Figure 5-9	PRA <sub>sim</sub> vs. PRA <sub>exp</sub> .....	100
Figure 5-10	Predictive Error $P$ at Different Equivalent Free-fall Heights.....	101

## List of Tables

Table 1-1	Testing Standards for Cushioning Materials .....	13
Table 1-2	Testing Standards for Packaged Products.....	14
Table 2-1	Proportion of Materials Manufactured for Packaging and Containers in Japan (2011) ..	34
Table 3-1	Calculation of Damping Coefficient $\zeta$ .....	59
Table 3-2	Calculation of Friction $F_c$ .....	61
Table 3-3	Corrected Impact Velocity $V_{new}$ .....	62
Table 3-4	Comparison of Experimental Results Analyzed by Traditional and Friction Theories...	62
Table 3-5	Example of dGs Calculation. $F_{before}$ , Pulp mould, Dummy: 6 kg. ....	68
Table 3-6	Example of dGs Calculation. $F_{after}$ , Corrugated Sleeve, Dummy: 6 kg. ....	68
Table 3-7	Observed and Expected Values Used in an Example of Chi-square Test. ....	72
Table 3-8	Results of Chi-square Tests of Homogeneity for Graphics 1–9 in Figure 3-12. ....	73
Table 3-9	Experimental Results of Corrugated Sleeve and Pulp Mould Cushions.....	75
Table 4-1	Relationship between $\Omega_{error}$ and $\zeta$ .....	86
Table 4-2	Comparison between $V$ and $V_{new}$ .....	87
Table 5-1	Results of Verification Experiments.....	94
Table 5-2	Calculation of $F_c$ .....	97
Table 5-3	Calculation of $c$ .....	98
Table 5-4	Predictive Error and Standard Deviation at Different Equivalent Free-fall Heights. ....	101
Table 7-1	DATA <sub>safety</sub> (10)↔DATA <sub>target</sub> (20–80).....	107
Table 7-2	DATA <sub>safety</sub> (20)↔DATA <sub>target</sub> (30–80).....	109
Table 7-3	DATA <sub>safety</sub> (30)↔DATA <sub>target</sub> (40–80).....	111
Table 7-4	DATA <sub>safety</sub> (40)↔DATA <sub>target</sub> (50–80).....	113
Table 7-5	DATA <sub>safety</sub> (50)↔DATA <sub>target</sub> (60–80).....	114
Table 7-6	DATA <sub>safety</sub> (60)↔DATA <sub>target</sub> (70, 80).....	115
Table 7-7	DATA <sub>safety</sub> (70)↔DATA <sub>target</sub> (80).....	115

This page is intentionally left blank